December 2017

Catalytic synthesis of biodiesel fuel under sub/supercritical conditions: kinetics and phase behavior

Jiuxu Liu
Syracuse University

Abstract

In this thesis, transesterification of triglycerides and esterification of free fatty acids were executed under subcritical and supercritical alcohol conditions, and discussed in Chapter 2-5. The project was initiated by studying the phase behavior and kinetics of transesterification reactions under severe reaction conditions (T: 300-400 ^{o}C, P=200 bar), since those conditions were suggested and commonly used in the literature. At these conditions, triglycerides reacted with alcohol within minutes, and the oil-alcohol mixture formed a homogeneous phase which minimized the boundary mass transfer resistance. The composition change of the reaction mixture made the critical point of the system approach supercritical region quickly, as calculated by RK Aspen EOS. The kinetic data were well fitted by a three-step second order model. However, thermal degradation of biodiesel fuel was found especially at temperatures higher than 325 ^{o}C. A thorough study on biodiesel thermal degradation clearly proves that the degradation at temperatures above 325 ^{o}C decreased the biodiesel quality, which suggests future experiments be performed at lower temperatures. The degradation reactions were found to be isomerization, polymerization, and pyrolysis reactions. Accordingly, catalysts were employed in order to reach a high product yield in short residence times at milder conditions. A trace amount of sulfuric acid and potassium ethoxide was separately used under subcritical conditions to catalyze the transesterification reactions (T: 175-225 ^{o}C, P: 200 bar). All the reactions were conducted in homogeneous phase. Lastly, esterification reaction of oleic acid was carried out in a packed-bed reactor containing unmodified gamma-alumina. A kinetic study suggests that the mass transfer resistance of the esterification reaction was not significant. Both reaction systems were capable of converting the oil feedstocks to biodiesel product in a few minutes with high conversions.

Catalytic synthesis of biodiesel fuel under sub/supercritical conditions: kinetics and phase behavior

By

Jiuxu Liu

B.S., Chemical Engineering, Hebei University of Technology, 2010

M.S., Chemical Engineering, Syracuse University, 2013

Dissertation

Submitted in partial fulfillment of the requirements for the degree of Doctor of Philosophy in Chemical Engineering

Syracuse University

December 2017

Acknowledgement

I would like to express my deepest gratitude to my academic advisor, Professor Lawrence L. Tavlarides, for providing me an opportunity to receive high-quality education and grow to be a researcher. Thank you for all your encouragement which becomes my motivation to keep me moving forward and to fully explore myself, and for all your guidance which leads me through these years of journey. Also, thank you for your great patience on teaching me many important qualities which should be mastered and benefit my life in terms of how to make a good presentation in front of people, how to fully present my work in publications, and most importantly always paying attention to details. You have given me huge support during my study, and always raised me up when I was lacking confidence to proceed. It is my great honor to be one of Prof. T's graduates and call myself your student.

I sincerely thank my department, Department of Biomedical and Chemical Engineering, for consecutively giving me an opportunity to serve as either a teaching assistant or a graduate assistant, for financially supporting my study through all these years, and for financially supporting me for conference travels. During these five years, I have been serving as a teaching assistant for multiple Professors in our department, and I want to thank you all (Professors Cadwell, Bond, Sangani, Mather, Nangia, Santanam, Henderson, Hosein, and Tavlarides) for teaching me valuable knowledge and training me to be a good TA. Also, my gratitude goes to the current and former secretaries (Sabina, Amelia, Jason, Barbara, Chris, Lynore, and Dawn) in our department, thank you for your help on all the reimbursement process and administrative issues.

I am grateful to our college, College of Engineering and Computer Science, for financially support my research. I also would like to thank the Graduate Students Organization (GSO) at Syracuse University for awarding me travel grant from 2015 to 2017.

I thank all my defense committee members including Professors Akih-Kumgeh, Ren, Sangani, Hosein, Bond, and Tavlarides for your time and help throughout the process to finalize my dissertation.

I am grateful to Professor Bond for allowing me to use his GC MS, FTIR, and TPD, and thank Argy and Xinlei for their sincere help and discussion on characterizing my biodiesel samples and alumina catalysts. I thank Mr. Mario Montesdeoca for your help on using the GC FID and letting me use your FID data receiver for all these years.

I would like to thank my current and former group members including Dr. Ronghong Lin, Yue Nan, and Professor Rice, for their friendship and valuable suggestions and discussions provided on our weekly group meetings. We have been a good and productive team during these years, and I wish all of you a happy life in the future.

My special thanks goes to my soccer teammates of SUCSSA, I am grateful that I can have the opportunities to share all the happy and memorable time with you guys on soccer fields.

In the end, my appreciation and dearest love go to my family including my parents Dongmei Wang and Yanbin Liu, my aunts Jing Wang and Song Wang-Heikari, my grandma Peiyu Wang, my wife Jing Zhang, and my sweet cats Shengsheng and Dingding. It was your encouragements which helped me get through my most struggling time during my first year of study when I was encountered by research difficulties. Thank you for all your endless love and the sacrifices you have made through this journey, I would not have been able to complete my study if without your support. More importantly, I have become a better person and grown up under your guidance and care. Thank you my family.

Table of content

List of Figures

List of Tables

Chapter 1. Introduction

1.1 Biodiesel

Biodiesel has been produced from multiple oil sources including refined vegetable oils, waste grease, and animal fats. It is a renewable and biodegradable fuel, and is registered with the U.S. Environmental Protection Agency (EPA) as a fuel and fuel additive. For example, B100 is referred to pure biodiesel fuel, and B20 represents a mixture of diesel fuel and biodiesel containing 20 vol% biodiesel, both can be directly used as a fuel in compression-ignition engines. The chemical reactions related to biodiesel synthesis include transesterification and esterification reactions, which covert triglycerides and free fatty acids to alkyl esters via reactions with alcohols. Biodiesel has a better lubricity than diesel fuel due to its higher viscosity, so it is largely used as a diesel fuel additive to improve the fuel lubricity. Good lubricity makes sure the fuel molecules stick on the surface of engine, pumps, and injectors so the fuel can be delivered and combusted smoothly. Some properties of biodiesel are similar with those of petroleum diesel fuel in terms of density and energy content. However, the cold flow properties are not as good as diesel fuel, as shown in **Table 1-1**. For example, cloud point of biodiesel is higher than that of diesel fuel, meaning crystals form more easily at cold temperatures in biodiesel fuel than in diesel fuel. The formation of crystals can block filters, which prevents fuel from being pumped to the engine. So instead of using B100, B20 is commonly used in the cold U.S. climates area in order to limit the cloud point at a reasonable value.

Table 1-1 Comparison of fuel properties [1].

Fuel Property	Diesel	Biodiesel
Fuel standard	ASTM D975	ASTM D6751
Higher heating value, Btu/gal	-138490	-119550
Lower heating value, Btu/gal	-129488	-127960
Kinematic viscosity @ 40 ºC	1.3-4.1	4.0-6.0
Specific gravity @15.5 ºC	0.85	0.88
Density, lb/gal @ 15.5 ºC	7.1	7.3
Carbon, wt%	87	77
Hydrogen, wt%	13	12
Oxygen, wt%	0	11
Sulfer, wt% (ppm)	0.0015 max. (15 ppm max)	0.0-0.0015 (0-15 ppm)
Boiling point, ºC	180-340	315-350
Flash point, ºC	60-80	100-170
Cloud point, ºC	-35 to 5	-3 to 15
Pour point, ºC	-35 to -15	-5 to 10
Cetane number	40-55	47-65

Greenhouse gas (GHG) emission will be reduced if petroleum diesel is replaced by biodiesel fuel, since the amount of life-cycle GHG generated from biodiesel fuel is 74% lower compared to diesel fuel, as reported by Argonne National Laboratory [1]. Similar life-cycle analysis was conducted and published by California Air Resources Board (CARB) [2]. The general components involved in the biodiesel Life Cycle Assessment (LCA) includes oilseed planting, oil extracting, biodiesel synthesis, and biodiesel combustion. In specific, CO_2 is adsorbed by oilseed plant via photosynthesis. The oilseed is then harvested and crushed to extract oil which is transported to biodiesel plant. The oil is converted to biodiesel fuel via transesterification and esterification reactions. All farming, harvesting, and transporting procedures above required energy either from electricity or petroleum fuel, which generates CO_2. When biodiesel fuel is being used in heating or combustion engine, CO_2 is generated and released to air. Part of the generated CO_2 will be then consumed in next round of oilseed

planting. If waste grease is adopted instead of soybean in biodiesel production, GHG emission can be more significantly reduced, as shown in **Figure 1-1**.

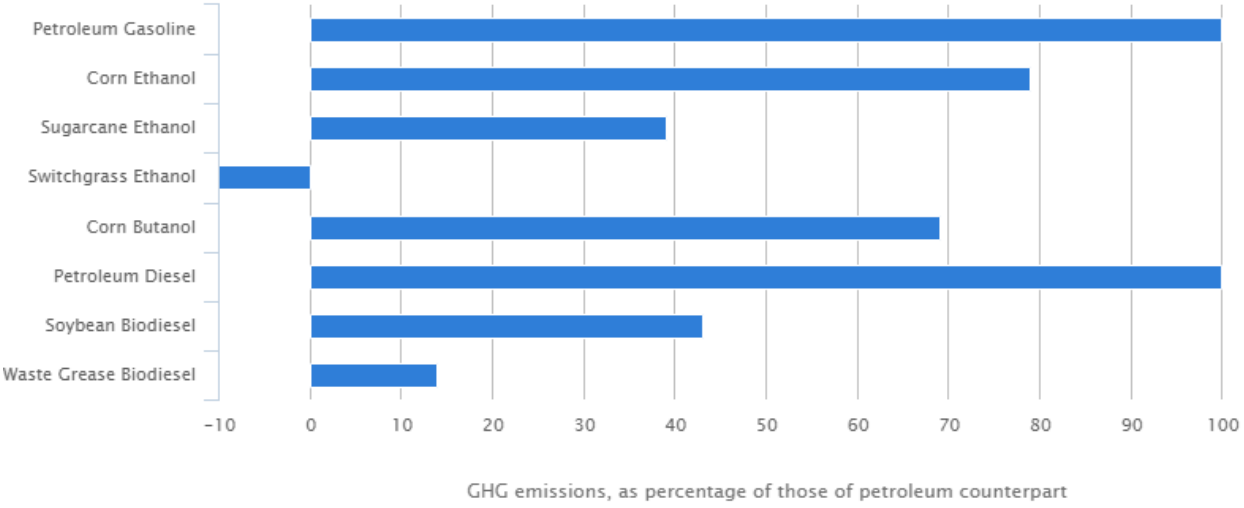

Figure 1-1. Green House Gases (GHG) emissions of biofuel as percentage of those of petroleum counterpart [3].

1.2 Market and policy of biodiesel production

Figure 1-2 shows trends in incentives and laws related to biodiesel fuel, enacted in all 50 states and the District of Columbia from 2002 to 2013. Among all states, California has issued the most policies which supports the usage and production of biodiesel fuel.

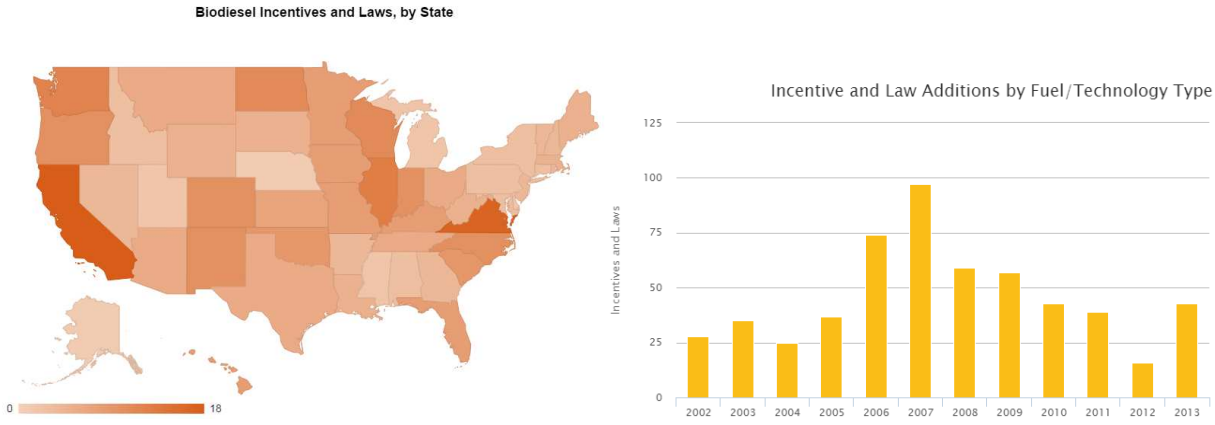

Figure 1-2. Biodiesel incentives and laws in the U.S. [4, 5]

In New York State, biofuel producers may be subsidized by $0.15 per gallon of biodiesel (B100) or denatured ethanol. The maximum annual subsidy available per taxpayer per production facility is $2.5 million, and the maximum consecutive time is limited up to four years [6]. For Federal tax incentive, biodiesel producers may be eligible for a $1.00 incentive per gallon of biodiesel. These polices encourages the usage and production of biodiesel fuel.

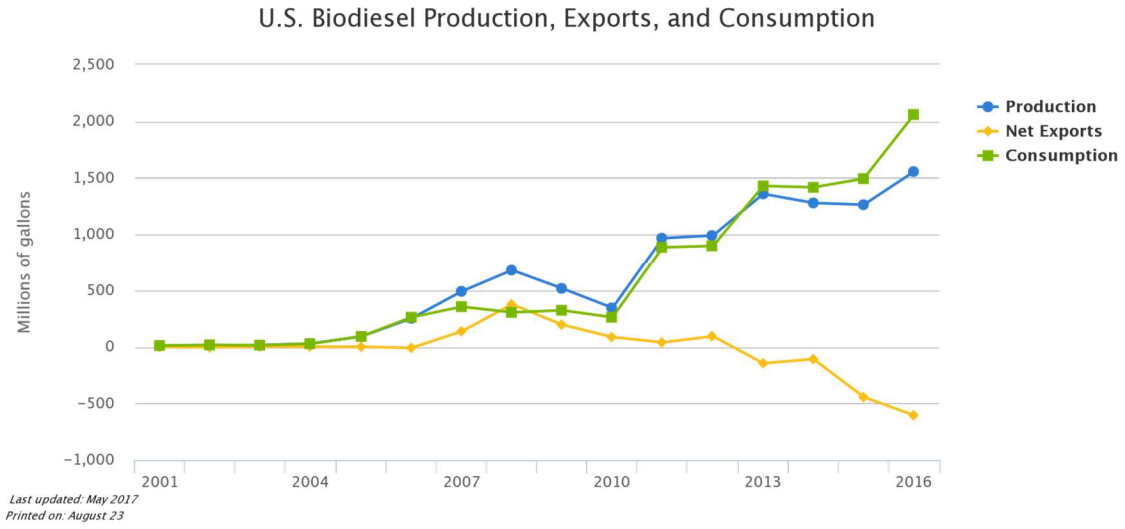

Figure 1-3. Biodiesel production, exports, and consumption in the U.S. from 2001 to 2016 [7].

Data of biodiesel in the U.S. from 2001 to 2016 including production, consumption, and export is summarized in **Figure 1-3** showing that consumption and production has been dramatically increased during last decade, and it is mainly caused by the execution of Renewable Fuel Standard. The decreasing trend of net exports reveals a fact that biodiesel imported to the states has exceeded the exported quantity [7].

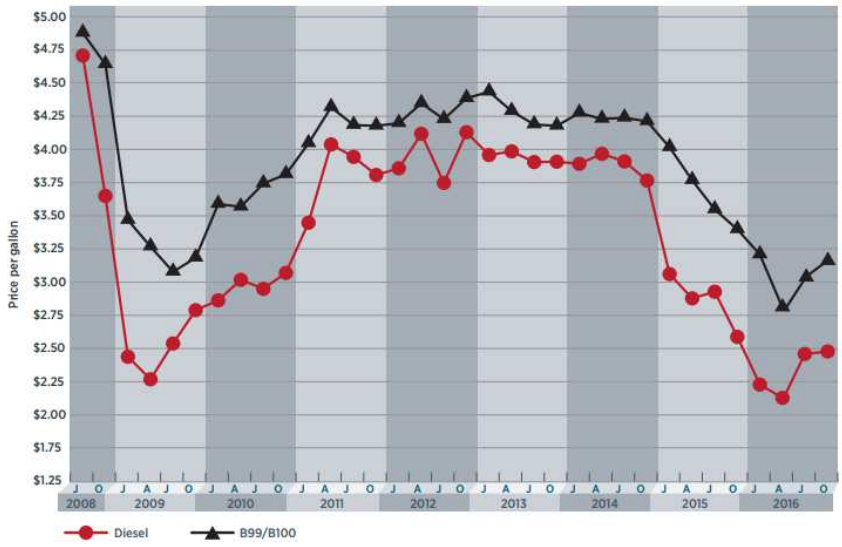

Figure 1-4. Price of biodiesel fuel compared to petroleum diesel fuel [8].

By looking at **Figure 1-4**, it is obvious to see that the price of biodiesel fuel is always higher compared to regular diesel fuel price. This is due to the fact that most of the biodiesel fuel is produced from relatively expensive refined soybean oil in the U.S. To make biodiesel fuel as competitive as diesel fuel, it is necessary to either choose less expensive oil feedstocks or apply new technologies which saves production cost.

1.3 Conventional production technology

1.3.1 One-step homogeneous method

The alcoholysis process, transesterification of triglycerides and esterification of free fatty acids reactions, has been employed in commercial biodiesel fuel production. For transesterification reaction, one triglyceride molecule reacts with three alcohol molecules to be fully consumed and generate three fatty acid alkyl esters (FAAE) and one molecule of glycerol. However, the complete conversion of triglycerides is difficult to reach, and intermediate product such as diglycerides and monoglycerides, can be detected in final product. For esterification reaction, free fatty acid molecule reacts with alcohol molecule to give FAEE and water. Multiple

kinds of catalysts have been tested and demonstrated as an effective compound to provide a high biodiesel yield, among all of them the homogeneous process is currently used in commercial biodiesel production due to its simple operation. The non-catalytic or catalytic supercritical process was proposed in early 2000 and has been developed to convert low quality oil feedstocks to biodiesel fuel. A summary of all proposed method in biodiesel production is presented via a branch tree plot as shown in **Figure 1-5** [9].

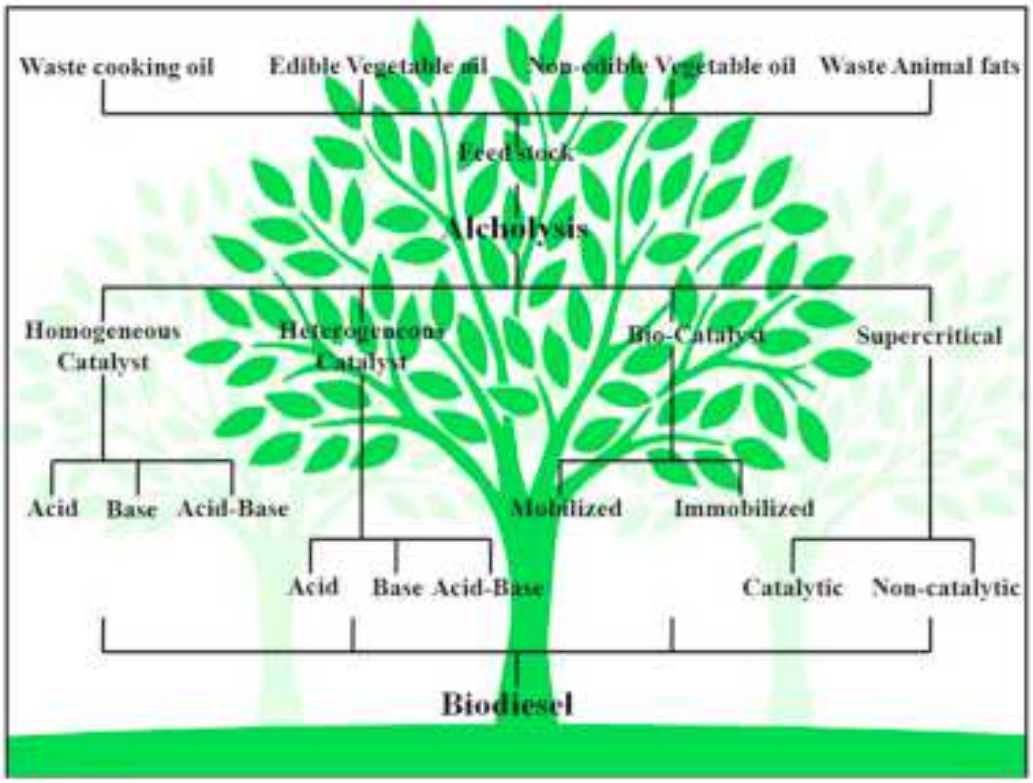

Figure 1-5. Schematic diagram for alcoholysis reaction [9]. The reuse of the figure has been permitted by Elsevier.

The catalysts used in the homogeneous process can be acidic or basic. The processes are not tolerant to low-quality feedstocks meaning high-purity and expensive raw materials are required. The catalysts are dissolved in the product and needed to be separated at the end of the

process. Considering that impurities such as free fatty acids and water will poison the catalysts, the industry now has to employ refined vegetable or soybean oils as the feedstocks. The necessity of using refined oil is the main cause of the high price of biodiesel fuel compared to diesel.

Basic catalysts are preferred in biodiesel industry since they provide faster reaction rates than acidic catalysts in general. Hydroxides and methoxides are the most commonly used compounds such as KOH, NaOH, $NaOCH_3$, and $KOCH_3$. The reactions are usually carried out under mild conditions, for example temperature of 65 ^oC, ambient pressure, catalyst concentration of 1 wt% based on oil mass, alcohol-to-oil molar ratio of 6, and one-hour reaction time. Since basic catalysts are easily poisoned by the presence of both water and FFAs, high quality of feedstocks and pretreatment of feedstocks are required to use meaning water and FFAs content should be limited below 0.06 wt% and 0.5 wt%, respectively, in order to reach the high product yield. The strict limitation is due to the fact that water in the feedsocks will react with triglycerides and biodiesel product, and convert them to FFAs via hydrolysis reactions. The formed FFAs then will further react with the basic catalysts to form soaps which makes the final separation procedure difficult. The final product received before separation consists of biodiesel, glycerol, FFAs, intermediate products as diglyceride and monoglycerides, unreacted alcohol, formed soap, and dissolved catalyst. The mixture must go through further separation and distillation to satisfy the ASTM standard, and this procedure is technically difficult and could cause a loss of product yield [9].

The advantage of acidic catalysts over the basic ones is that the acidic system is tolerant to the presence of FFAs, since they can catalyze the esterification reaction of FFAs and transesterification reaction of triglycerides, which makes it applicable to use low quality of oil

feedstocks in biodiesel production. However, the acidic systems are very sensitive to water, since the acids tends to bind with water, which decreases the biodiesel product yield. The water content should be limited below 0.1 wt%. The most popular acid being employed is sulfuric acid with a concentration of 1-5 wt% based on oil mass. Similar to reactions with basic catalysts, the reaction catalyzed by sulfuric acid can be carried out under mild conditions (T: ~80 ^{o}C, ambient P), but requires a higher alcohol-to-oil molar ratio (~30:1) and longer reaction time (3-20 h) to approach a high biodiesel yield.

The pretreatment procedure to remove water and FFAs in the feedstocks is one of the main technical difficulty in biodiesel production, and it drives up the production cost. The other difficulty consist of product separation and purification. After the reactions, the product mixtures are usually separated via static settlement into two layers. Most of the dissolved catalysts remain in the glycerol layer on the bottom, and the unreacted glycerides and some of the catalysts are in the ester layer on the top. The unreacted alcohol exist in both layers. In order to remove the catalysts, the product is washed by water, and large amount of wastewater is being generated in this process.

1.3.2 Two-step homogeneous method

In order to directly use low-quality oils containing high amount of FFAs, a two-step homogeneous method was proposed. This method is a combination of acidic and basic catalytic reactions. In the first step, an acidic catalyst is applied, so the FFAs in the oils can be eliminated via esterification reactions. This step prevents a further contact of FFAs with basic catalysts in the second step, and generates biodiesel product. In the second step, basic catalyst is added to the reaction mixture, the unreacted glycerides from the first step is then converted to biodiesel product via transesterification reactions. A 97% biodiesel yield was reported by Wang et al., and

the reaction was conducted by the two-step method [10]. In their first step, the esterification reaction of FFAs was performed under 95 ^{o}C for four hours with 2 wt% ferric sulfate and a methanol-to-oil molar ratio of 10:1. The second step was to run the transesterification reaction under 65 ^{o}C for 1 hour with 1 wt% potassium hydroxide and a methanol-to-oil molar ratio of 6:1. However, the two-step method still require pretreatment of feedstocks to remove water, and separation product with catalyst is mandatory at the end of each step, which increases production time and cost.

1.3.3 Heterogeneous method

In order to avoid dealing with the technical difficulty in the product purification process of the homogeneous catalytic system, the synthesis has been carried out over heterogeneous catalysts. But the problem related to presence of water and FFAs has not been solved yet. A study from DiSerio et al. explored the possibility of converting soybean oil to biodiesel over both acidic and basic heterogeneous catalysts [11]. Yields of 75 % and 92 % were reached for catalysts of MgO and hydrotalcites, respectively. Due to the basicity of the solids, soap formation was observed when adding FFAs to the reaction mixture. Besides, soap formation was found when water is present, since FFAs were generated from hydrolysis reaction of triglycerides with water. In terms of acid solids, supported titanium oxide over silica TiO_2/SiO_2 and vanadyl phosphate VOP were used, and biodiesel yields of 40% and 70% were reported for each catalytic system, respectively. The VOP catalyst was found unstable due to significant deactivation. Water content was found to poison both catalysts, and FFAs slightly influenced the reaction. In Chapter 5, a thorough review of the topic of heterogeneous biodiesel synthesis is prepared with more details and examples.

1.3.4 Enzyme method

The problems, associated with acidic/basic catalytic technology, caused by the impurities from the feedstocks can be perfectly eliminated by the enzyme method which employs lipase as the catalyst to convert triglycerides and FFAs to biodiesel fuel [12]. Water does not poison the catalyst also. High biodiesel yields were reported via this method, and the product separation procedure is easy. The main drawback of the enzyme method is the expensive cost the enzyme itself. No commercial application of this method has been found so far.

1.4 Subcritical and supercritical (SC) technology

1.4.1 Properties of alcohol under SC conditions

When the temperature and pressure exceed the critical values of a substance, the compound then becomes supercritical. A general pressure-temperature diagram can be found below. Supercritical fluids have been widely used in chemical reactions and separations as a perfect reaction media and solvent.

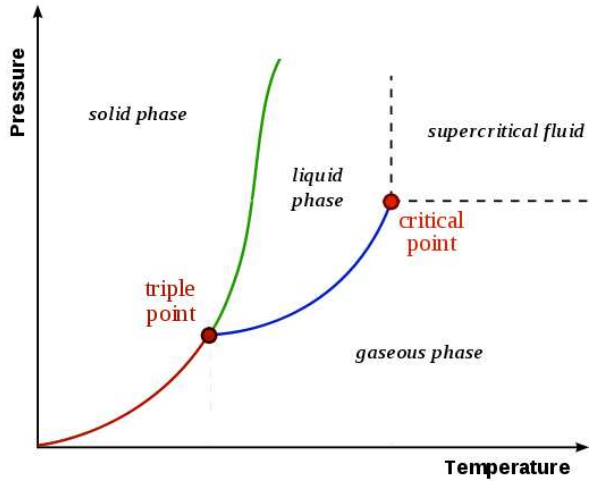

Figure 1-6. General P-T diagram [13].

The SC alcohol conditions are created by increasing the reaction temperature and pressure to values near or above the critical point of alcohol. Under such severe conditions, the

properties of alcohol are changed such as density of hydrogen bonding in alcohols significantly decreases, and alcohols become nearly non-polar. Bazaev et al. experimentally measured the density change of pure ethanol [14] and methanol [15] under SC conditions. Physical properties change of SC ethanol is presented in **Figure 1-7 - 1-9**. At near-supercritical region (T: ~250 ^{o}C, P: 50-70 bar), the density of ethanol significantly changes with pressure fluctuation, and becomes less sensitive in the supercritical region (T: >300 ^{o}C, P: > 100 bar). The values are much less condense compared to the density of liquid ethanol.

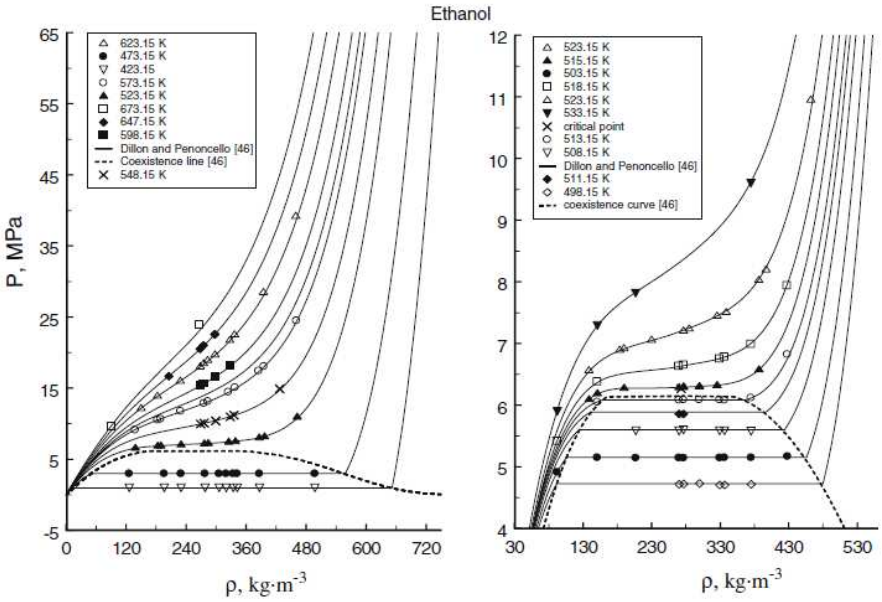

Figure 1-7. Measured values of pressure of SC ethanol as a function of density at different temperatures [14]. The reuse of the figure has been agreed by Springer.

The polarity and hydrogen-bond strength are significantly decreased with enhancing the temperature above the critical value, meaning the polar ethanol can be turned to a nearly non-polar compound with reduced hydrogen bond at supercritical conditions [16, 17]. Under conventional conditions, triglycerides (nonpolar) are not miscible within alcohol (polar). Under supercritical conditions, since alcohol is turned to be nearly non-polar, the two compounds

become miscible with each other, and a homogeneous phase is formed which diminishes the boundary mass transfer so the reaction rate is significantly improved. More details of this topic will be discussed in the phase behavior experiments in Chapter 2. The viscosity of alcohol also changes with density as shown in **Figure 1-9**.

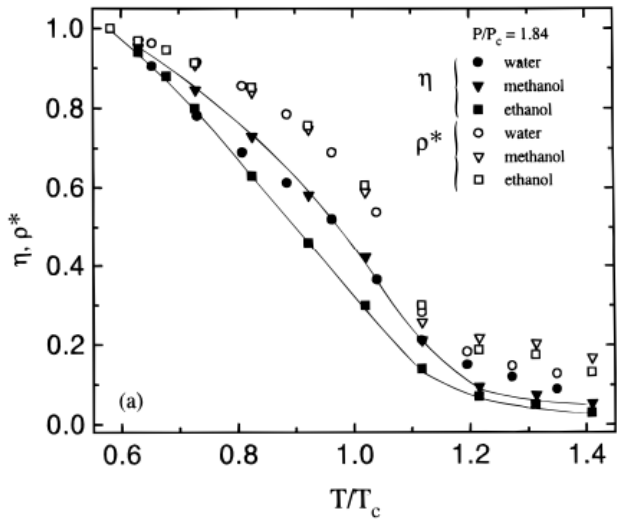

Figure 1-8. The extent of hydrogen bonding η for water, methanol, and ethanol as a function of reduced temperature at a reduced pressure of 1.84 [17]. The reuse of the figure has been agreed by American Chemical Society Publications.

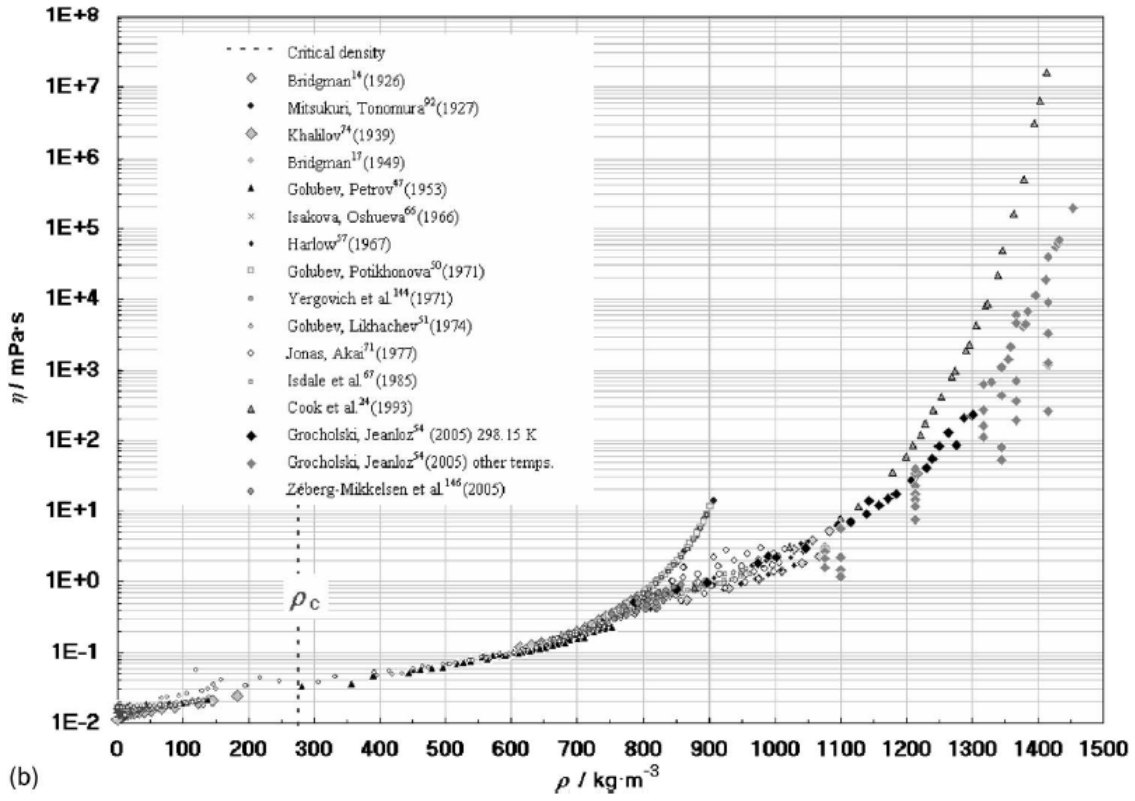

Figure 1-9. Density dependence of the viscosity data of methanol. Reproduced from Xiang, Hong Wei, Arno Laesecke, and Marcia L. Huber. "A new reference correlation for the viscosity of methanol." Journal of physical and chemical reference data 35.4 (2006): 1597-1620. [18], with the permission of AIP Publishing.

1.4.2 Biodiesel synthesis under SC conditions

With the elimination of mass transfer resistance at the oil-ethanol boundary, the reaction rate is also accelerated by the high temperatures (T> 250 ^{o}C), and high product yield can be reached in a few minutes of reaction time even without employing any catalysts. The supercritical process is more tolerant to low-quality feedstocks, and accordingly the production process can be simplified in terms of fewer pretreatment and purification units. When water and FFAs are present in the reaction mixture under supercritical conditions, all the reactions including hydrolysis of triglycerides, transesterification of triglycerides, and esterification of FFAs, can occur simultaneously [20]. No soap will be formed, which is the main problem related

to the basic catalytic process since FFAs react with the bases to generate soap. Besides, the final separation of biodiesel from glycerol is simple, because the two compounds are not miscible with each other at the conditions of being collected (ambient temperature) and there is not catalysts to remove in either phase. Also considering its ability of handling inexpensive feedstocks, the cost of biodiesel could be dramatically dropped since most of cost for biodiesel comes from the feedstocks including refined vegetable oil and soybean oil. The reaction mechanism of the supercritical process is similar to the homogeneous acidic reaction in terms of that the proton is disassociated from alcohol and acting as the catalyst. Environmentally speaking, supercritical process is greener compared to the conventional methods considering it does not have to use catalyst, wastewater is generated from catalyst separation step.

However, the supercritical process has been criticized due to its higher pressure (P> 70 bar, temperature (T> 250 ^{o}C), and alcohol-to-oil molar ratio (~>42:1). The high pressure and temperature would require more energy and more expensive and stable equipment for production. The required high amount of alcohol would make the recovery process of the excess alcohol more complicated and energy consuming. There is no conclusion in the literature to compare which method is more superior, the supercritical or conventional. Some studies of supercritical process showed that with application of cheap waste cooking oil as the feedstock and optimal process design, the total investment and operation costs can be less than those of the conventional method applying homogeneous catalysts [20, 21, 22]. More effort on economic analysis of different supercritical processes are needed, and the environmental impacts as well.

1.5 Research overview

From a scientific perspective, the supercritical reaction systems has not been well explored yet leaving much unknowns including the kinetics and mechanism. In terms of the

kinetics, most studies in the literature only focused on one-step global reaction rate equation, the information of elementary reaction steps remains unknown. Similarly, another important topic, phase behavior, is rarely brought up and explained in the literature. It is unclear that after oil is mixed with supercritical alcohol, if the reaction mixture keeps as supercritical or turns to other state. Currently, high alcohol-to-oil molar ratio is suggested by researchers in order to ensure a homogeneous reaction phase. With a better understanding of phase behavior, the single phase can be reached at a lower ratio, which simplifies the alcohol recovery procedure and thereby reduce the processing cost.

Accordingly, in Chapter 2, we examined the phase behavior of the SC reaction mixtures. Meanwhile, significant degradation of biodiesel was found when the reaction conditions were too severe. In Chapter 3, we explored the mechanism of the degradation reactions, and demonstrated that these degradations lower the quality of biodiesel in terms of viscosity and cold flow qualities when the synthesis was performed beyond 325 ^{o}C. In order to avoid the decompositions, we specifically limited the reaction temperature below 325 ^{o}C, and applied two newly proposed catalytic systems on biodiesel synthesis, as discussed in Chapter 4 and 5.

The content in Chapter 2, 3, and 4 are reproduced or reused from our publications with Elsevier's permission.

1.6 References

[1] Edition, Fifth. "Biodiesel Handling and Use Guide." (2016). DOE/GO-102016-4875.

[2] Stefan Unnasch (2015). Required Document No.2 – Pathway Life Cycle Analysis Report. Retrieved Nov 14, 2017, from https://www.arb.ca.gov/fuels/lcfs/2a2b/apps/ful-ftd-rpt-123015.pdf

[3] Retrieved June 10, 2017, from http://www.afdc.energy.gov/data/10328

[4] Retrieved June 10, 2017, from http://www.afdc.energy.gov/data/10372

[5] Retrieved June 10, 2017, from http://www.afdc.energy.gov/data/10360

[6] Reference New York Tax Law 28*2 and 187-c

[7] Retrieved June 10, 2017, from http://www.afdc.energy.gov/data/10325

[8] Retrieved June 10, 2017, from http://www.afdc.energy.gov/uploads/publication/alternative_fuel_price_report_oct_2016.pdf

[9] Avhad, M. R., and J. M. Marchetti. "A review on recent advancement in catalytic materials for biodiesel production." Renewable and Sustainable Energy Reviews 50 (2015): 696-718.

[10] Wang, Yong, et al. "Preparation of biodiesel from waste cooking oil via two-step catalyzed process." Energy conversion and management 48.1 (2007): 184-188.

[11] Di Serio, M., et al. "From homogeneous to heterogeneous catalysts in biodiesel production." Industrial & Engineering Chemistry Research 46.20 (2007): 6379-6384.

[12] Fukuda, Hideki, Akihiko Kondo, and Hideo Noda. "Biodiesel fuel production by transesterification of oils." Journal of bioscience and bioengineering 92.5 (2001): 405-416.

[13] Retrieved June 10, 2017, from http://lessons.chemistnate.com/phase-diagrams.html

[14] Bazaev, A. R., et al. "PVT measurements for pure ethanol in the near-critical and supercritical regions." International journal of thermophysics 28.1 (2007): 194-219

[15] Bazaev, A. R., et al. "PVT measurements for pure methanol in the near-critical and supercritical regions." The Journal of supercritical fluids 41.2 (2007): 217-226.

[16] Lu, Jie, et al. "Nearcritical and supercritical ethanol as a benign solvent: polarity and hydrogen-bonding." Fluid Phase Equilibria 198.1 (2002): 37-49.

[17] Hoffmann, Markus M., and Mark S. Conradi. "Are there hydrogen bonds in supercritical methanol and ethanol?" The Journal of Physical Chemistry B102.1 (1998): 263-271.

[18] Xiang, Hong Wei, Arno Laesecke, and Marcia L. Huber. "A new reference correlation for the viscosity of methanol." Journal of physical and chemical reference data 35.4 (2006): 1597-1620. https://doi.org/10.1063/1.2360605

[19] Kusdiana, Dadan, and Shiro Saka. "Effects of water on biodiesel fuel production by supercritical methanol treatment." Bioresource technology 91.3 (2004): 289-295.

[20] Warabi, Yuichiro, Dadan Kusdiana, and Shiro Saka. "Reactivity of triglycerides and fatty acids of rapeseed oil in supercritical alcohols." Bioresource technology 91.3 (2004): 283-287.

[21] West, Alex H., Dusko Posarac, and Naoko Ellis. "Assessment of four biodiesel production processes using HYSYS. Plant." Bioresource Technology 99.14 (2008): 6587-6601.

[22] Zhang, Yea, et al. "Biodiesel production from waste cooking oil: 2. Economic assessment and sensitivity analysis." Bioresource technology 90.3 (2003): 229-240.

Chapter 2: Evaluation of transesterification under supercritical conditions

This chapter has been published as: Liu, Jiuxu, Ronghong Lin, Yue Nan, and Lawrence L. Tavlarides. "Production of biodiesel from microalgae oil (Chlorella protothecoides) by non-catalytic transesterification: Evaluation of reaction kinetic models and phase behavior." The Journal of Supercritical Fluids 99 (2015): 38-50. It has been reused with permission from Elsevier.

2.1 Abstract

The non-catalytic transesterification of triglycerides with methanol was conducted at 300-400 ^{o}C, 150-300 bar, methanol-to-oil molar ratio (MOMR) of 6-12, and residence time of 0.5-10 min. A visualization system was built to study the phase transition, and it shows that at the conditions (T: 300~400 ^{o}C, P: 200 bar, τ: 0.5~10 min, MOMR of 9), the reactions were performed in homogeneous state. The dynamic phase behavior of the reacting systems was also investigated by RK-Aspen Equation of State. The results indicate that at 200 bar, MOMR of 9, and 300-385 ^{o}C, the reacting mixtures were in liquid state and moved towards supercritical region, while at 400 ^{o}C the reacting system was initially in liquid state and quickly approached supercritical state due to the fast reaction conversion. The critical points of the reaction mixtures were estimated. Thermal degradation of biodiesel fuel was observed if residence time was extended.

2.2 Introduction

Biodiesel, a renewable diesel alternative, can be produced by transesterification reactions from various sources such as plant oils, animal fats and other renewable oils. The first generation

commercial biodiesel fuels are produced primary from plant oils (e.g. soybean oil in USA [1], rapeseed oil in Germany, and palm oil in Malaysia [2]). Some current concerns of the first generation biodiesel fuels are that they contribute to higher food prices due to competition with food crops and they are expensive without government grants and subsidies [3]. Therefore, efforts have been made to develop processes to produce next generation biodiesel from other renewable sources such as microalgae which offers many potential advantages as a non-food feedstock for biodiesel production and has been recognized as a promising alternative source for oil production. Microalgae can accumulate substantial amounts of lipids - up to 50% of dry cell weight in certain species [4], which is at least as much as 40 times more oil per acre than other plants used for biofuel production [5]. Various design options for cultivating systems for more efficient microalgae growth and oil production have been developed. These cultivating systems mainly include 1) open pond systems, 2) closed pond systems, 3) plastic bag systems, 4) tubular systems, and 5) photo-bioreactor systems [6]. Despite some advantages of microalgae (e.g. non-food feedstock and high oil content), the commercialization of microalgae oil biodiesel is still limited due to high production cost. The estimated production cost of biodiesel from microalgae was $4.92/gallon in 2011, higher than most of other advanced biofuel production costs [7], although the cost might be reduced if appropriate technology could be applied [8].

Commercial biodiesel fuels are produced using conventional transesterification methods in which either base or acid catalysts are used. The main drawbacks of the conventional methods are: they are energy intensive, recovery of glycerol is difficult, catalysts have to be removed from the product, waste water requires treatment, and free fatty acids and water interfere with the transesterification reactions [9]. A non-catalytic biodiesel production process was proposed to address these issues associated with the conventional methods [10]. The core of the non-catalytic

method is to bring the reaction temperature to above the critical temperature of an alcohol (e.g. above 240 ^{o}C for methanol) to form a homogeneous reaction phase; this phase is not necessary to be in a supercritical state as claimed in most literature, as will be discussed in this chapter. The major advantages of the non-catalytic transesterification reaction method are that it significantly reduces reaction time, pretreatments for free fatty acid and water are not required, and the purification of products is much simpler because it is not necessary to remove and recycle the catalysts [10]. Engineering design and economic studies to make biodiesel using the various feed stocks discussed have concluded that the non-catalytic process has the potential to produce biodiesel in an economically sustainable manner [11- 15]. Three recent economic analyses [16-18] performed on the non-catalytic process are very encouraging with regard to the possibility of scaling up the process to industrial levels. In China, an industrial demonstration unit for non-catalytic production of biodiesel from soybean oil, palm oil and waste cooking oil has been in operation since 2009 [19]. Production of biodiesel from microalgae by transesterification at supercritical methanol conditions has also been reported [20-22].

The main objective of this chapter is to address the reaction phase behavior related to produce biodiesel fuel from triglycerides using the non-catalytic continuous flow transesterification method at relatively severe conditions (T: 300-400 ^{o}C, P: 200 bar), which has not been thoroughly addressed in the literature. The information on phase equilibrium is important to determine if reactions are rate controlled or mass transfer controlled [23]. In the reaction phase behavior section of this work, the phase transition was physically observed from a high-pressure high-temperature visualization system, and the results show that at a methanol-to-oil molar ratio (MOMR) of 9, pressure of 200 bar, temperature ranging from 300 to 400 ^{o}C, the methanol-oil flows formed homogeneous streams. Also a suitable thermodynamic model (RK-

Aspen EOS) was employed to simulate the changing critical properties of the reaction system, and the conditions to provide supercritical state of the reaction mixtures were determined. This approach has not been done in previous studies.

2.3 Materials and experimental methods

2.3.1 Materials

Refined microalgae oil (Chlorella protothecoides) was supplied by the Soley Institute in Turkey. The oil density measured at room temperature was 0.96 g/ml. n-Methyl-n-(trimethylsilyl) trifluoroacetamide (MSTFA) (GC derivatization synthesis grade), reference fatty acid methyl esters (FAMEs) standard GLC-10 FAME mix (1891-1AMP), individual standard solutions for triolein, diolein, and monoolein, and internal standards kit (44918-U) were purchased from Sigma Aldrich. The GLC-10 FAME standard contains equal weight percent of methyl palmitate (C16:0), methyl stearate (C18:0), methyl oleate (C18:1), methyl linoleate (C18:2) and methyl linolenate (C18:3). Methanol (HPLC grade) and n-heptane (HPLC grade) were purchased from Thermo Fisher Scientific. Sulfuric acid (98%, ACS reagent grade) was purchased from Sigma Aldrich. Gases (ultrahigh purity grade) used in gas chromatograph analysis were supplied by Airgas.

2.3.2 Transesterification of the oil by the conventional catalytic method

To verify the supplier's measurements and to establish an accurate fatty acid profile, transesterification of the oil with methanol was performed using the conventional acid-catalyzed method. The reactants were prepared by mixing methanol, microalgae oil and sulfuric acid at the volume ratio of 1.32:1:0.148, and the corresponding methanol-to-oil molar ratio was 30:1. The reactants were well stirred with a magnetic stirrer and the reaction was conducted at 65 ^{o}C and 1

bar for 24h. The reaction product consisted of two layers; the upper layer consisted of mainly biodiesel and the lower layer was made up of mainly methanol, glycerol and sulfuric acid. The upper biodiesel layer was separated, collected, and washed by DI water for GC analysis.

2.3.3 Transesterification of the oil by the non-catalytic method

Non-catalytic transesterification of the oil with methanol was performed in two coiled tubular stainless steel reactors (ID 1.753 mm × 4 m, and ID 1.753 mm × 10 m). Experimental runs at 385 ºC and 400 ºC with residence time longer than 4 minutes were performed in the 4 meters long reactor, others were done in the ten meters long reactor. **Figure 2-1** illustrates the continuous flow reactor system.

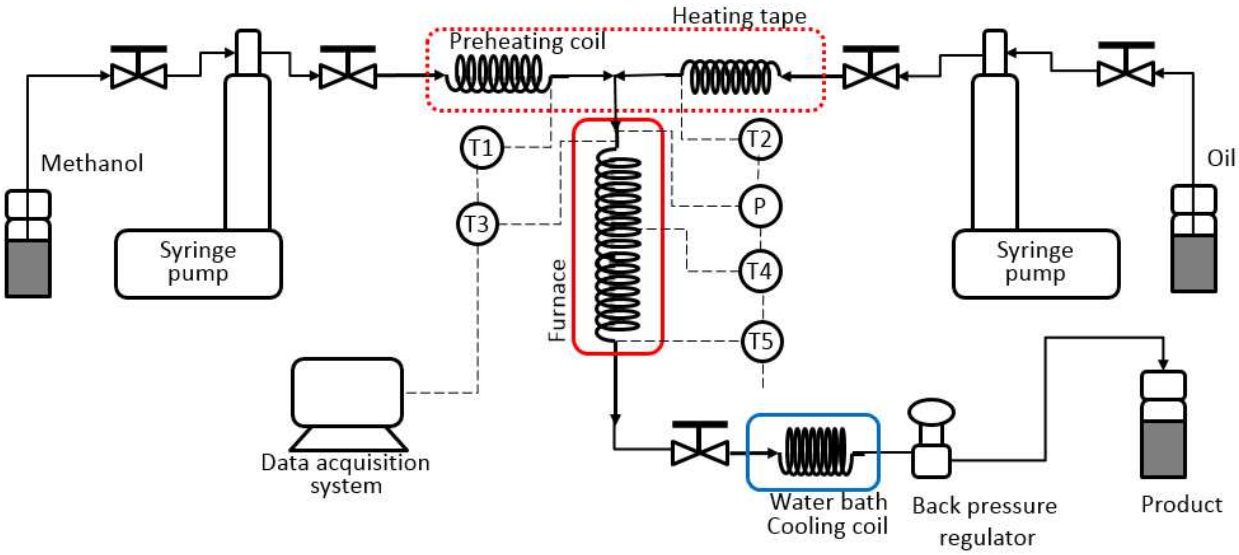

Figure 2-1 Schematic diagram of the experimental setup for non-catalytic transesterification of oil. P – pressure indicator, T1-T5 – thermocouples.

Oil and methanol were pressurized and delivered by two high pressure syringe pumps (Teledyne ISCO 100D and 260D) and then preheated by two heating tapes. Since methanol and oil were immiscible at ambient conditions, heating and pressurizing the two streams separately

before mixing will be beneficial to form a homogeneous state. The two preheated streams were mixed in a mixing tee and then entered the coiled tubular reactor. The reactor was located inside and heated by an electrical furnace (Briskheat). The reaction products were cooled down to room temperature by passing them through a stainless steel coil immersed in a water/ice bath and then collected in glass vials. The reaction pressure (P) was controlled by a back pressure regulator (Swagelok) and monitored by a pressure gauge (Ashcroft, model 1082, 0-10000 psig). The temperatures were controlled by portable controllers (Briskheat). The preheated temperatures (T1 and T2) and the reaction temperatures at the inlet (T3), in the middle (T4), and at the outlet (T5) of the reactor were monitored by thermocouples and recorded by a data acquisition system (National Instruments, model TBX-68T).

Pump flow rates to reach a desired residence time τ is determined by firstly estimating the molar volume (m^3/mol) of methanol-oil mixture at reaction conditions using RK-Aspen EOS; secondly calculating the mass flow rate at reaction conditions by combining information of the reactor volume, the mixture molar volume, the molar weight for methanol and oil, and required residence time; then finally using this mass flow rate information to calculate the flow rates of the pumps. This method was compared with another estimation by using Eq 2-1, and achieved near same calculation result:

$$\tau = \frac{V}{F_M(\rho_M/\rho'_M)+F_O(\rho_O/\rho'_O)} \qquad \text{Eq2-1}$$

where V is the reactor volume, F is the volume flow rate in the pumps, ρ is the density in the pump (ambient temperature, reaction pressure), ρ' is the density at reaction conditions. M and O represent methanol and oil, respectively.

In the preliminary experiments in this work, MOMR (6:1, 9:1 and 12:1), pressures (150, 200 and 300 bar), temperatures (350, 385 and 400 ^oC) were employed, and residence times

varied from 4 to 10 min. In the experiments executed to study thermodynamics and kinetics, MOMR of 9:1, pressure of 200 bar, temperatures (300, 325, 350, 385, and 400 ^{o}C), and residence time from 0.5-10 min for 300 and 325 ^{o}C, 0.5-8 min for 350 ^{o}C, 0.5-4 min for 385 and 400 ^{o}C, respectively, were employed. Different residence time ranges at different temperatures were employed here to avoid biodiesel decompositions. In each run, methanol was preheated and pumped into the reactor to pressurize the system and the reactor was preheated as well before adding oil to the system. After the reactor reached the desired temperature and the system reached the desired pressure, oil was preheated and pumped into the system. Methanol was preheated to 350-385 ^{o}C depending on the reaction temperature, while oil was preheated to 300~ 350 ^{o}C for all runs. For each condition, steady state were normally reached in three residence times, which was judged by minimal fluctuations of T1-T5. When the reaction system reached steady state, products were collected. Runs at residence times from half to 2 minutes were repeated twice. Since the pressure and temperature were well controlled, and the flow streams were very stable and in homogeneous state as shown in section 2.5.3, the runs for longer residence times were not repeated. Multiple reaction products were collected for each run for analysis. Average values, as shown in **Table 2-4**, were calculated and further used in the phase behavior and kinetics simulation. The relative error among the collected samples at same condition was negligible.

2.3.4 Phase transition of methanol-oil mixing streams

A flow visualization system was built up, as shown in **Figure 2-2**. Similar to the reactor system, oil and methanol were pumped separately by two high-pressure syringe pumps (Teledyne ISCO 260D) and then preheated by two heating tapes. The two preheated streams were mixed in a mixing tee and then entered a high-pressure view cell. The length from the

mixing tee outlet to the view cell inlet was the same as the length from the mixing tee outlet to the tubular reactor inlet in the reaction experiments. The view cell was heated by a heating tape. A charge-coupled-device (CCD) camera with a micro-lens (Photron, model# FASTCAM-512PCI) and a light source were used to observe the streams flowing inside the view cell. Similar with the experimental set-up shown in Figure 2-1, the system pressure (P) was controlled by a back pressure regulator (Swagelok) and monitored by a pressure gauge (Ashcroft, model 1082, 0-10000 psig). The preheated temperatures (T1 and T2), and the temperatures at the view cell inlet (T3) and in the view cell (T4) were monitored by thermocouples and recorded by a data acquisition system (National Instruments, model TBX-68T).

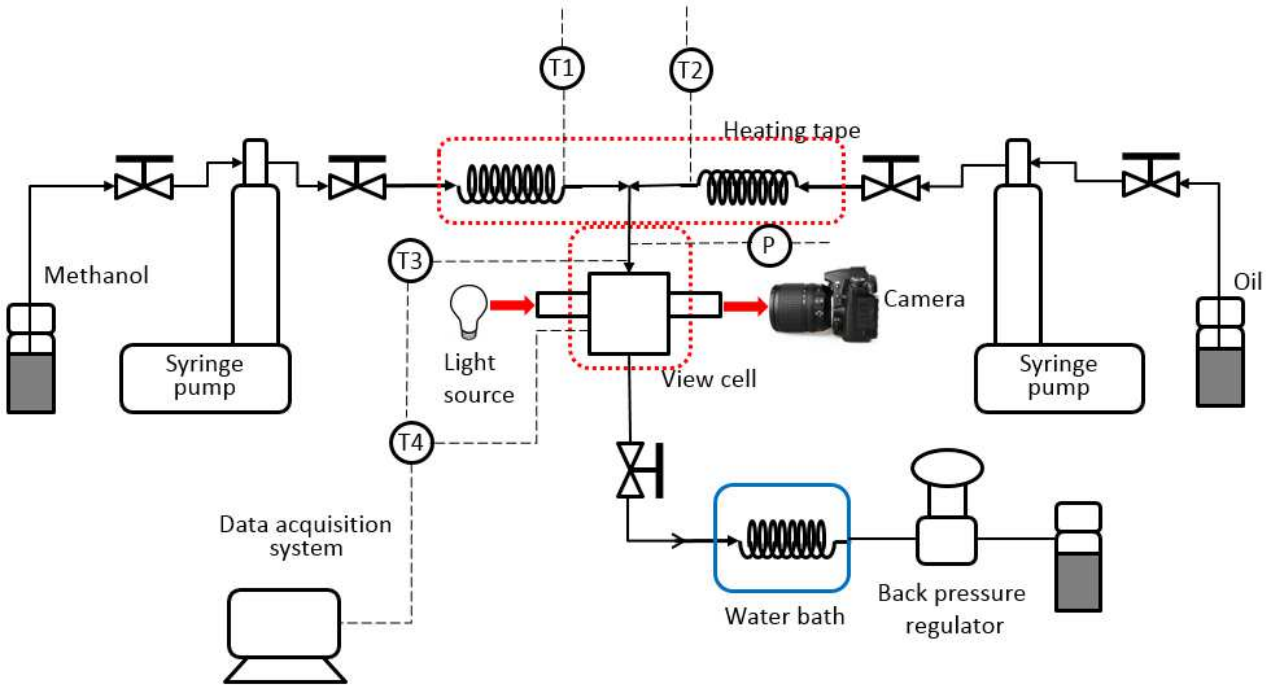

Figure 2-2. Schematic diagram of the experimental setup for phase transition study. P – pressure indicator, T1-T4 – thermocouples.

In this section, a MOMR of 9, pressures (from ambient pressure to 200 bar), temperatures (from 130 to 400 ^{o}C), and flow rates (low, medium, and high) were employed. The values of

low, medium, and high flow rates were taken from the flow rates to create a 10, 2, and half minute residence times as in the tubular reactor in the reaction experiments.

The objective of these experiments was to study oil-methanol mixing phenomena and phase transitions during heating and pressurizing process, and to demonstrate the transesterification reactions were controlled by reaction kinetics rather than mass transfer at conditions studied (T: 300-400 ^{o}C, P: 200 bar, methanol-to-oil molar ratio: 9, residence time: 0.5-10 min).

2.3.5 Analytical Methods

2.3.5.1 Sample preparation

Biodiesel samples collected from the conventional catalytic transesterification reaction were first washed with deionized water three times to remove impurities such as methanol, glycerol and sulfuric acid and then analyzed by gas chromatographs.

Pretreatment of biodiesel samples collected from the non-catalytic transesterification reaction were performed in three different ways for comparison, since the biodiesel layer of samples contains a non-negligible amount of methanol. a) Methanol was removed by washing with deionized water at water-to-biodiesel volume ratio of 3:1, and then the washed biodiesel layer was analyzed, b) methanol was removed by heating in a vacuum oven at 65 ^{o}C, and then the heated biodiesel layer was analyzed, and c) crude biodiesel layer was analyzed by using GC FID without any purification. Methanol concentration in the crude biodiesel layer was measured by a refractometer (ABBE Mark II, American Optical Scientific Instruments), and its value was then deducted from the GC FID result to calculate the content of each compound if all methanol was removed. The procedures are as follows. Standard solutions with methanol concentrations from 0-10 wt% in deionized water were prepared, the refractive indexes of the standards were

measured, and a linear calibration curve of methanol mass concentration versus refractive index, was constructed. A known amount of a crude biodiesel sample was washed by a known amount of deionized water in order to extract the dissolved methanol, and the refractive index of the water solution was measured. Finally, the methanol concentration in the crude biodiesel sample was determined with the calibration curve and a simple mass balance calculation.

The above three different pretreatment methods were determined to have consistent results, so most samples were purified by the deionized water washing method according to its simple operation.

Biodiesel characterization includes the quantitative analysis of the FAME profile and determination of the concentrations of monoglycerides, diglycerides and triglycerides present in the reaction products. For the analysis of the FAME profile, biodiesel samples were prepared by diluting 1 μl biodiesel into 1 ml hexane, making a total biodiesel concentration of 1000 ppm by volume. Calibration curves for individual FAMEs were made using the analytical standard GLC-10 FAME mix [24]. For the analysis of glycerides species, calibration curves for each compound was develop by similar, but not the same, procedures with the ASTM D6584 [25] protocol. Wider concentration ranges were employed to build calibration curves in order to accurately measure concentrations at low reaction conversions. Triolein, diolein, and monoolein were used to represent triglycerides, diglycerides, and monoglycerides. The results are shown in Table 2-4. It is necessary to clarify that since samples are washed by DI water to remove methanol and glycerol, the values for those two compounds in **Table 2-4** were determined from a mass balance calculation by combining the information of initial content of methanol and triglycerides (MOMR of 9:1), content of glycerides and FAMEs in the collected samples, and the three-step reaction mechanism.

2.3.5.2 GC-FID analysis

The quantitative analysis of FAMEs, monoglycerides, diglycerides and triglycerides were done by gas chromatograph (HP 5890 series II) equipped with a flame ionization detector (FID) and a Rtx® Biodiesel TG column (Restek, 10 m × 0.32 mm × 0.1 μm). Helium was used as the carrier gas. For the FAME analysis, the GC temperature program follows: held at 60 °C for 2 min), ramp at 6 °C/min from 60 ºC to 150 °C, held at 150 °C for 10 min, ramp at 10 °C/min from 150 ºC to 350 °C, and finally held at 350 °C for 2 min. For the glycerol and glycerides analysis, a different temperature program was applied: held at 60 °C for 2 min, ramp at 15 ºC/min from 60 ºC to 180 ºC, and finally ramp at 7 ºC /min from 180 ºC to 360 ºC. Both the injection and the detection temperatures were 360 ºC in both analyses.

2.4 Theory

2.4.1 Thermodynamics

Triglycerides and alcohols are immiscible and form inhomogeneous reaction systems during conventional catalytic biodiesel production processes, which greatly limits mass transfer and hence the rates of reactions. The non-catalytic method breaks the mass transfer barrier and accelerates reaction rates by bringing the reaction system to elevated temperature and pressure conditions to form a homogeneous reaction environment. A better understanding of dynamic phase behavior and transition encountered during the implementation of transesterification reactions is required for the design and optimization of the non-catalytic biodiesel production process. A high-pressure high-temperature visualization system allows direct observation of phase behavior, and thermodynamic models provide a powerful tool for predicting phase behavior. Bunyakiat et al. [26] used Lorentz-Berthelot (LB) mixing rules to calculate the critical

points for mixtures of oil and methanol. In a recent review article by Anitescu and Bruno [27], based on the estimation of the critical points of the methanol and oil mixtures by the Lorentz-Berthelot (LB) mixing rules, the authors concluded that at relative high temperatures, the supercritical transesterification reaction can be achieved at relatively low methanol-to-oil ratios. For example, at 350 ºC and 400 ºC, the required methanol-to-oil ratios would be 15 and 8, respectively. However, as pointed out by Pinnarat and Savage [28], even though the LB mixing rules are very convenient to use, the properties calculated from the rules are actually pseudocritical properties, not true critical points, which are generally expected to be very different to the true mixture critical properties. Similar discussion was also made by Poling et al. [29]. So, an appropriate equation of state is suggested to use to determine the actual critical point of a mixture [28].

Tang et al. [30] reported that the predictions of the Peng-Robinson (PR) equation of state (EOS) agreed reasonably well the experimental measurements of phase behavior of the methanol-triolein system. Fang et al. [31] applied the PR EOS for the methanol-C18 methyl esters system and found that the model could not predict well the composition of the vapor phase. Andreatta et al. [32] evaluated the group contribution with association equation of state (GCA-EOS) and the A-UNIFAC model for prediction of phase equilibrium of the methyl oleate-methanol-glycerol ternary system and found that the GCA-EOS model had a good predictive capability. The GCA-EOS was later applied by Hegel et al. [33] to predict phase equilibrium of the vegetable oil-methanol-methyl esters-glycerol system and the predictions agreed well with experimental observation. Glisic et al. [34] examined PR, Soave-Redlich-Kwong (SRK) and Redlich-Kwong-Aspen (RK-Aspen) EOS and different mixing rules for predicting phase behavior of the triglycerides-methanol system and concluded that the RK-Aspen EOS with the

Van der Waals (VdW) mixing rule could best calculate the liquid-vapor phase distribution of the system. Glisic and Skala [23] further demonstrated that the RK-Aspen EOS was able to predict the dynamic phase behavior of the reacting mixtures during the transesterification reactions at subcritical and supercritical conditions.

In this work, the RK-Aspen EOS was applied to predict the changing critical points of the reacting microalgae oil-methanol system. The RK-Aspen EOS is an extension of the SRK EOS and applies the VdW mixing rule, as shown in Eqs. 2-(2-11) [34-36].

$$P = \frac{RT}{V - b_m} - \frac{a_m}{V^2 + b_m V} \quad \text{Eq 2-2}$$

$$a_m = \sum_i \sum_j x_i x_j (a_i a_j)^{0.5} (1 - k_{a,ij}) \quad \text{Eq 2-3}$$

$$b_m = \sum_i \sum_j x_i x_j \frac{(b_i + b_j)}{2} (1 - k_{b,ij}) \quad \text{Eq 2-4}$$

$$a_i = 0.42747 \alpha_i \frac{R^2 T_{ci}^2}{P_{ci}} \quad \text{Eq 2-5}$$

$$b_i = 0.08664 \frac{R T_{ci}}{P_{ci}} \quad \text{Eq 2-6}$$

$$\alpha_i = \left[1 + m_i (1 - T_{Ri}^{0.5}) - \eta_i (1 - T_{Ri})(0.7 - T_{Ri}) \right]^2 \quad \text{Eq 2-7}$$

$$T_{Ri} = \frac{T}{T_{ci}} \quad \text{Eq 2-8}$$

$$m_i = 0.48508 + 1.5519 \omega_i - 0.15613 \omega_i^2 \quad \text{Eq 2-9}$$

$$k_{a,ij} = k_{a,ij}^0 + k_{a,ij}^1 \frac{T}{1000} \quad \text{Eq 2-10}$$

$$k_{b,ij} = k_{b,ij}^0 + k_{b,ij}^1 \frac{T}{1000} \quad \text{Eq 2-11}$$

where ω is the acentric factor, R is the universal gas constant, k is the binary interaction parameter, and η is the polar factor.

The transesterification reaction system involves reactants (i.e. triglycerides and methanol), intermediates (i.e. diglycerides and monoglycerides) and final products (i.e. FAMEs, glycerol and other side-reaction products). As determined in section 2.5.1, over 90% of FAMEs

is unsaturated C18. Accordingly, triolein, diolein, monoolein and methyl oleate were used as surrogates in the thermodynamic model for triglycerides, diglycerides, monoglycerides and FAMEs, respectively, and other side-reaction products were neglected. It is extremely challenging to include in the thermodynamic calculations all chemicals that are present in the system. Thermodynamic parameters for triolein, diolein, monoolein, methyl oleate, methanol and glycerol used as inputs in the ASPEN Plus program [23, 36] were given in **Table 2-1**. The compositions of the reaction system were determined by experiments, as shown in **Table 2-4**.

Table 2-1 Thermodynamics parameters for ASPEN Plus Simulation of the transesterification reaction system.

Parameters	Triolein [23]	Diolein [16]	Monoolein [16]	Methyl Oleate [16]	Methanol [36]	Glycerol [36]
M (g/mol)	885.45	621.00	356.55	296.49	32.04	92.09
T_C (K)	977.88	920.20	835.06	721.02	512.50	850.00
P_C (MPa)	0.334	0.505	1.056	1.103	8.084	7.500
V_C (m^3/kmol)	3.250	2.830	1.254	1.108	0.117	0.264
ω	1.9782	1.7632	1.5324	1.0494	0.5650	0.5130
T_B (K)	827.40	765.03	674.82	595.93	337.85	561.00
V_B (m^3/kmol)	2.708	1.106	0.533	0.489	0.043	0.087
V_l (298K) (m^3/kmol)	0.958	0.623	0.360	0.341	0.040	0.073
ΔG_f (298K) (kJ/kmol)	-1.80E+05	-3.00E+05	-3.23E+05	-1.20E+05	-1.62E+05	-4.47E+05
ΔH_f (298K) (kJ/kmol)	1.97E+05	8.08E+05	5.69E+05	-6.40E+05	-2.01E+05	-5.78E+05
ΔH_v (298K) (kJ/kmol)	3.02E+05	2.19E+05	9.01E+04	6.36E+04	3.51E+04	6.57E+04

Values of the binary interaction parameter k and the polar factor η for reacting species are required for the phase equilibrium simulation. Glisic et al. [34] reported triolein-methanol binary interaction parameters based on experimental data obtained at 200-230 ^oC. No data were found

in the literature for binary interaction parameters for other pairs of components. Also, no data are available in the literature for polar factors for those components present in the reaction system. Accordingly, the triolein-methanol binary interaction parameter reported by Glisic et al. [34] was used, and all other binary interaction parameters and the polar factors were set to zero.

2.4.2 Reaction kinetics

It is well known that transesterification consists of a number of consecutive, reversible reactions [37]. Noureddini and Zhu [38] reported a three-step reversible reaction model with considering mixing of the reaction system for catalytic transesterification of soybean oil with methanol. Modifications of the model have been proposed and applied to both catalytic and non-catalytic transesterification of triglycerides. Modifications were made mainly by considering the order and reversibility of the reactions. Representative models are summarized in **Table 2-2**. Diasakou et al. [39] used a three-step first-order irreversible model to fit the kinetic data for non-catalytic transesterification of soybean oil at 220-235 ^{o}C and found that the evolution of the concentration of each component in the ester phase could be well predicted by the kinetic model. Kusdiana and Saka [40] simplified the three-step model to a one-step first-order irreversible model by ignoring all the intermediates and the model fitted reasonably well with experimental data. The simplified model was later used by other researchers in their work [41, 42]. In these models, the reactions were considered to be first-order because methanol was present in large excess and hence the effect of the decrease in methanol concentration as transesterification proceeded on reaction kinetics was assumed to be negligible [39-41]. However, when methanol was not in large excess, treating methanol as a solvent rather than a reactant could be problematic. For this situation, second order reaction kinetic models were considered by others [38, 43-45]. D'Ippolito et al. [43] applied the three-step model and considered all reactions

second-order and partially reversible.

Table 2-2 Summary of kinetic models for transesterification of triglycerides with methanol.

Reaction Model	Formula	Order of Reaction	References
Three-step, reversible	$TG + MeOH \underset{k_{-1}}{\overset{k_1}{\rightleftharpoons}} DG + ME$ $DG + MeOH \underset{k_{-2}}{\overset{k_2}{\rightleftharpoons}} MG + ME$ $MG + MeOH \underset{k_{-3}}{\overset{k_3}{\rightleftharpoons}} GL + ME$	2^{nd}	[38, 45]
Three-step, partial reversible	$TG + MeOH \xrightarrow{k_4} DG + ME$ $DG + MeOH \underset{k_{-5}}{\overset{k_5}{\rightleftharpoons}} MG + ME$ $MG + MeOH \underset{k_{-6}}{\overset{k_6}{\rightleftharpoons}} GL + ME$	2^{nd}	[43]
Three-step, irreversible	$TG + MeOH \xrightarrow{k_7} DG + ME$ $DG + MeOH \xrightarrow{k_8} MG + ME$ $MG + MeOH \xrightarrow{k_9} GL + ME$	1^{st}	[39]
		2^{nd}	[44]
One-step, irreversible	$uME + MeOH \xrightarrow{k_{11}} GL + ME$	1^{st}	[40,41]

2.5 Results and discussions

2.5.1 Oil characterization

Transesterification of the oil with methanol by the conventional catalytic method resulted in a 98.7% FAME yield. The GC-FID analysis showed that the FAMEs were composed of 5.5 wt% C16:0, 2 wt% C18:0, 91.5 wt% unsaturated C18 and 1wt% other species. A comparison of the fatty acid profiles with other oil species is given in **Table 2-3**. Individual C18:1, C18:2 and

C18:3 concentrations were not determined due to the limitation of the current analytic method, and they were combined.

Table 2-3 Fatty acid profiles of the refined oil used in this work and other biodiesel syntheses studies.

Fatty Acids (wt%)	Chlorella protothecoides (this work)	C. vulgaris [21]	D. tertiolecta [20]
C12:0	ND [a]	0	0
C14:0	ND	0.4	0
C15:0	ND	0	0
C16:0	5.5	17.8	44.3
C16:1	ND	0	0
C17:0	ND	0	0
C18:0	2	2.1	7.8
C18:1		45.5	
C18:2	91.5 [b]	9	47.9 [b]
C18:3		12.7	
others	1	12.5	0

[a] ND-not detectable. [b] the total weight percent of C18:1, C18:2 and C18:3.

2.5.2 Non-catalytic transesterification of oil

From observing GC chromatograms of products, biodiesel decomposition appears to be negligible at 300 and 325 ºC with residence time up to 10 min, 350 ºC with residence time up to 8 min, and 385 and 400 ºC with residence time up to 4 min. Therefore, in order to minimize the influence of the decomposition reactions, in the experiments for phase behavior simulation and reaction kinetic models evaluation, pressure and MOMR were set to 200 bar and 9:1, respectively, while temperature varied from 300-400 ºC, and residence time from 0.5-10 min for

300 and 325 ºC, 0.5-8 min for 350 ºC, 0.5-4 min for 385 and 400 ºC, respectively. Experimental results are shown in **Table 2-4** and **Figure 2-3**.

Table 2-4 Summary of experimental data (200 bar, methanol-to-oil molar ratio of 9:1).

Run #	T (°C)	τ (min)	Product composition (mole fraction)						X
			GL	MG	DG	TG	ME	MeOH	
1	300	0.5	0.0053	0.0012	0.0068	0.0828	0.0228	0.8812	0.092
2	300	2	0.0145	0.0019	0.0173	0.0672	0.0489	0.8502	0.1359
3	300	4	0.0192	0.0064	0.0234	0.0509	0.1023	0.7978	0.1929
4	300	8	0.0193	0.0117	0.0355	0.0368	0.1260	0.7707	0.1597
5	300	10	0.0233	0.0138	0.0339	0.0287	0.1320	0.7683	0.2358
6	325	0.5	0.0118	0.0014	0.0096	0.0772	0.0477	0.8523	0.1181
7	325	2	0.0424	0.0022	0.0148	0.0406	0.1341	0.7659	0.4240
8	325	4	0.0555	0.0048	0.0095	0.0301	0.1918	0.7083	0.5559
9	325	8	0.0679	0.0083	0.0072	0.0164	0.2500	0.6502	0.6808
10	325	10	0.0785	0.0091	0.0049	0.0082	0.2596	0.6397	0.778
11	350	0.5	0.0252	0.0018	0.0111	0.0618	0.0905	0.8096	0.2528
12	350	2	0.0589	0.0053	0.0155	0.0231	0.1841	0.7131	0.5598
13	350	4	0.0734	0.0065	0.0067	0.0132	0.2403	0.6599	0.7357
14	350	8	0.0827	0.0083	0.0047	0.0042	0.2696	0.6305	0.8284
15	385	0.5	0.0244	0.0038	0.0174	0.0543	0.0985	0.8016	0.2452
16	385	2	0.0746	0.0133	0.0058	0.0059	0.2569	0.6435	0.7488
17	385	4	0.0875	0.0092	0.0028	0.0003	0.2842	0.6160	0.8771
18	400	0.5	0.0397	0.0045	0.0196	0.0360	0.1480	0.7522	0.3980
19	400	2	0.0877	0.0062	0.0038	0.0022	0.2855	0.6146	0.8784
20	400	4	0.0954	0.0039	0.0005	0.0000	0.2948	0.6054	0.9552

At a given residence time, a higher reaction temperature resulted in lower concentrations of the reactants and higher concentrations of products. The concentration of intermediate diglycerides increased first and then decreased as the residence time increased. This trend occurred regardless of the reaction temperatures. For the dynamic concentration profile for monoglycerides (**Figure 2-5C**), at 300 ºC, 325 and 350 ºC, the concentration of monoglycerides

increased with residence time, which indicates longer residence times are needed to consume the monoglycerides and complete the reactions. At higher temperatures (385 and 400 ºC), the concentration of monoglycerides reached maximum values within 2 min and then decreased as the residence time increased.

The reaction conversion increases with temperature and residence time, as shown in **Table 2-4**. Temperature of 300, 325, and 350 ºC were not high enough to reach complete reaction conversion at the residence times employed. The reaction conversion at 4 min increased from 73.6% to 95.5% as temperature increased from 350 to 400 °C (**Table 2-4**). The reaction conversions were nearly complete (>97) at 400 ºC and residence time longer than four minutes, but the biodiesel yield decreased due to product decomposition.

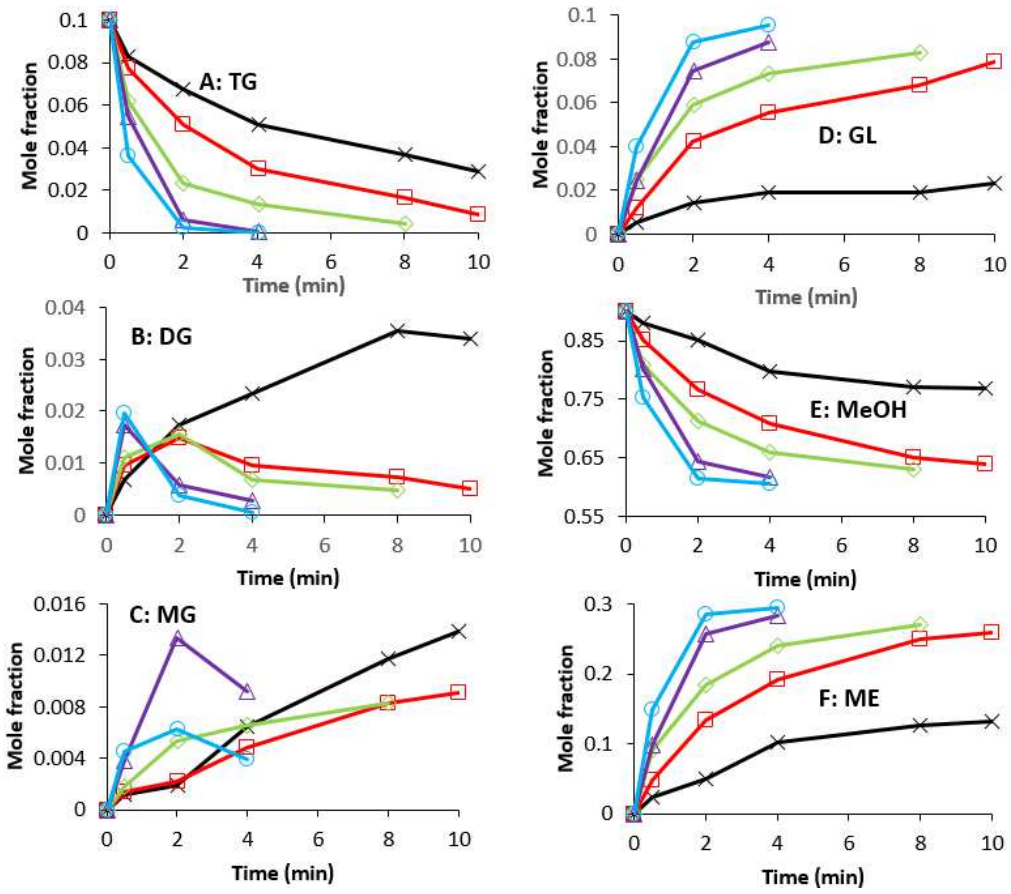

Figure 2-3. Concentration profiles for triglycerides (TG), diglycerides (DG), monoglycerides (MG), glycerol (GL), methanol (MeOH) and fatty acid methyl esters (ME) at 300 °C (×), 325 °C (□), 350 °C (◊), 385 °C (Δ) and 400 °C (○).

2.5.3 Phase behavior of non-catalytic transesterification

Most of the previous studies that claimed supercritical transesterification were performed at high MOMR of 40-42 and at around 300 °C. One of the reasons to choose this high molar ratio is to have the reaction performed in a homogeneous state, so the mass transfer issue can be minimized. In this work, we employed a visualization system to study the phase transitions at various conditions. As shown in **Figure 2-4**, the images on the first row describe phase transition during heating and pressurizing procedure at low pump flow rates (τ= ~10 min).

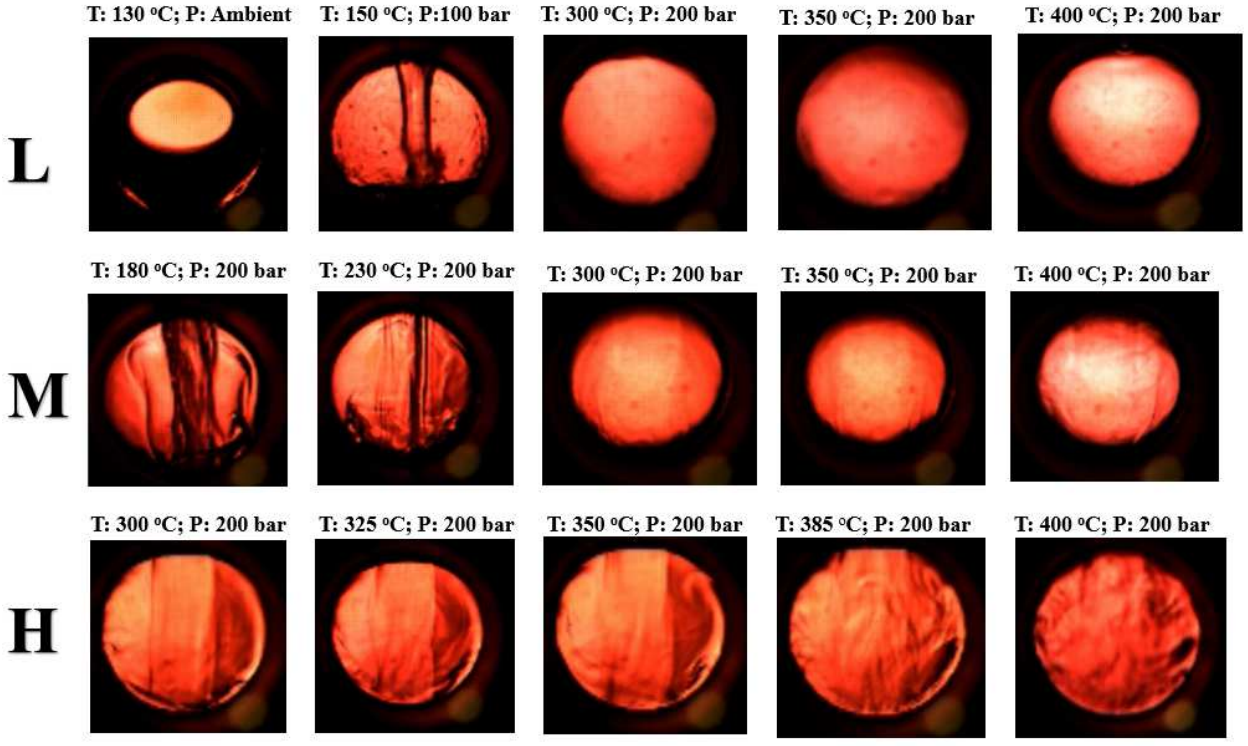

Figure 2-4. Mixtures of microalgae oil-methanol (MeOH/Oil molar ratio of 9) flowing through a view cell (V~1 mL) at various conditions (T= 130~400 °C, P= ambient~200 bar, flow rates from low to high). Images on the first row are at low (L) flow rates, images on the second row are at medium (M) flow rates, and images on the third row are at high (H) flow rates.

At 130 ºC and ambient pressure, two immiscible phases formed, the light phase was methanol flow, and the dark phase was oil flow. When temperature and pressure reached 150 ºC and 100 bar, a flow jet formed, the out layer of the flow jet was oil, and the oil and methanol were partially miscible under this flow condition. Homogeneous flows were observed at temperature higher than 300 ºC, pressure of 200 bar, and current low flow rate. The images on the second row show phase transition during heating from 180 to 400 ºC at pressure of 200 bar and medium flow rates (τ= ~2 min). Flow jets can be observed at 180 and 230 ºC, and multiple phases existed due to limited methanol-oil solubility. Similar with images at low flow rate, in the temperature range from 300 to 400 ºC, homogeneous flows were observed at 200 bar and medium flow rate. Images on the third row in Figure 2-6 show flow behavior at temperature from 300 to 400 ºC, pressure of 200 bar, and high flow rates (τ= ~0.5 min). The pump flow rates here were four times larger than medium flow rates, and nineteen times larger than low flow rates. Homogeneous flows jets were observed. The mixing at high flow rates appears to be much more dynamic than that at lower flow rates.

As stated in section 2.3.4, low, medium, and high flow rates represent residence time of 10, 2, and half min in the tubular reactor. In summarization from images in **Figure 2-6**, at temperature from 300 to 400 ºC, pressure of 200 bar, methanol-to-oil molar ratio of 9, and residence times from low to high, the methanol-oil mixture streams were in a homogeneous state. These results also indicate that the transesterification reactions in this study were controlled by kinetic rates, rather than mass transfer.

Figure 2-5 plots the critical points of methanol-triolein mixture as a function of the mole composition obtained by the LB mixing rules and the RK-Aspen EOS. The critical temperatures

and pressures estimated by the LB mixing rules are lower than those obtained by the RK-Aspen EOS. The difference in the critical temperature (**Figure 2-7A**) generally decreases, while the difference in the critical pressure (**Figure 2-7B**) increases and then slightly decreases, as the methanol-to-oil molar ratio increases. Experimental determination of true critical properties is required to address this issue. In the lack of experimental data, the estimates by the RK-Aspen EOS is preferred because previous studies showed that the EOS could well predict phase behavior of the methanol-oil mixtures [23, 34].

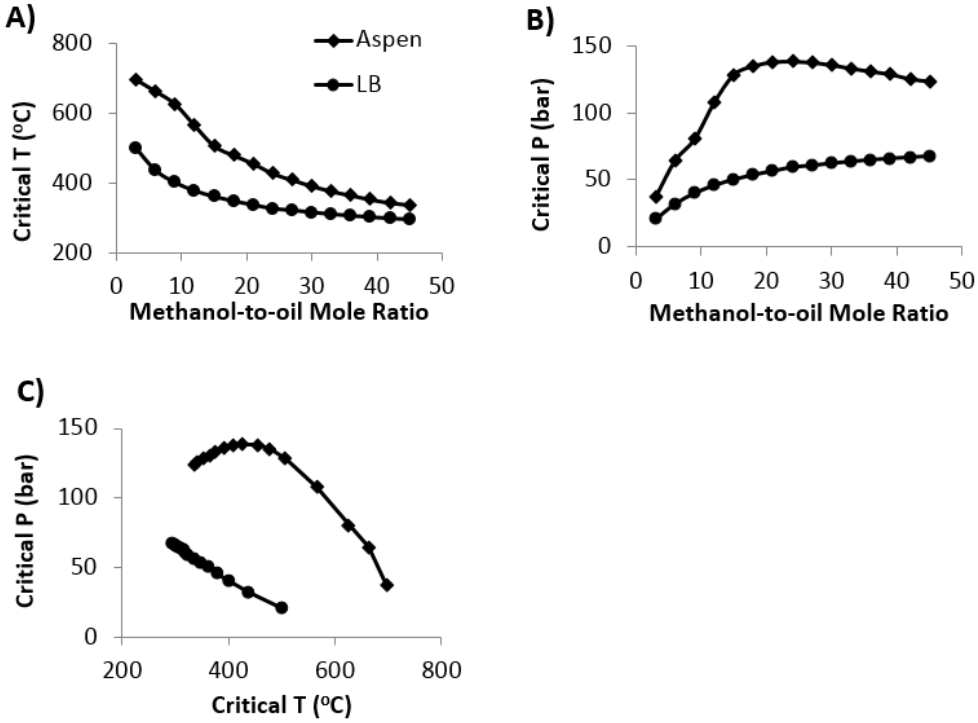

Figure 2-5. Comparison of critical temperature and pressure of methanol and oil (triolein) mixtures as a function of methanol-to-oil ratio predicted by the RK-Aspen EOS (♦) and the Lorentz-Berthelot (LB) (●) mixing rules.

Data in **Table 2-4** were used to estimate critical points of the reaction system and calculate P-T relation curves. **Figure 2-6** shows dynamic P-T diagrams of the reacting systems at

300, 325, 350, 385 and 400 ºC. It was found that as the reactions progressed, the critical temperatures decreased significantly. The critical pressures also decreased with reactions.

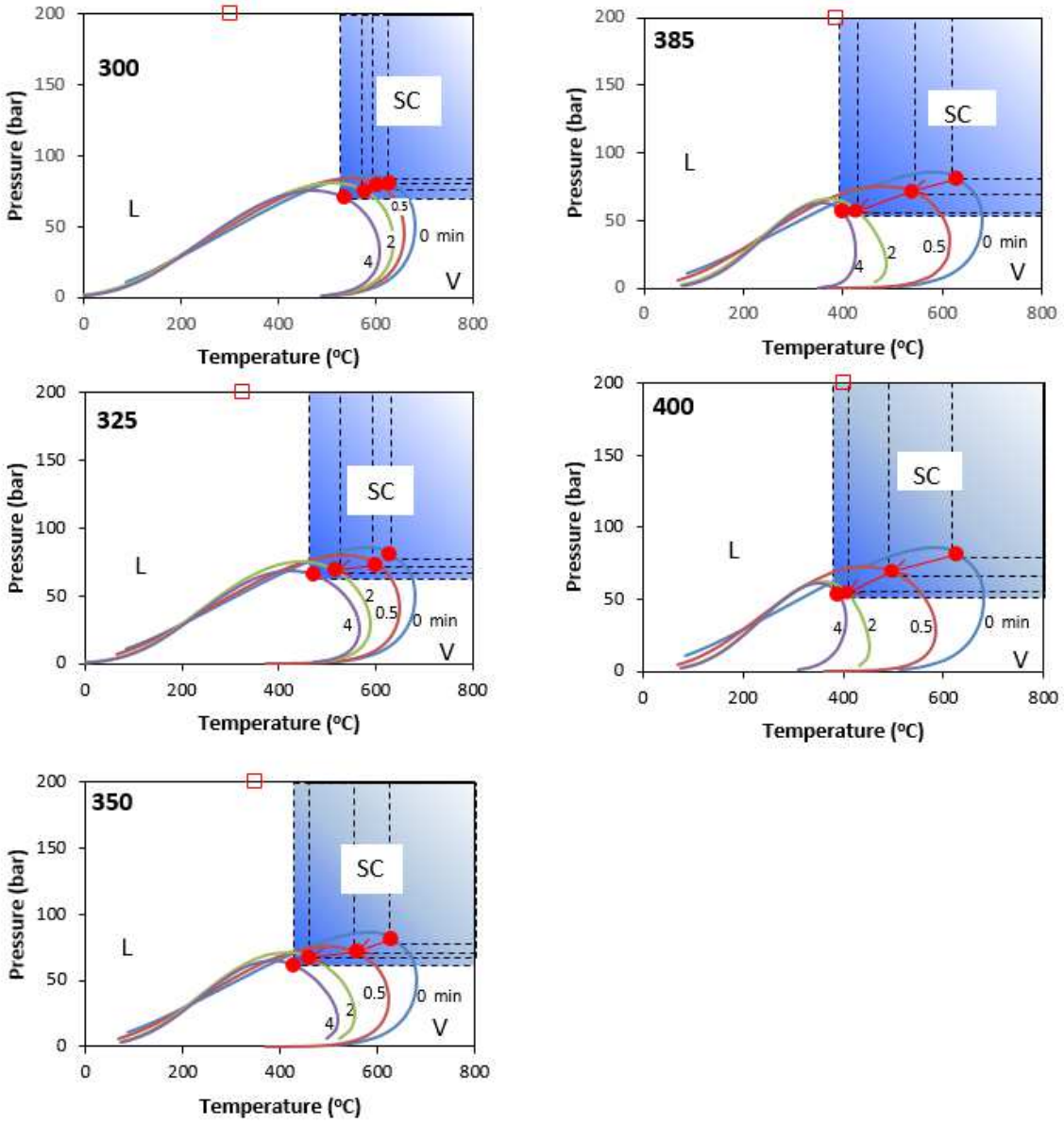

Figure 2-6. Dynamic P-T phase envelope (solid curves) of the transesterification reaction systems at 300, 325, 350, 385 and 400 ºC, 200 bar, and methanol-to-oil ratio of 9:1. (●) critical points; (□) reaction conditions. Dash lines indicate the moving boundary of the supercritical region. Red arrows indicate the change of the critical points of the reacting systems. L: liquid; V: vapor; SC: supercritical.

At 300 ^{o}C, the critical temperature of the final products at 4 min was higher than the reaction temperature, which indicates that the reacting mixtures was in liquid state and moved towards supercritical region during the course of the transesterification reaction. This similar phase behavior was observed at 325, 350 and 385 ^{o}C. When the reaction temperature was increased to 400 ^{o}C, the critical temperature of the mixtures reduced significantly from 628 ^{o}C to 408 ^{o}C within 2 min. This result indicates that at 400 ^{o}C, the reacting system was initially at liquid state and quickly approached supercritical state due to the fast reaction conversion. The reaction pressure for all runs were kept at 200 bar which was much higher than the critical pressures as shown in **Figure 2-6**. Therefore, considering the information obtained in **Figures 2-4** and **2-6**, it is expected that the transesterification reactions were carried out in a homogeneous liquid state or supercritical state under current reaction conditions (300, 325, 350, 385, and 400 ^{o}C; 200 bar; 9:1 molar ratio). Also this suggests that this high pressure is not necessary, a lower pressure should be employed in the future work in order to minimize the operation cost.

2.5.4 Thermal decomposition of biodiesel fuel

The thermal decomposition of methyl esters occurs at temperatures above 350 °C [24, 46]. **Figure 2-9** shows formation of smaller molecules at 400 ^{o}C, 6min due to decomposition of biodiesel.

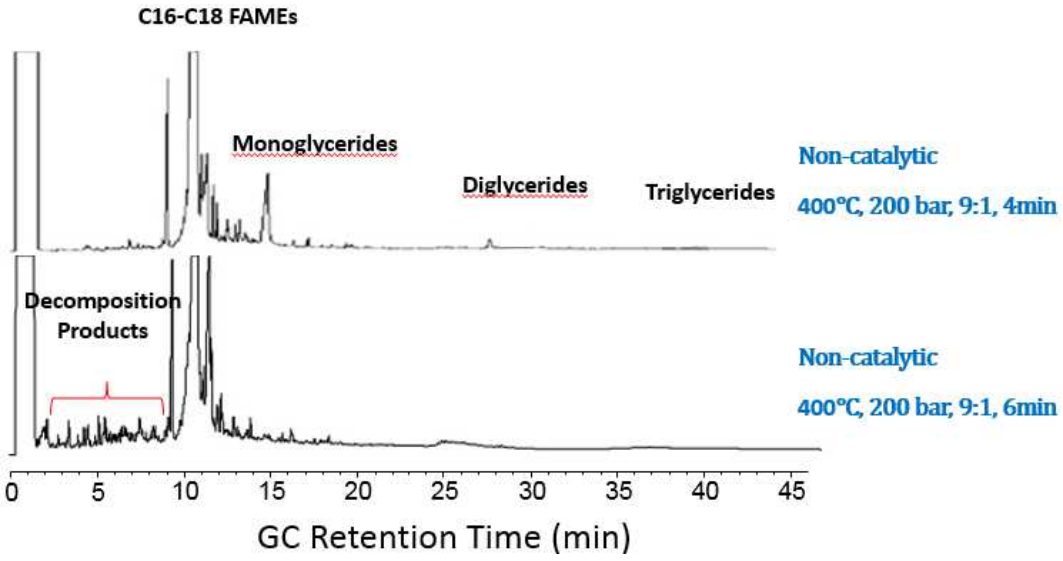

Figure 2-7. Comparison of gas chromatograms of biodiesel produced by non-catalytic methods at 400 ºC, 200 bar, MOMR of 9:1, residence time of 4 and 6 min.

The decomposition products mainly consisted of C_6 - C_{15}, saturated and unsaturated methyl esters and C_{10}-C_{17} hydrocarbons [3, 27], which could have a significant effect on biodiesel properties [47]. An investigation of the decomposition reactions and the effect on the fuel properties will be discussed in Chapter 3.

2.6 Conclusions

The non-catalytic transesterification of oil with methanol was conducted at 300-400 ºC, 150-300 bar, MOMR of 6-12, and residence time of 0.5-10 min. At 200 bar, 9 molar ratio and 4 min reaction time for temperature from 300-400 ºC, the reaction conversion increased from 19.3% to 95.5%. A high-pressure high-temperature visualization system was applied to study the phase transitions, and the results show that at temperature of 300 to 400 ºC, pressure of 200 bar, MOMR of 9, and residence time from half to ten minutes, the methanol-oil flow streams formed a homogeneous state. The dynamic phase behavior of the reacting systems was investigated by the advanced the RK-Aspen EOS. The simulation results indicate that the

transesterification reactions occurred in liquid phase for all conditions considered (300-400 ºC, 200 bar, 9:1 MOMR) except several cases at 400 ºC at high conversion where the system is near/ in supercritical state. Also critical points under which supercritical state could be reached were calculated. Thermal degradation of biodiesel fuel was found at extended residence times, and the effect of the degradation reactions on biodiesel qualities will be discussed in the next chapter.

Acknowledgements

We would like to thank Professor Michael Sponsler in the Department of Chemistry at Syracuse University for providing the vacuum oven. We are also grateful to Mario Montesdeoca in the Department of Civil and Environmental Engineering at Syracuse University for training on the GC-FID.

Nomenclature

Alphabet

a, a_i, a_j, a_{ci}, b, b_i, b_j	Coefficients used in the RK-Aspen EOS
k_1, k_{-1}, k_2, k_{-2}, k_3, k_{-3}, k_4, k_5, k_{-5}, k_6, k_{-6}, k_7, k_8, k_9, k_{10}, k_{-10}, k_{11}, k_{12}	Reaction rate constants
$k_{a,ij}$, $k^0_{a,ij}$, $k^1_{a,ij}$, $k_{b,ij}$, $k^0_{b,ij}$, $k^1_{b,ij}$	Binary parameters used in the RK-Aspen EOS
m	Characteristic constant used in the RK-Aspen EOS
M	Molar weight
$MOMR$	Methanol to oil molar ratio
P	Pressure
P_c	Critical pressure

P_{ci}	Critical pressure of component i
R	Universal gas constant
T	Temperature
T_B	Normal boiling point
T_c	Critical temperature
T_{ci}	Critical temperature of component i
T_R	Reduced temperature
T_{Ri}	Reduced temperature of component i
V	Volume
V_B	Liquid volume at normal boiling point
V_c	Liquid molar volume at critical point
V_l	liquid molar volume
X	Reaction conversion

Abbreviations

DG	Diglycerides
EOS	Equation of state
GL	Glycerol
MeOH	Methanol
ME	Methyl esters
MG	Monoglycerides
RK	Redlich- Kwong
TG	Triglycerides
uME	Un-methylesterified compounds

Greek Letters

α_i	Dimensional factor
ω	Acentric factor
η	Polar factor
τ	Residence time
$\triangle G_f$	Standard Gibbs energy
$\triangle H_f$	Standard enthalpy of formation
$\triangle H_v$	Standard enthalpy of vaporization

2.7 References

[1] M. Ash, Oil crops outlook: abundant U.S. soybean supplies propel 2013/14 exports. Technical Report OCS-13f. United States Department of Agriculture Economic Research Service, June 2013.

[2] V. Rathore, G. Madras, Synthesis of biodiesel from edible and non-edible oils in supercritical alcohols and enzymatic synthesis in supercritical carbon dioxide, Fuel. 86 (2007) 2650-2659.

[3] V.F. Marulanda, G. Anitescu, L.L. Tavlarides, Biodiesel fuels through a continuous flow process of chicken fat supercritical transesterification, Energy Fuels. 24 (2009) 253-260.

[4] Y. Chisti, Biodiesel from microalgae, Biotechnol. Adv. 25 (2007) 294-306.

[5] P.M. Schenk, S.R. Thomas-Hall, E. Stephens, U.C. Marx, J.H. Mussgnug, C. Posten, O. Kruse, B. Hankamer, Second generation biofuels: high-efficiency microalgae for biodiesel production, Bioenergy Research. 1 (2008) 20-43.

[6] L. Rodolfi, G. Chini Zittelli, N. Bassi, G. Padovani, N. Biondi, G. Bonini, M.R. Tredici, Microalgae for oil: Strain selection, induction of lipid synthesis and outdoor mass cultivation in a low‐cost photobioreactor, Biotechnol. Bioeng. 102 (2009) 100-112.

[7] M. Solecki, A. Dougherty, B. Epstein, Advanced Biofuel Market Report 2012, Environmental Entrepreneurs (E2). Available from: http://www.e2.org/ext/doc/E2AdvancedBiofuelMarketReport2012.pdf;jsessionid=05D790033BAF5608DE02E740480E3B76.

[8] M. Kizililsoley, S. Helvacioglu, Micro-algae growth technology systems, 2008. Available from: http://iimsam.org/images/growthtech.pdf.

[9] L. Meher, D. Vidya Sagar, S. Naik, Technical aspects of biodiesel production by transesterification—a review, Renewable and sustainable energy reviews. 10 (2006) 248-268.

[10] S. Saka, D. Kusdiana, Biodiesel fuel from rapeseed oil as prepared in supercritical methanol, Fuel. 80 (2001) 225-231.

[11] J. Van Kasteren, A. Nisworo, A process model to estimate the cost of industrial scale biodiesel production from waste cooking oil by supercritical transesterification, Resour. Conserv. Recycling. 50 (2007) 442-458.

[12] G. Anitescu, A. Deshpande, L.L. Tavlarides, Integrated technology for supercritical biodiesel production and power cogeneration, Energy Fuels. 22 (2008) 1391-1399.

[13] L. Canoira, M. Rodríguez-Gamero, E. Querol, R. Alcántara, M. Lapuerta, F. Oliva, Biodiesel from low-grade animal fat: production process assessment and biodiesel properties characterization, Ind Eng Chem Res. 47 (2008) 7997-8004.

[14] S. D'ippolito, J. Yori, M. Iturria, C. Pieck, C. Vera, Analysis of a two-step, noncatalytic, supercritical biodiesel production process with heat recovery, Energy Fuels. 21 (2007) 339-346.

[15] V.F. Marulanda, G. Anitescu, L.L. Tavlarides, Investigations on supercritical transesterification of chicken fat for biodiesel production from low-cost lipid feedstocks, The Journal of Supercritical Fluids. 54 (2010) 53-60.

[16] A. Deshpande, G. Anitescu, P. Rice, L. Tavlarides, Supercritical biodiesel production and power cogeneration: technical and economic feasibilities, Bioresour. Technol. 101 (2010) 1834-1843.

[17] S. Lee, D. Posarac, N. Ellis, Process simulation and economic analysis of biodiesel production processes using fresh and waste vegetable oil and supercritical methanol, Chem. Eng. Res. Design. 89 (2011) 2626-2642.

[18] V.F. Marulanda, Biodiesel production by supercritical methanol transesterification: process simulation and potential environmental impact assessment, J. Clean. Prod. 33 (2012) 109-116.

[19] Z. DU, Z. TANG, H. WANG, J. ZENG, Y. CHEN, E. MIN, Research and development of a sub-critical methanol alcoholysis process for producing biodiesel using waste oils and fats, Chinese Journal of Catalysis. 34 (2013) 101-115.

[20] B.J. Krohn, C.V. McNeff, B. Yan, D. Nowlan, Production of algae-based biodiesel using the continuous catalytic Mcgyan® process, Bioresour. Technol. 102 (2011) 94-100.

[21] R.B. Levine, T. Pinnarat, P.E. Savage, Biodiesel production from wet algal biomass through in situ lipid hydrolysis and supercritical transesterification, Energy Fuels. 24 (2010) 5235-5243.

[22] P.D. Patil, V.G. Gude, A. Mannarswamy, S. Deng, P. Cooke, S. Munson-McGee, I. Rhodes, P. Lammers, N. Nirmalakhandan, Optimization of direct conversion of wet algae to biodiesel under supercritical methanol conditions, Bioresour. Technol. 102 (2011) 118-122.

[23] S.B. Glišić, D.U. Skala, Phase transition at subcritical and supercritical conditions of triglycerides methanolysis, The Journal of Supercritical Fluids. 54 (2010) 71-80.

[24] R. Lin, Y. Zhu, L.L. Tavlarides, Mechanism and kinetics of thermal decomposition of biodiesel fuel, Fuel. 106 (2013) 593-604.

[25] ASTM D6584-10a. Standard Test Method for Determination of Total Monoglycerides, Total Diglycerides, Total Triglycerides, and Free and Total Glycerin in B-100 Biodiesel Methyl Esters by Gas Chromatography. West Conshohocken (PA): ASTM International; 2012.

[26] K. Bunyakiat, S. Makmee, R. Sawangkeaw, S. Ngamprasertsith, Continuous production of biodiesel via transesterification from vegetable oils in supercritical methanol, Energy Fuels. 20 (2006) 812-817.

[27] G. Anitescu, T.J. Bruno, Fluid properties needed in supercritical transesterification of triglyceride feedstocks to biodiesel fuels for efficient and clean combustion–a review, The Journal of Supercritical Fluids. 63 (2012) 133-149.

[28] T. Pinnarat, P.E. Savage, Assessment of noncatalytic biodiesel synthesis using supercritical reaction conditions, Ind Eng Chem Res. 47 (2008) 6801-6808.

[29] B. Poling, J. Prausnitz, J. O'Connell, The Properties of Gases and Liquids, 5th ed., McGraw-Hill, New York, 2001.

[30] Z. Tang, Z. Du, E. Min, L. Gao, T. Jiang, B. Han, Phase equilibria of methanol–triolein system at elevated temperature and pressure, Fluid Phase Equilib. 239 (2006) 8-11.

[31] T. Fang, Y. Shimoyama, T. Abeta, Y. Iwai, M. Sasaki, M. Goto, Phase equilibria for the mixtures of supercritical methanol C18 methyl esters and supercritical methanol α-tocopherol, The Journal of Supercritical Fluids. 47 (2008) 140-146.

[32] A.E. Andreatta, L.M. Casás, P. Hegel, S.B. Bottini, E.A. Brignole, Phase equilibria in ternary mixtures of methyl oleate, glycerol, and methanol, Ind Eng Chem Res. 47 (2008) 5157-5164.

[33] P. Hegel, A. Andreatta, S. Pereda, S. Bottini, E.A. Brignole, High pressure phase equilibria of supercritical alcohols with triglycerides, fatty esters and cosolvents, Fluid Phase Equilib. 266 (2008) 31-37.

[34] S. Glišić, O. Montoya, A. Orlović, D. Skala, Vapor-liquid equilibria of triglycerides-methanol mixtures and their influence on the biodiesel synthesis under supercritical conditions of methanol, Journal of the Serbian Chemical Society. 72 (2007) 13-27.

[35] P.M. Mathias, A versatile phase equilibrium equation of state, Industrial & Engineering Chemistry Process Design and Development. 22 (1983) 385-391.

[36] ASPEN PLUS, Version 7.3.2. Cambridge, MA 02141. Aspen Technology, Inc.: 2012.

[37] F. Ma, M.A. Hanna, Biodiesel production: a review, Bioresour. Technol. 70 (1999) 1-15.

[38] H. Noureddini, D. Zhu, Kinetics of transesterification of soybean oil, J. Am. Oil Chem. Soc. 74 (1997) 1457-1463.

[39] M. Diasakou, A. Louloudi, N. Papayannakos, Kinetics of the non-catalytic transesterification of soybean oil, Fuel. 77 (1998) 1297-1302.

[40] D. Kusdiana, S. Saka, Kinetics of transesterification in rapeseed oil to biodiesel fuel as treated in supercritical methanol, Fuel. 80 (2001) 693-698.

[41] H. He, S. Sun, T. Wang, S. Zhu, Transesterification kinetics of soybean oil for production of biodiesel in supercritical methanol, J. Am. Oil Chem. Soc. 84 (2007) 399-404.

[42] M.N. Varma, G. Madras, Synthesis of biodiesel from castor oil and linseed oil in supercritical fluids, Ind Eng Chem Res. 46 (2007) 1-6.

[43] S. D'ippolito, J. Yori, M. Iturria, C. Pieck, C. Vera, Analysis of a two-step, noncatalytic, supercritical biodiesel production process with heat recovery, Energy Fuels. 21 (2007) 339-346.

[44] D. Darnoko, M. Cheryan, Kinetics of palm oil transesterification in a batch reactor, J. Am. Oil Chem. Soc. 77 (2000) 1263-1267.

[45] M.R. Shahbazi, B. Khoshandam, M. Nasiri, M. Ghazvini, Biodiesel production via alkali-catalyzed transesterification of Malaysian RBD palm oil–Characterization, kinetics model, Journal of the Taiwan Institute of Chemical Engineers. 43 (2012) 504-510.

[46] H. Imahara, E. Minami, S. Hari, S. Saka, Thermal stability of biodiesel in supercritical methanol, Fuel. 87 (2008) 1-6.

Chapter 3: Thermal degradation of ethanol-based biodiesel: mechanism, kinetics, and effect on viscosity and cold flow property

This chapter has been published as: Liu, Jiuxu, Yujie Shen, Yue Nan, and Lawrence L. Tavlarides. "Thermal decomposition of ethanol-based biodiesel: Mechanism, kinetics, and effect on viscosity and cold flow property." Fuel 178 (2016): 23-36. It has been reproduced with permission from Elsevier.

3.1 Abstract

In Chapter 2, thermal degradation of biodiesel was observed under SC conditions, however it is not clear how the degradation reactions influence the fuel properties, which will be answered in this Chapter. Thermal degradation of the ethanol-based biodiesel (FAEEs) was evaluated in batch reactors by thermal exposure at 250-425 ºC for durations from 3 to 63 min, with and without the presence of ethanol. The results of GC analysis show that FAEEs were relatively stable at 250 and 275 ºC, and stability reduced as temperature and heating time increased. Major decomposition reactions consisted of isomerization, polymerization, and pyrolysis reactions to form isomers, dimers/polymers, smaller chain FAEEs, hydrocarbons, and carboxylic acids the latter of which are not generated in the decomposition of methanol-based biodiesel (FAMEs). This suggests that when applying the sub/supercritical ethanol technology to produce FAEEs, the reaction temperatures must be modest to avoid generating acids which increases the acid value of the final product. A three-lump model was used to predict concentrations of compounds in the FAEEs stressed at 250-325 ºC. The decomposition degree of the FAEEs biodiesel was simulated by using first order one-step reaction models (reversible and

irreversible), and results show that the reversible model performed better than the irreversible model except for data of 425 ^{o}C. The data show that FAEEs are less stable and decompose more completely than FAMEs. The presence of ethanol was shown to reduce the decomposition. Dynamic viscosity was measured, and differential scanning calorimetry (DSC) was used to determine the crystallization onset temperatures to represent cold flow properties. The values are significantly influenced by the polymerization and pyrolysis reactions.

3.2 Introduction

Currently commercial biodiesel is produced via transesterification reactions in which oils, fats and alcohols act as reactants. Methanol is the most widely used alcohol due to its low cost. It makes biodiesel not a completely renewable fuel as methanol is produced from petroleum resources and natural gas. Ethanol can be derived from renewable sources through fermentation processes, and it has been studied as an alternative alcohol in the biodiesel industry [1]. If part of the methanol is replaced by ethanol, there would be less dependency on the synthetic sources for methanol.

Ethanol is more miscible with oil compared to methanol, which decreases mass transfer resistance during the transesterification reaction [2]. Fatty acid ethyl esters (FAEEs, biodiesel produced with ethanol) have improved cold flow properties over fatty acid methyl esters (FAMEs, biodiesel produced with methanol) [3- 6]. Also FAEEs emit fewer greenhouse gases (GHG), such as carbon dioxide and nitrogen oxides (NOx), and are more biodegradable in water than FAMEs. However, since current biodiesel industry employs catalytic transesterification processes which require anhydrous alcohol, the high cost of anhydrous ethanol and the more

complex purification process to separate ethanol from biodiesel make the industry hesitate to use anhydrous ethanol for biodiesel production.

The advanced non-catalytic technology has great potential to lower the production cost by using hydrated ethanol and waste oils. Since the process has high tolerance for low quality of oils and alcohols, impurities such as water and free fatty acids are acceptable in this technology. This situation makes hydrated ethanol, a cheaper and renewable alcohol, become a possible choice for biodiesel production for the non-catalytic processes. Also this technology is becoming much more competitive and is under development. The first industrial demonstration unit of this process with a scale of 60 kton/year biodiesel was implemented in China in 2009, and another unit with a scale of 100 kton/year is currently being built by SINOPEC, China [7, 8]. Also Agron Bioenergy in California, U.S. is commercially producing biodiesel with a scale of 50 kton/year by using similar technology [9].

The kinetics and optimization of non-catalytic transesterification have been well studied [10-14], these results have demonstrated that the production yield of ethanol-based biodiesel is nearly as high as methanol-based biodiesel under optimal reaction conditions. However, the required high temperatures (250-400 ºC) in this technology will thermally decompose biodiesel which further affects yields of product and biodiesel properties.

Thermal decomposition of FAMEs under sub/supercritical alcohol conditions at 350-500 °C was first observed by the Saka group [10]. This phenomena was reported and analyzed at different temperature ranges by other research groups since then [15- 19]. Three types of reactions were found during FAMEs biodiesel decomposition: isomerization reactions which transfer cis-type unsaturated FAMEs to trans-type isomers [17, 18], polymerizations reactions (the Diels-Alder reaction) which combines FAMEs to form higher molecular weight compounds

such as dimers and polymers [17, 20], and pyrolysis reactions which break down FAMEs to form gas products, hydrocarbons, and lower molecular weight FAMEs [15, 17, 21]. In addition, dehydrogenation [21] and hydrogenation [18] may also be involved. These reactions occur at different temperature ranges which overlap. The reactions have been found to influence biodiesel quality significantly.

Imahara et al. [17] observed that isomerization reactions occurring in supercritical methanol slightly increased cloud point and pour point of FAMEs biodiesel. Dunn et al. [22] found that the polymerization reactions increased the viscosity of biodiesel, and the cold flow properties were changed a little for temperatures up to 150 ^{o}C. Windom and Bruno [23] found that the volatility of biodiesel was significantly affected by the pyrolysis of unsaturated FAMEs. During the previous studies from our group [24, 25] on thermal decomposition of FAMEs, the three types of decomposition reactions were observed (isomerization, polymerization, and pyrolysis reactions). A simplified one-step reversible model was proposed to describe the experimental data [24], and polymerization and pyrolysis reactions were determined to greatly influence the viscosity and cold flow property of FAMEs [25].

Also some researchers reported that during non-catalytic transesterification reactions, excess alcohol was found to decrease the esters thermal decomposition to some extent. Olivares-Carrillo et al. [26] found less thermal decomposition of FAMEs at higher methanol-to-oil molar ratio, which demonstrates methanol has some protective effect on the decomposition of esters. Bertoldi et al. [27] showed that the decomposition of FAEEs clearly decreased with a rise in ethanol-to-oil molar ratio. However the mechanism has not been studied, and it is not clear how the three decomposition reactions (isomerization, polymerization and pyrolysis) are influenced by the alcohol. In this study, we evaluate the influence ethanol has on ethyl esters decomposition.

Most studies of biodiesel decomposition at sub/supercritical alcohol conditions focused on FAMEs, whereas detailed studies on the decomposition of FAEEs has not been well addressed in the literature. The aim of the current work is to study thermal stability of FAEEs as a parallel study and provide a comparison to the thermal decomposition of FAMEs biodiesel from our previous work [24, 25]. In this work, prepared FAEEs were thermally treated at temperatures ranging from 250 to 425 ºC for 3 to 63 min in batch reactors. The mechanisms of decomposition were studied based on information from GC chromatograms, and a three-lump model and two simplified one-step models were applied to describe the reaction kinetics. The presence of ethanol was shown to influence the pyrolysis reactions. Viscosity and crystallization onset temperature of the FAEEs before and after thermal treatment were also measured to determine the effects of thermal decomposition on these properties.

3.3 Material and methods

3.3.1 Material

Ethanol-based biodiesel (FAEEs) was synthesized in the laboratory via base-catalyzed transesterification. Refined vegetable oil was purchased from a local market, and fresh diesel fuel was provided by a local gas station. Biodiesel-diesel blends were prepared by mixing fresh FAEEs with diesel at volume percentages of 20%, 40%, 60%, and 80% to make B20, B40, B60, and B80, respectively. 200 proof ethanol was purchased from Decon Laboratories, Inc. Potassium hydroxide pellets, glycerol, hexadecane, GC analytical standards for FAEEs (customized), palmitic acid, stearic acid, oleic acid, and linoleate acid were purchased from Sigma Aldrich. N-Heptane (HPLC grade) was supplied by Thermo Fisher Scientific. Gases (ultrahigh purity grade) used in gas chromatograph analysis were supplied by Airgas.

3.3.2 FAEEs preparation

Before executing the thermal stressing experiments, pure FAEEs were synthesized in our laboratory, since FAEEs biodiesel are not commercially available in North America. A two-step base-catalyzed (potassium hydroxide) method was employed. Firstly, oil was mixed with ethanol at a molar ratio of 1:12, and 1.5 wt% KOH based on total weight was added. The reaction was conducted in a glass flask with constant stirring at a temperature of 65 ^{o}C. After two-hour reaction time, the reaction was stopped by ceasing stirring and cooling down to room temperature. Glycerol at 25 wt% (based on total weight of the mixtures) was added into the homogeneous reaction mixtures in order to extract most unreacted ethanol, generated glycerol, and KOH. After 24 hours settling, the clear upper phase was removed to a new glass reactor, ethanol at a molar ratio of 6:1 based on initial amount of oil and 1.5 wt% KOH based on total weight was added to start the second step reaction. After two-hour reaction time at 65 ^{o}C, the reactor was cooled down to room temperature to stop the reaction, and glycerol at 25 wt% was added to separate most unreacted ethanol from the FAEEs. Then the crude FAEEs phase was removed and washed with DI water. Finally the FAEEs were heated in an oven at 40 ^{o}C for 24 hours to vaporize all water and ethanol.

Pure FAEEs produced from the above method were analyzed by gas chromatography. The results show that the FAEEs are composed of 19 wt% C16:0, 7.5 wt% C18:0, 72.5 wt% unsaturated C18 and 1 wt% other species.

3.3.3 Thermal stressing experiment

Thermal stressing of FAEEs biodiesel was performed in coiled stainless steel reactors (ID = 1.524 mm, L = 0.5 m, V = 0.913 ml). The batch reactors were immersed in a fluidized sand bath (Techne SBL-2) and heated at temperatures of 250-425 ^{o}C for 3 to 63 min. Duplicated runs

for each condition were performed to address the experimental uncertainty. The experimental setup and operation procedure were similar to our previous work [24].

To study the effect of ethanol on FAEEs decomposition, fresh FAEEs were mixed with ethanol at volume ratio of 1:1. The two compounds were soluble with each other at room conditions. Then the mixture was loaded into the reactors and heated by following the same procedures of the pure FAEEs thermal stressing experiments. The reaction temperature ranged from 300 to 425 ^{o}C.

3.3.4 Viscosity measurements

An m-VROC viscometer (RheoSense, Inc.) was used to measure dynamic viscosity of four types of fuels (fresh diesel fuel, fresh FAEEs biodiesel, FAEEs-diesel blends, and all thermally treated FAEEs biodiesel) at 40 ± 0.15 ^{o}C. The fuel samples were injected to the instrument at flow rates of 20-500 μl/min. More viscous samples required lower injection rates.

3.3.5 Crystallization onset temperature measurements

The crystallization onset temperature is used to represent the cold flow properties (e.g. cloud point, pour point, and cold filter plugging point), since previous studies proved that the crystallization onset temperature had a good linear correlation with those cold flow properties [28- 30]. The crystallization onset temperatures of four types of fuels (fresh diesel fuel, fresh FAEEs biodiesel, FAEEs-diesel blends, and all thermally stressed FAEEs biodiesel) were determined by Differential Scanning Calorimetry or DSC (Q200, TA Instruments). During the DSC analysis, samples of 5-7 mg were loaded in Tzero aluminum hermetic pans (TA Instruments) and sealed, the temperature of samples were first held at -40 °C for 3 min, then ramped to 50 °C at 3 °C/min and equilibrated for 3 min, and cooled down to -40 °C at

3 °C/min. Additional details to determine the onset temperatures based on DSC analysis can be found in our previous study [25].

3.3.6 Gas chromatogram analysis

3.3.6.1 GC-FID analysis

To quantitatively determine the decomposition degree of FAEEs, the FAEEs samples were analyzed by gas chromatography (HP 5890 Series II) equipped with a flame ionization detector (FID), an autosampler (HP 5890 Series II), and a Rtx-Biodiesel TG column (10 m × 0.32mmID × 0.10 μm, Restek) at splitless mode. FAEEs standard solutions were prepared as 500, 750, 1000, 1250, 1500 and 2000 ppm to construct calibration curves. FAEEs biodiesel samples of 1 μl were diluted into 1 ml heptane to make a concentration of 1000 ppm by volume. The temperature of both injector and detector were 300 °C. The oven temperature started at 60 °C and held for 2 min, then ramped at 6 °C/min to 150 °C and held for 10 min, and finally ramped at 10 °C/min to 350 °C and held for 1 min. The temperature program in this section was the same with our previous work [24].

3.3.6.2 GC-MSD analysis

Quantitative and qualitative analysis of selected FAEEs samples were performed by using gas chromatography (Agilent 7890A, 5975C) equipped with a mass selective detector (MSD) and an HP-INNOWAX capillary column (30 m × 0.25mmID × 0.25 μm, Agilent) at a split ratio of 20:1. The temperatures of injector and the GC-MSD interface were 250 °C. The oven temperature was held at 50 °C for 1 min, ramped at 3 °C/min to 250 °C and held at 250 °C for 10 min.

Quantitative analysis based on GC-MSD data were used to determine concentration of compounds in the FAEEs samples stressed at 250-325 ºC, and the information was further used

to develop the three-lump model. Calibration curves for FAEEs and carboxylic acids (C16, 18, 18:1, and 18:2) were constructed by using standards purchased from Sigma Aldrich. The calibration curve for trans-type C18:2 FAEE isomers was assumed to be the same with that of the original cis-type C18:2 FAEE.

Qualitative analysis based on GC-MSD data were used to identify compounds in all stressed samples, and some of the results are provided in **Figure 3-2**.

3.4 Results and discussion

Figure 3-1 shows selected photographs of thermally stressed FAEEs.

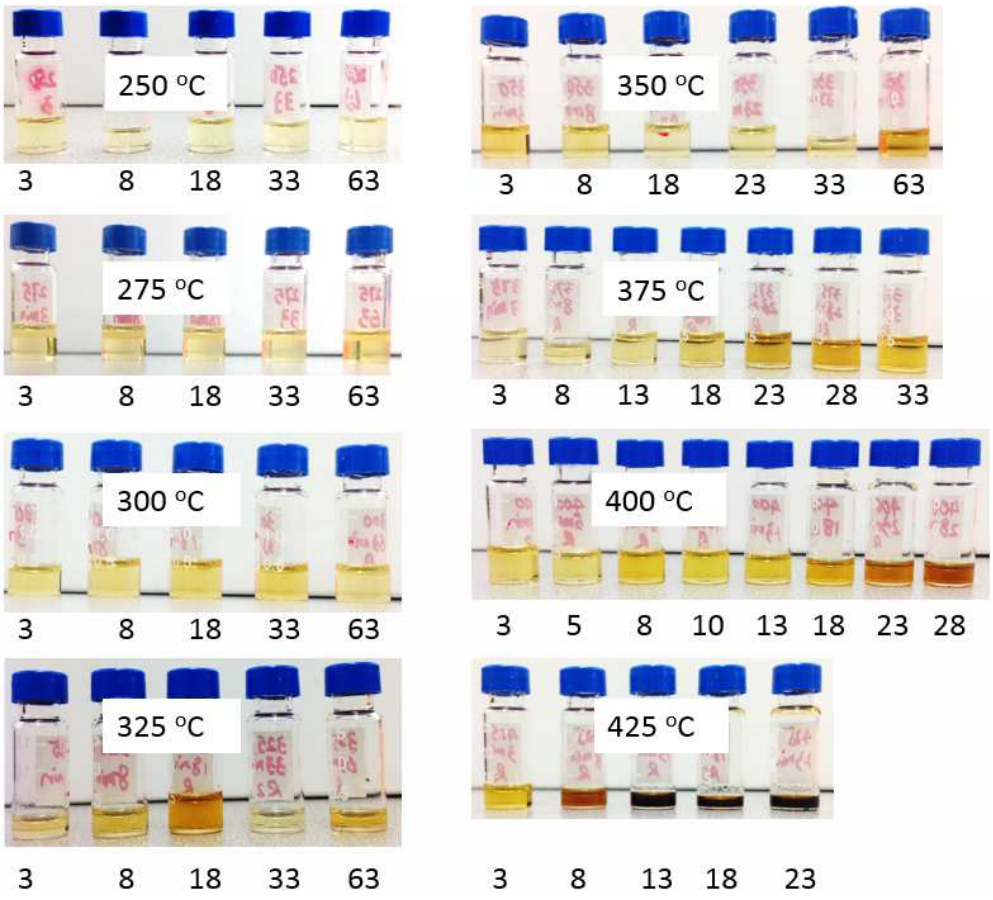

Figure 3-1. Selected photographs of thermally stressed FAEEs samples under temperatures from 250 to 425 °C and different stressing times. Numbers indicated under each vial represent thermal stressing time in minutes.

Color change of FAEEs stressed at 250, 275, and 300 ºC is negligible. At 350 ºC, yellowish fuel samples change to dark yellow at 63 min. With temperature increasing to 375, 400, and 425 ºC, the color change of FAEEs became more distinct, and at 425 ºC and 13 min and above the fuel samples were coked to dark brown mixtures. In general at 325-425 ºC, where color change was not negligible, a darker color was observed at higher temperature and longer heating time. This phenomena suggest that the thermal stability of FAEEs decrease with thermal stressing temperature and time, however FAEEs are relatively stable at 300 ºC and below. An exception is found at 325 ºC that the sample of 18 min is darker than 33 and 63 min, this might be caused by accidental contact of the coiled stainless steel reactor with the heating element.

3.4.1 Mechanism of FAEEs degradation

Figure 3-2 describes the changing presence of decomposition products during the thermal stressing process. It shows that FAEEs remained stable at 250 ºC before 33 min, and the unsaturated FAEEs were found to almost decompose completely at 375 ºC and 33 min or above, 400 ºC and 13 min or above, and 425 ºC and 3min or above.

At 250 ºC and 275 ºC at 33 min and longer, new peaks were observed and were identified via GC-MSD analysis as trans-type C18:2 isomers, and this indicates that the cis-trans isomerization reaction occurred at temperatures of 250 and 275 ºC. As stated in **Figure 3-2**, at 250-325 ºC, the trans-type isomers peaks were increasing with heating duration. At 350, 375 and 400 ºC, the peaks of the isomers first increased then decreased with heating time. Higher thermal stressing temperature required less time to reach the maximum. Similar behavior was found in our previous work on the FAMEs decomposition， and it was concluded that the isomerization of FAMEs was an equilibrium reaction [24]. Accordingly, these results imply that the isomerization of FAEEs is an equilibrium reaction as well. No isomer peaks were found at 425

ºC, and it suggests that the isomers were decomposed as soon as they were formed. Based on the above observations, the cis-trans isomerization reaction of the FAEEs are reversible and observed at temperature range of 250-400 ºC, and the isomers are not stable above 325 ºC.

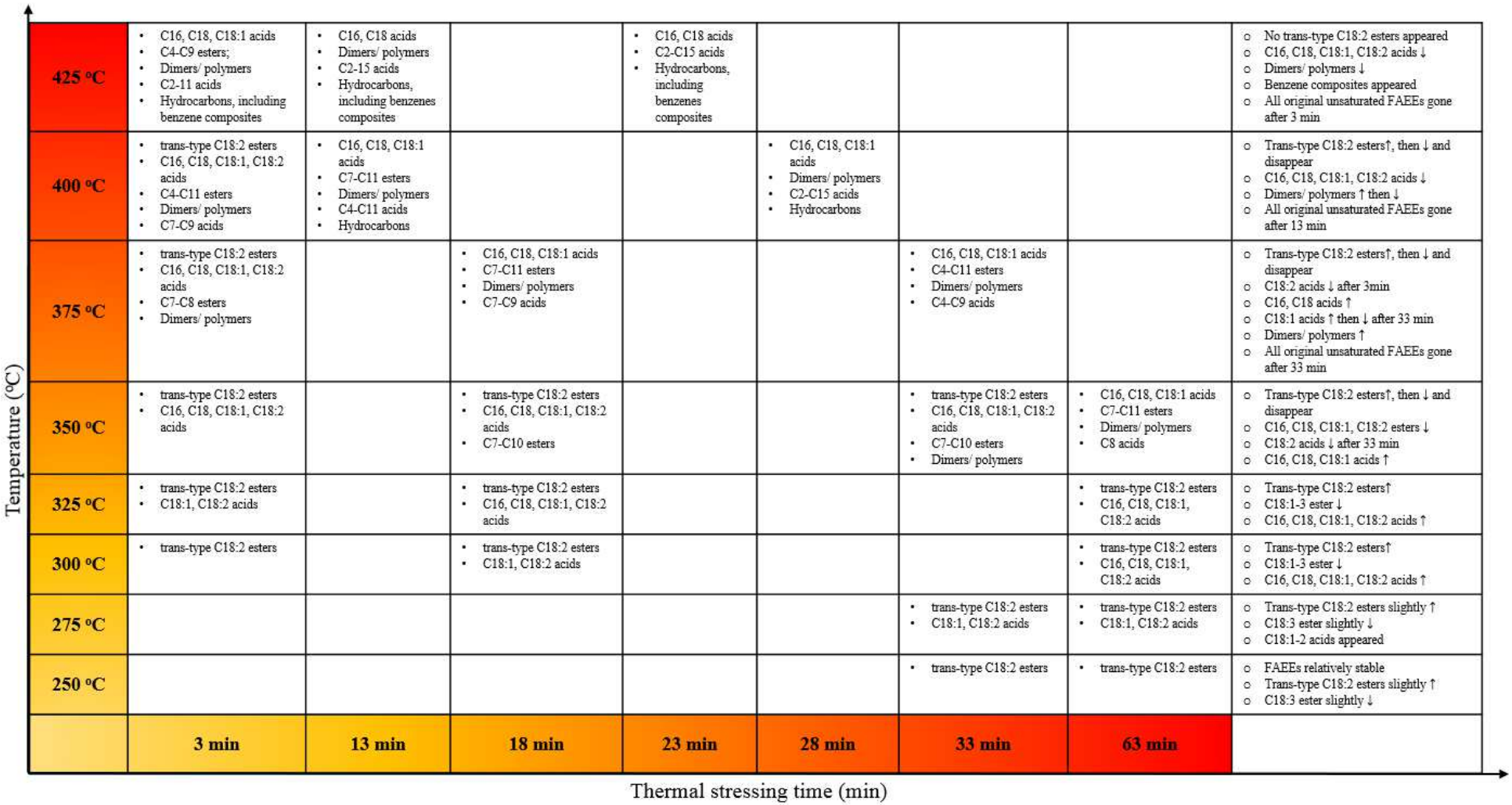

Figure 3-2. Summary of decomposition products that appeared in the stressed FAEEs.

In our previous study, FAMEs biodiesel was decomposed via pyrolysis reactions at high temperatures into gas products, hydrocarbons, and short chain FAMEs. The pyrolysis reactions for FAMEs biodiesel start at 350 ºC [24]. Unlike the pyrolysis products of FAMEs which consisted of small chain FAMEs, hydrocarbons, and gases [24], the liquid pyrolysis products of FAEEs include carboxylic acids. For example the FAEEs stressed at 275 ºC and 63 min included unsaturated C18 carboxylic acids, and those stressed at 300 ºC and 63 min included saturated (C16, C18) and unsaturated (C18:1, C18:2) carboxylic acids. The unsaturated C18 carboxylic acids appear to occur due to the degradation of corresponding unsaturated C18 ethyl esters, and the saturated C16 and C18 carboxylic acids appear to occur from degradation of corresponding saturated C16 and C18 ethyl esters, respectively. The process to thermally decompose the ethyl esters to carbonyl acids is suggested to follow the irreversible pyrolysis reaction route below [31-39].

$$RCOOC_2H_5 \xrightarrow{\Delta} RCOOH + CH_2CH_2 \qquad \text{Eq 3-1}$$

As summarized in Figure 3-2, at 300 and 325 ºC, all the long chain carboxylic acids (C16, C18, C18:1-2) accumulated with the heating process. At 350 ºC, linoleic acid (C18:2) started to decrease after 33 min, octanoic acid (C8) acid was observed, and all other long chain acids (C16, C18, and C18:1) kept increasing during the heating period. At 375 ºC, linoleic acid (C18:2) started to decrease after appearance at 3 min, oleic acid (C18:1) was observed to increase and then decrease after 33 min, and shorter chain carboxylic acids (C4-C9) were first detected at 18 min. For all conditions at 400 and 425 ºC, all the long chain carboxylic acids (C16, C18, C18:1-2) started to decrease after appearance at 3 min, and shorter chain carboxylic acids were observed at 3 min. In summary, linoleic acid, oleic acid, and the two long chain saturated carboxylic acids (C16, C18) were not stable after being formed at and above 350, 375,

and 400 ºC, respectively; and some of these compounds were decomposed into shorter chain carboxylic acids. The above observations also suggest that when applying non-catalytic technology to produce FAEEs biodiesel, it is necessary to keep the reaction conditions as modest as possible in order to avoid generating acids from decomposition which increases the acid value of the final product.

Other decomposition products such as shorter chain FAEEs (C7-C11) and hydrocarbons were detected when original FAEEs were stressed at 350 ºC and above. Obvious gas products were observed to appear at 350 ºC and 18 min and above, 375 ºC and 8 min and above, 400 ºC and 3min and above, and 425 ºC when the reactors were opened. Again as stated in **Figure 3-2**, at temperatures of 400 and 425 ºC, liquid pyrolysis products were mostly composed of carboxylic acids with different carbon number (C2-C18), short chain FAEEs and hydrocarbons. Benzene composites were found in the product at 425 ºC. These observations demonstrate that the pyrolysis reactions at 350 ºC and above result via multiple reaction routes.

In addition, a peak was observed at retention time of 70 min in the GC-MSD analysis of the decomposition products, which cannot be identified via the GC MSD data library. However based on further analysis, this peak appears to represent a complex mixture of dimers/polymers generated via the well-known Diels-Alder reaction. The identification procedure is presented and discussed later in detail in **Figure 3-12** and Section 3.4.5 along with the viscosity data.

According to all the experimental observations discussed above, the mechanism of FAEEs thermal decomposition is summarized and presented in **Figures 3-3** and **3-4**. **Figure 3-3** shows the reaction pathways of ethyl linoleate (C18:2 FAEE) decomposition, where ethyl linoleate was converted to trans-type isomers and linoleic acid (C18:2) starting from 250 and 275 ºC, respectively. At 350 ºC and above, ethyl linoleate was further decomposed to

dimers/polymers, shorter chain FAEEs, hydrocarbons, and gases. The generated isomers and linoleic acid were not thermally stable at 350 °C and above, and converted to dimers/polymers and some smaller molecular weight compounds.

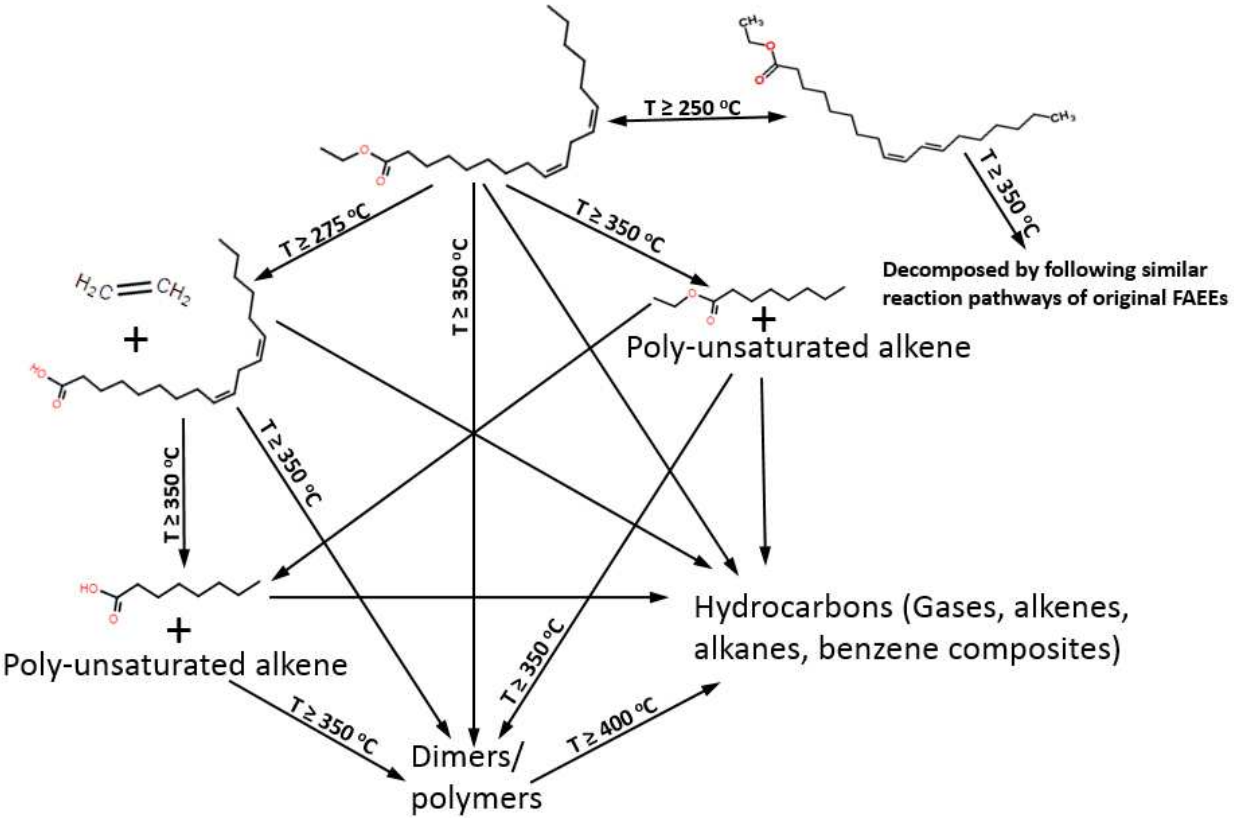

Figure 3-3. Mechanism of ethyl linoleate (C18:2 FAEE) thermal decomposition.

Figure 3-4 presented a proposed eight-lump model to describe the thermal decomposition of the FAEEs. It shows that isomerization reactions occur starting from 250 °C which convert the original cis-type ester to trans-type isomers. The original FAEEs were transformed via pyrolysis reactions into multiple products, such as long chain carboxylic acids starting from 275 °C, shorter chain FAEEs starting from 350 °C, and hydrocarbons starting from 350 °C. Also, the long chain carboxylic acids and shorter chain FAEEs were not stable at

temperatures above 350 °C and converted to shorter chain carboxylic acids, hydrocarbons, and gases. Polymerization reactions were observed at 350 °C and above. Any chemical compounds with multiple double bonds are expected to undergo these reactions, such as unsaturated FAEEs, unsaturated carboxylic acids, and unsaturated hydrocarbons. The generated dimers/polymers were not stable at temperatures above 375 °C, as discussed in Section 3.4.5.

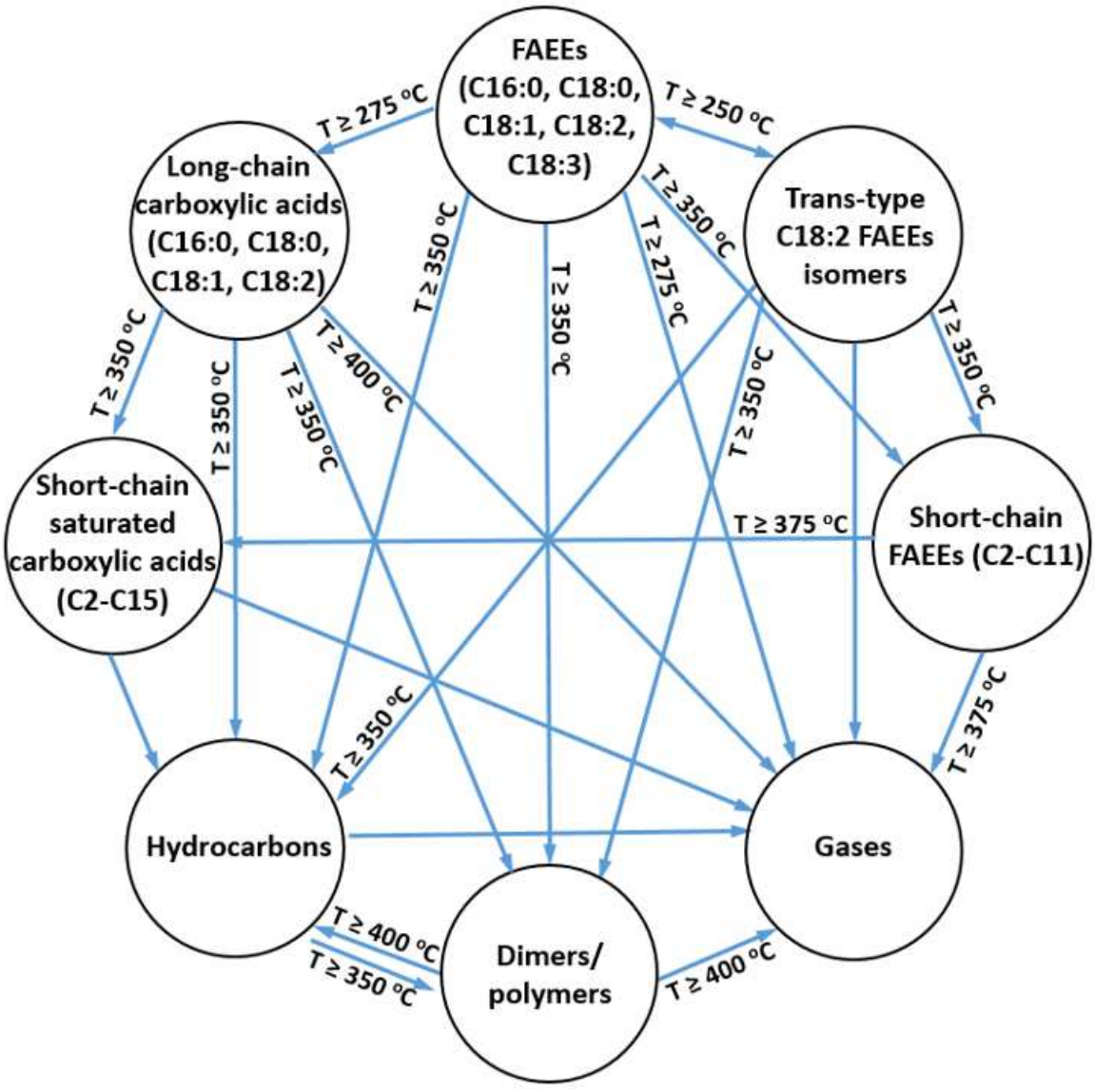

Figure 3-4. A proposed eight-lump model to describe the mechanism of FAEEs thermal decomposition reactions.

3.4.2 Kinetics of FAEEs degradation

Kinetic analysis in this work consists of two steps. First, experimental data of the FAEEs stressed at 250-325 ºC were simulated by employing a three-lump model. Second, two simplified one-step models were used to predict the degree of FAEEs decomposition at all temperatures.

As discussed above, the thermal decomposition reactions of FAEEs were less complex at temperatures of 325 ºC and below. At 250-325 ºC, some FAEEs were converted to corresponding trans-type isomers and carboxylic acids, the generated isomers and acids were not found to be further decomposed, and no polymerization products were detected. Based on this evidence, a three-lump model was proposed and presented in Eq3-2 in which original cis-type FAEEs were converted to trans-type isomers via a reversible reaction step and to carboxylic acids via an irreversible reaction step. Here k_{FC}, k_{FI}, and k_{IF} are reaction rate constants for reaction step of FAEEs→Carboxylic acids, FAEEs→Isomers, and Isomers→FAEEs, respectively. As the reactions are much more complex when temperatures are above 325 ºC, the three-lump model was not used to predict experimental data for the range of 350-425 ºC.

$$Carboxylic\ acids \xleftarrow{k_{FC}} FAEEs \underset{k_{IF}}{\overset{k_{FI}}{\rightleftharpoons}} Isomers\ of\ FAEEs \qquad \text{Eq 3-2}$$

The three-lump model was firstly employed to predict data of a single compound of the FAEEs, ethyl linoleate, and its corresponding reactions products including isomers and linoleic acid. Then this model was used to predict data of the entire FAEEs group and their reactions products including isomers and carboxylic acids. Simulation results are presented in **Figure 3-5** and **3-6**. Both figures show that the amount of ethyl esters biodiesel decreased along with thermal stressing, while the amount of isomer and carboxylic acids were accumulating during the process. The data fitting was performed using the Micromath Scientist 3.0 software from

Micromath Research. The model prediction was determined to agree well with the experimental data, and the reaction rate constants were shown in **Table 3-1**.

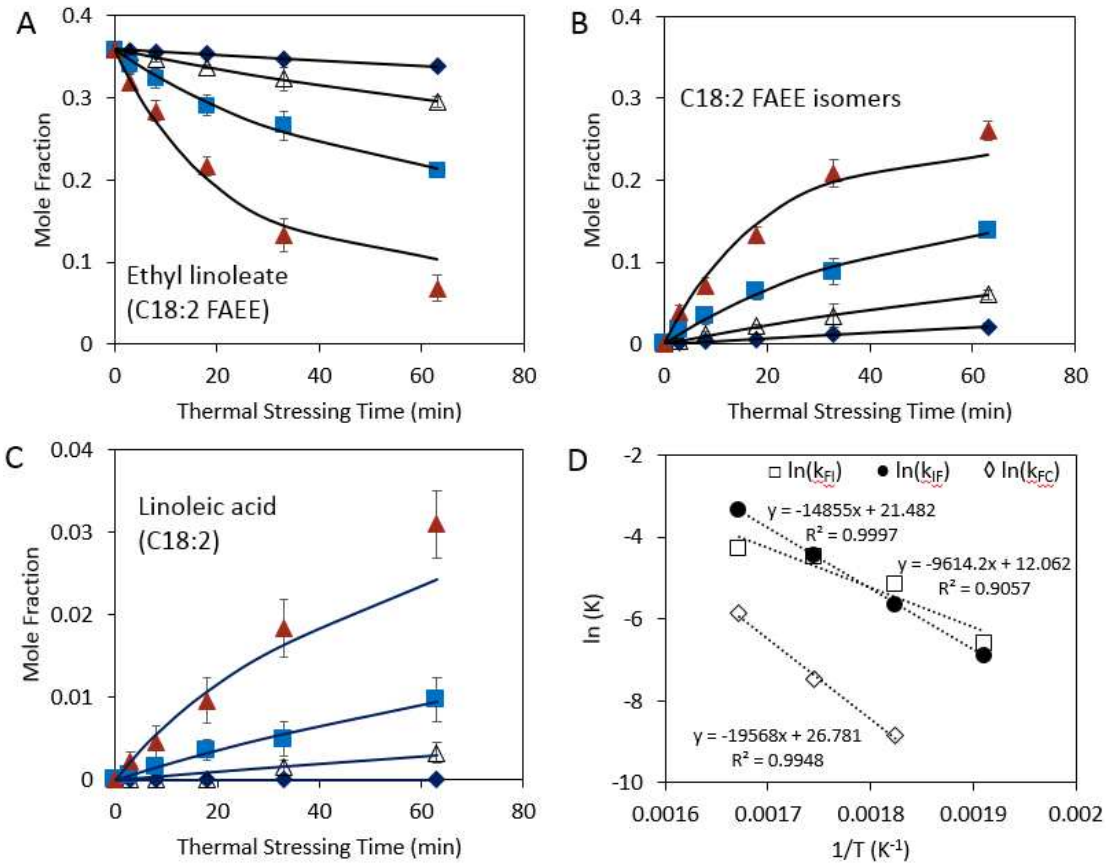

Figure 3-5. Simulation results of the proposed three-lump model for the reactions of ethyl linoleate at 250 °C (♦), 275 °C (Δ), 300 °C (■), and 325 °C (▲). (A) Data of the original ethyl linoleate, (B) data of the isomers generated from isomerization reactions, (C) data of linoleic acid generated from pyrolysis reactions, and (D) Arrhenius equation of reaction rate constants. Solid lines are predictions of the model.

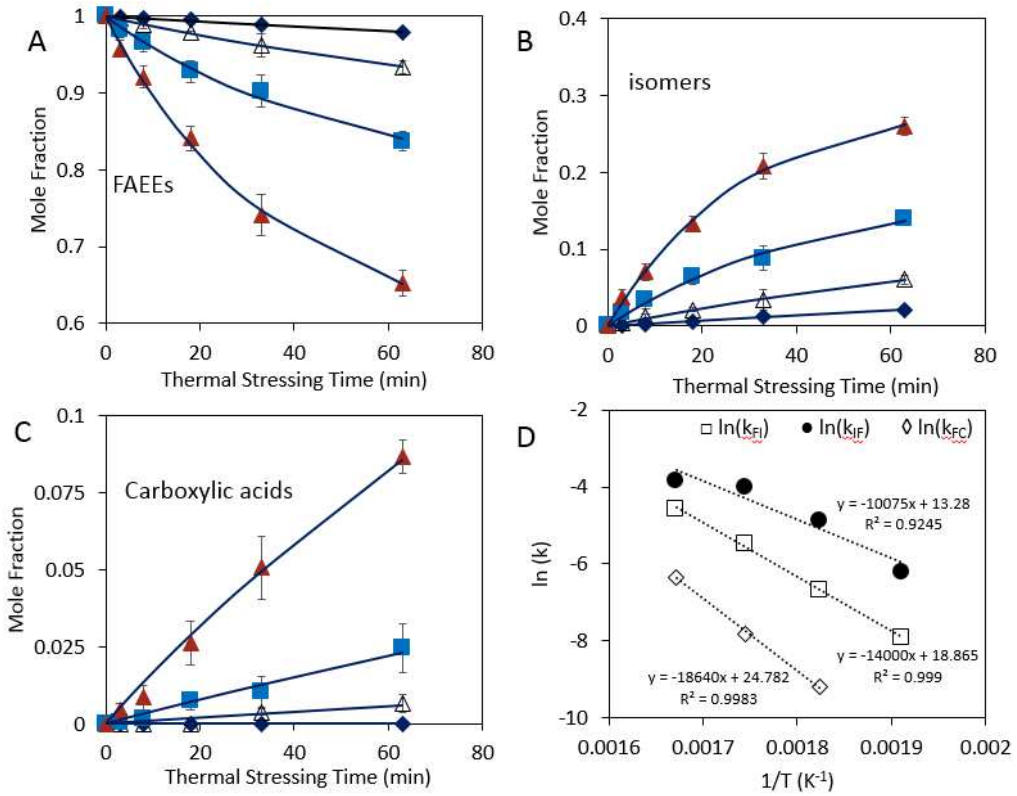

Figure 3-6. Simulation results of the proposed three-lump model for the reactions of the FAEEs at 250 ºC (♦), 275 ºC (Δ), 300 ºC (■), and 325 ºC (▲). (A) Data of the original FAEEs, (B) data of the isomers generated from isomerization reactions, (C) data of carboxylic acids generated from pyrolysis reactions, and (D) Arrhenius equation of reaction rate constants. Solid lines are predictions of the model.

Table 3-1. Reaction rate constants of the three-lump model for ethyl linoleate and the FAEEs thermal decomposition reactions.

T (°C)	k_{FI} (min^{-1})	k_{IF} (min^{-1})	k_{FC} (min^{-1})
Ethyl linoleate			
250	0.0010 ± 0.0003	0.0014 ± 0.0004	NA
275	0.0035 ± 0.0001	0.0057 ± 0.001	0.0001 ± 0.00003
300	0.0116 ± 0.0006	0.0114 ± 0.002	0.0006 ± 0.0002
325	0.0358 ± 0.0033	0.0137 ± 0.0036	0.0028 ± 0.0009
FAEEs			
250	0.0004 ± 0.00002	0.0020 ± 0.0016	NA
275	0.0013 ± 0.00005	0.0076 ± 0.0014	0.0001 ± 0.00002
300	0.0041 ± 0.0002	0.0182 ± 0.0024	0.0004 ± 0.00005
325	0.0102 ± 0.0004	0.0214 ± 0.0018	0.0018 ± 0.00009

The standard reaction enthalpy and entropy change for the reversible isomerization reaction were estimated by plotting the Van't Hoff equation with data in **Table 3-1**. Accordingly, the standard reaction enthalpy change for the isomerization of ethyl linoleate is estimated to be 78.6 kJ/mol, and the standard reaction enthalpy change for the isomerization of FAEEs mixture is calculated to be 55.5 kJ/mol. Similarly, the standard reaction entropy change for the isomerization of ethyl linoleate is determined to be 138.8 J/mol/K, and the standard reaction entropy change for the isomerization of FAEEs mixture is estimated as 85.8 J/mol/K. These analyses indicate that the isomerization reaction is endothermic and entropically favorable.

Data from GC-FID analysis were used to quantitatively study the degree of FAEEs thermal decomposition. The degree of decomposition is defined as:

$$Decomposition\ ratio = \frac{\sum C_{i,fresh} - \sum C_{i,TS}}{\sum C_{i,fresh}} \quad \text{Eq 3-3}$$

where the subscript *i* represents C16:0, C18:0, C18:1-3, respectively. Data points in **Figure 3-7** illustrate FAEEs decomposition increased with reaction time at 250-425 ^{o}C. FAEEs were relatively stable at 250 and 275 ^{o}C, since only less than 5% of FAEEs were decomposed. At 300 ^{o}C and 63 min, the decomposition increased gradually to 14.8%. These experimental data in **Figure 3-7** also show that the decomposition became more significant when temperature increased to 325 ^{o}C and above. FAEEs were almost completely decomposed in ten minutes at 400 and 425 ^{o}C.

In our previous study of FAMEs thermal decomposition [24], two simple one-step reaction models were used and compared to simulate the decomposition reactions, and the results showed that the reversible model worked better than the irreversible model on predicting FAMEs thermal decomposition. Equation 3-4 represents the reversible first order reaction model, while Equation 3-5 represents the irreversible first order reaction model.

$$A \underset{k_2}{\overset{k_1}{\rightleftharpoons}} P \qquad \text{Eq 3-4}$$

$$A \xrightarrow{k_3} P \qquad \text{Eq 3-5}$$

Here P represents all reaction products, k_1 and k_2 are reaction rate constants for the forward and reverse reaction in Equation 3-4, and k_3 is the rate constant in Equation 3-5.

In the current study, the same two models were applied to simulate degree of the FAEEs thermal decomposition reactions as a function of thermal stressing time. Rate constants and activation energies were determined and compared with previous FAMEs decomposition. The simulation results of each model is presented as solid lines in **Figure 3-7**.

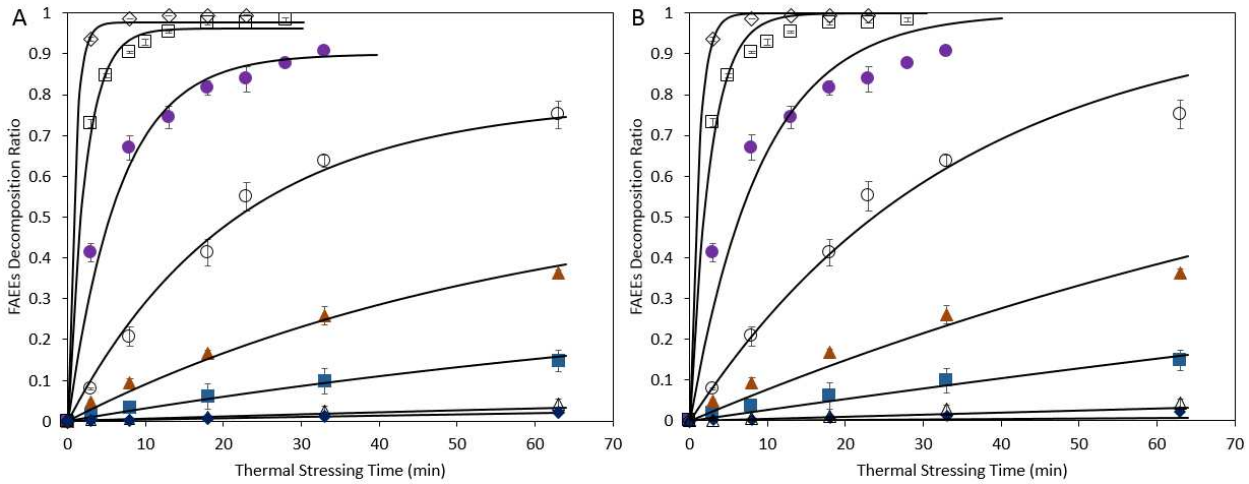

Figure 3-7. Simulation of FAEEs thermal decomposition degree using the one-step first order (A) reversible and (B) irreversible reaction models. Decomposition temperatures were 250 ºC (♦), 275 ºC (Δ), 300 ºC (■), 325 ºC (▲), 350 ºC (○), 375 ºC (●), 400 ºC (□), and 425 ºC (◊). Solid lines are model predictions.

It shows that the reversible model (**Figure 3-7A**) fits the data better than the irreversible model (**Figure 3-7B**) except for the highest temperature 425 ºC. This is because that at 425 ºC the dominant reactions were pyrolysis reactions, and the isomerization reactions, which are reversible, were not observed at 425 ºC since the isomer would be decomposed rapidly at this high temperature, as stated in **Figure 3-2** and discussed in the previous section.

Estimated reaction rate constants for both models (k_1, k_2, and k_3) and the reaction equilibrium constant ($K=k_1/k_2$) for the reversible model are presented in **Table 3-2**.

Table 3-2. Reaction rate constants and equilibrium constants of the one-step models for FAEEs thermal decomposition reactions.

T (°C)	k_1 (min^{-1})	k_2 (min^{-1})	k_3 (min^{-1})	K
250	0.0004 ± 0.00002	0.0020 ± 0.0016	0.0003 ± 0.000006	0.1593
275	0.0008 ± 0.00003	0.0034 ± 0.0022	0.0007 ± 0.00001	0.2294
300	0.0032 ± 0.0003	0.0053 ± 0.0031	0.0028 ± 0.0001	0.6084
325	0.0098 ± 0.0007	0.0070 ± 0.0026	0.0081 ± 0.0004	1.3926
350	0.0365 ± 0.0021	0.0100 ± 0.0023	0.0293 ± 0.0013	3.6374
375	0.1357 ± 0.0058	0.0150 ± 0.0025	0.1088 ± 0.0073	9.0267
400	0.4294 ± 0.0156	0.0173 ± 0.0032	0.3877 ± 0.0194	24.8766
425	1.1268 ± 0.1458	0.0254 ± 0.0086	0.9155 ± 0.0258	44.3134

The Arrhenius equation was applied to show the linear relationship between natural logarithms of reaction rate constants and inverses of reaction temperature. The reaction activation energies E_a were further determined according to the slope of the linear function. E_a for the forward and reverse reactions in the reversible model are 144.6 and 41.5 kJ/mol, respectively, and E_a for the forward reaction in the irreversible model is 143.0 kJ/mol. For the reversible reaction model, the van't Hoff equation was used to describe the relationship between the reaction equilibrium constant K and the temperatures to estimate the standard reaction enthalpy. By doing so, the reversible reaction enthalpy ΔH_0 was determined as 103.5 kJ/mol which indicates the FAEEs thermal decomposition is an overall endothermic reaction.

A comparison of rate constants and equilibrium constants between FAEEs and FAMEs thermal decomposition determined previously [24] is shown in **Figure 3-8**. The rate constants of the forward step (k_1 and k_3) for FAEEs are slightly higher than those of FAMEs at temperatures above 350 °C, and very close to those of FAMEs at temperatures below 350 °C. It also clearly shows that the rate constants of the reverse step (k_2) for FAEEs are much smaller than the ones

for FAMEs. The reaction equilibrium constants for FAEEs are higher than those of FAMEs at all temperatures, and it indicates that FAEEs decomposed more completely than FAMEs at high temperatures.

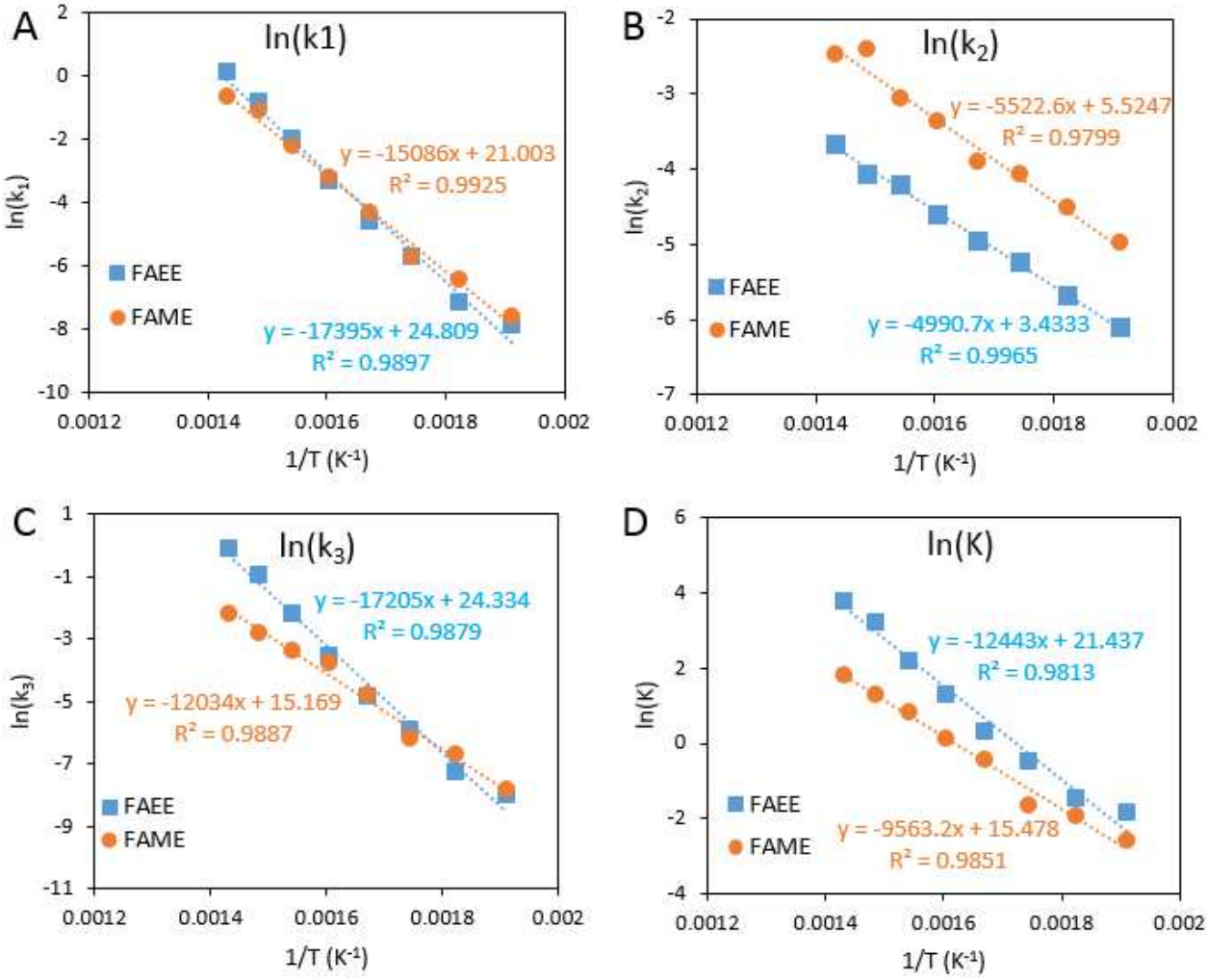

Figure 3-8. Comparison of temperature dependency of the decomposition reaction rate constants and equilibrium constants between FAMEs (●) [24] and FAEEs (■). The data from our previous work [24] are reused here with Elsevier's permission.

3.4.3 Effect of ethanol on FAEEs degradation

Thermal decomposition of FAEEs in a FAEEs-ethanol mixture was studied in this section to compare with that of pure FAEEs. The temperature range was selected as 300-425 ^{o}C. All heated samples were analyzed by using GC-FID, and selected samples were analyzed by using

GC-MSD. Thermal decomposition data are plotted in **Figure 3-9**, and it shows that the FAEEs-ethanol mixtures were less decomposed than pure FAEEs under same stressing conditions. The potential mechanism of this observation could be that FAEEs were first decomposed to C16-18 carboxylic acids, then part of the acids reacted with ethanol via esterification to form the original compound FAEEs.

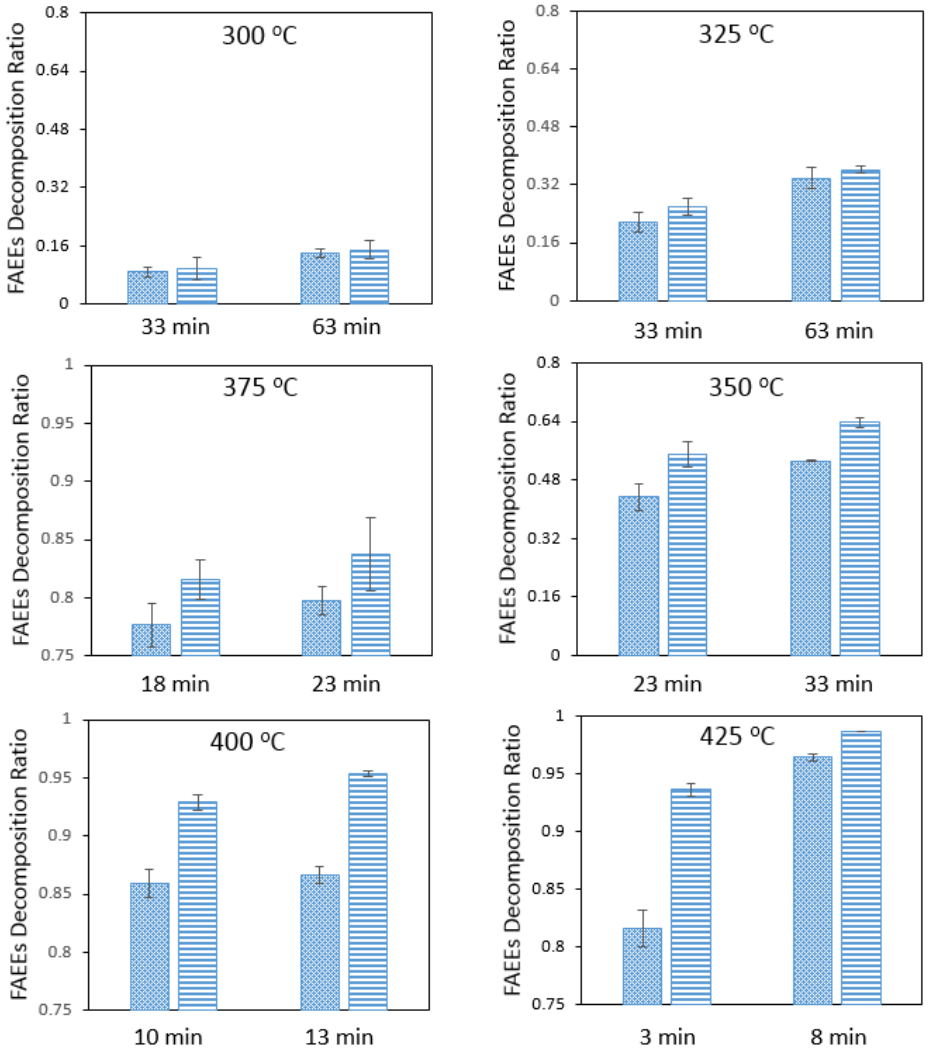

Figure 3-9. Thermal decomposition of FAEEs without ethanol (▤) and with presence of ethanol at a FAEEs-to-ethanol volume ratio of 1:1 (▩).

Figure 3-10(A, B) clearly shows esterification reactions happened during stressing FAEEs-ethanol mixtures. After being heated at 400 ºC and 13 min, the pure FAEEs sample

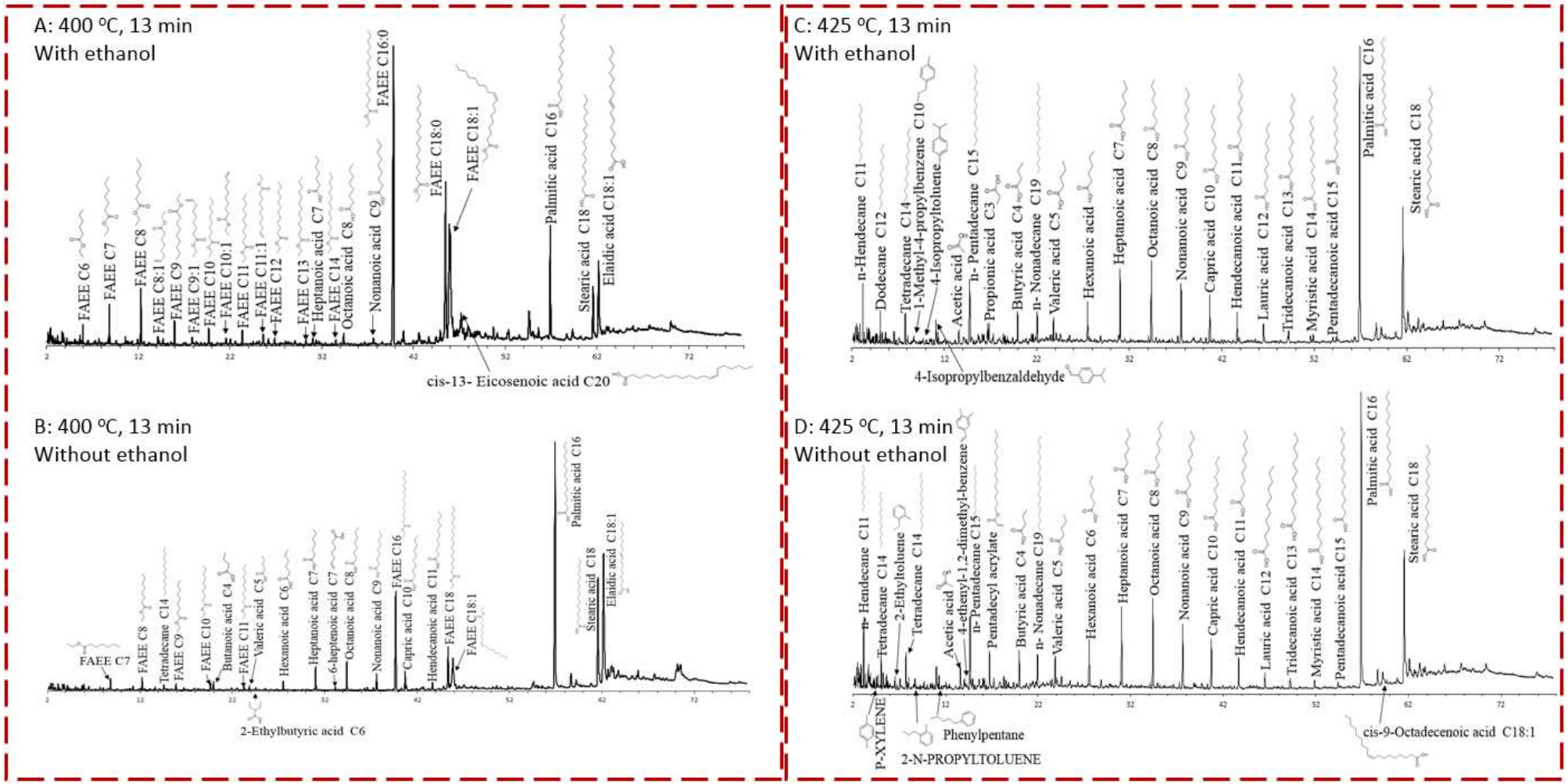

Figure 3-10. GC MS chromatogram for FAEEs thermally stressed at 400 and 425 ºC and 13 min (A, C) with presence of ethanol and (B, D) without ethanol.

(**Figure 3-10B**) generated large amounts of short chain carboxylic acids (C4-C11), however the short chain compounds in FAEEs-ethanol sample (**Figure 3-10A**) are mainly ethyl esters. This result demonstrates esterification reactions of carboxylic acids with ethanol did occur at this experimental condition. **Figure 3-10(C, D)** shows that when the temperature increased to 425 ^{o}C at 13 min stressing duration, no short chain ethyl esters were found in either FAEEs-ethanol mixture or pure FAEEs samples, since those esters were not stable at this high temperature and further decomposed to corresponding carboxylic acids. In conclusion, ethanol was found to reduce the pyrolysis reactions by esterification reactions at temperatures of 400 ^{o}C and below.

3.4.4 Viscosity of diesel, fresh FAEEs, and fresh FAEEs-diesel blends

Dynamic viscosities of fresh diesel fuel, fresh FAEEs biodiesel prepared in the laboratory, and fresh FAEEs-diesel blends were measured at 40 ^{o}C, and the results are provided in **Table 3-3**, and plotted in **Figure 3-11** along with the ASTM standards limit for biodiesel [40] and for diesel fuel [41]. Since the ASTM standards only specify the limits of kinematic viscosity instead of dynamic viscosity, the standard limits were converted to the dynamic viscosities by considering the density of the fuels. The viscosity of FAEEs biodiesel was 4.78 mPa·s which satisfies the ASTM standard (1.76-5.55 mPa·s or 1.9-6.0 mm^2/s). As expected, the viscosities of FAEEs-diesel blends increase with increasing concentration of FAEEs. The values for B20-60 FAEEs-diesel blends (2.55-3.54 mPa·s) satisfy the ASTM standard for diesel fuel (1.65-3.56 mPa·s or 1.9-4.1 mm^2/s).

Table 3-3. Experimental data for thermally stressed FAEEs, fresh FAEEs, DF, and FAEEs-DF blends.

T (ºC)	t (min)	Decomposition ratio	Viscosity @ 40 ºC (mPa·s)	Crystallization onset T (ºC)
250	3	0.001	3.96	-4.45
250	8	0.003	4.06	-4.12
250	18	0.005	4.15	-3.59
250	33	0.012	4.19	-3.45
250	63	0.021	4.18	-3.78
275	3	0.001	4.10	-3.28
275	8	0.006	4.15	-3.55
275	18	0.011	4.17	-3.83
275	33	0.028	4.27	-3.44
275	63	0.043	4.33	-3.32
300	3	0.018	4.12	-3.64
300	8	0.035	4.26	-3.28
300	18	0.061	4.50	-3.64
300	33	0.098	4.62	-3.66
300	63	0.148	5.77	-4.22
325	3	0.048	4.36	-3.69
325	8	0.093	4.28	-3.61
325	18	0.168	5.28	-3.37
325	33	0.259	6.19	-3.36
325	63	0.362	8.38	-2.39
350	3	0.079	4.86	-3.49
350	8	0.207	6.31	-3.08
350	18	0.412	9.85	-0.77
350	23	0.551	14.60	3.3
350	33	0.637	17.90	6.46
350	63	0.751	28.29	9.48
375	3	0.413	9.43	-1.62
375	8	0.670	16.41	4.39
375	13	0.744	18.55	9.74
375	18	0.816	28.91	11.21
375	23	0.838	29.36	10.71
375	28	0.877	35.19	11.34
375	33	0.907	56.68	12.86
400	3	0.730	18.63	9.66
400	5	0.845	30.27	8.94
400	8	0.904	40.49	10.43
400	10	0.929	46.95	10.88
400	13	0.953	45.56	11.42
400	18	0.975	46.20	10.76
400	23	0.977	41.87	9.49
400	28	0.983	36.97	8.7
425	3	0.936	28.28	9.34
425	8	0.987	26.82	7.48
425	13	0.994	11.03	1.64
425	18	0.994	10.67	-0.95
425	23	0.995	7.94	-5.87
DF			2.11	-14.42
BD100			4.78	-2.99
BD80			4.16	-5.63
BD60			3.54	-7.89
BD40			3.00	-10.29
BD20			2.55	-12.52

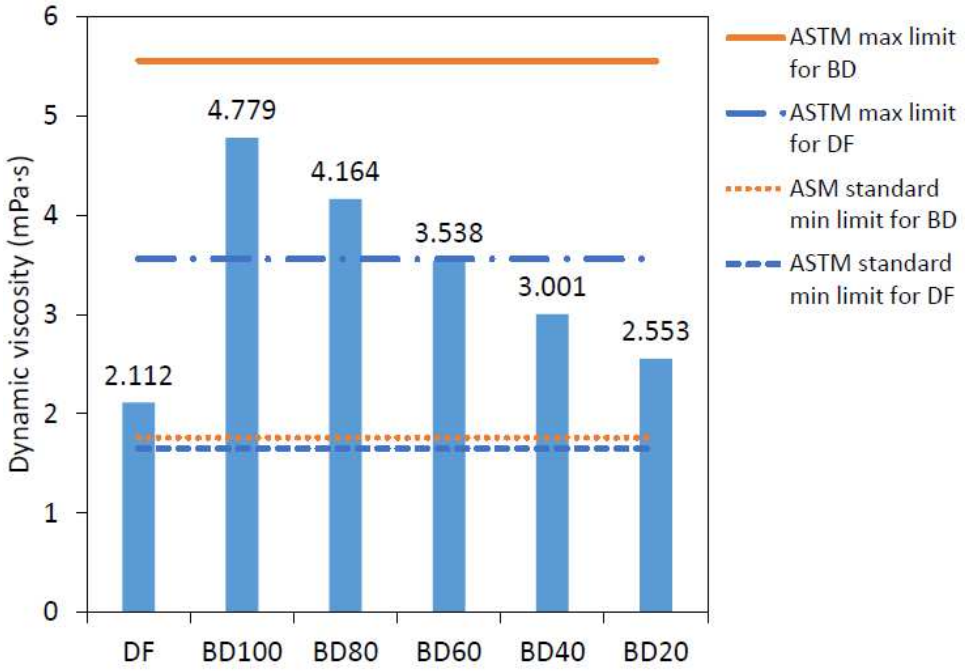

Figure 3-11. Dynamic viscosities at 40 ºC of fresh FAEEs biodiesel fuel (BD), diesel fuel (DF) and FAEEs-diesel blends.

3.4.5 Effect of thermal degradation on FAEEs viscosity

Viscosities of all stressed FAEEs are given in **Table 3-3** and plotted in **Figure 3-12**. In **Figure 3-12A**, negligible increase of viscosity was observed at 250 and 275 ºC. At 300 ºC, the viscosity increased negligibly up to 33 min, and increased slightly as the heating time increased to 63 min. The highlighted area between viscosity value of fresh FAEEs (BD100) and diesel fuel (DF) represents an acceptable range for viscosity. The viscosity of all samples stressed at 250-300 ºC falls in this range except for the sample of 300 ºC and 63 min. At 325-375 ºC, obvious increases of viscosity along with temperature and stressing time were observed. At 400 and 425 ºC, the viscosity reached to a maximum value at heating time of 10 min and 3 min, respectively, and it decreased subsequently. **Figure 3-12B** illustrates the change of viscosity of FAEEs as a function of the degree of decomposition. Within 15% decomposition, the viscosity was nearly the same with fresh FAEEs and within the limit of ASTM biodiesel standards. Sharper increase

of viscosity was observed as the decomposition ratio extended beyond 20%, especially beyond 40%. The viscosity reduced when the decomposition ratio exceed 90% at 400 and 425 ºC.

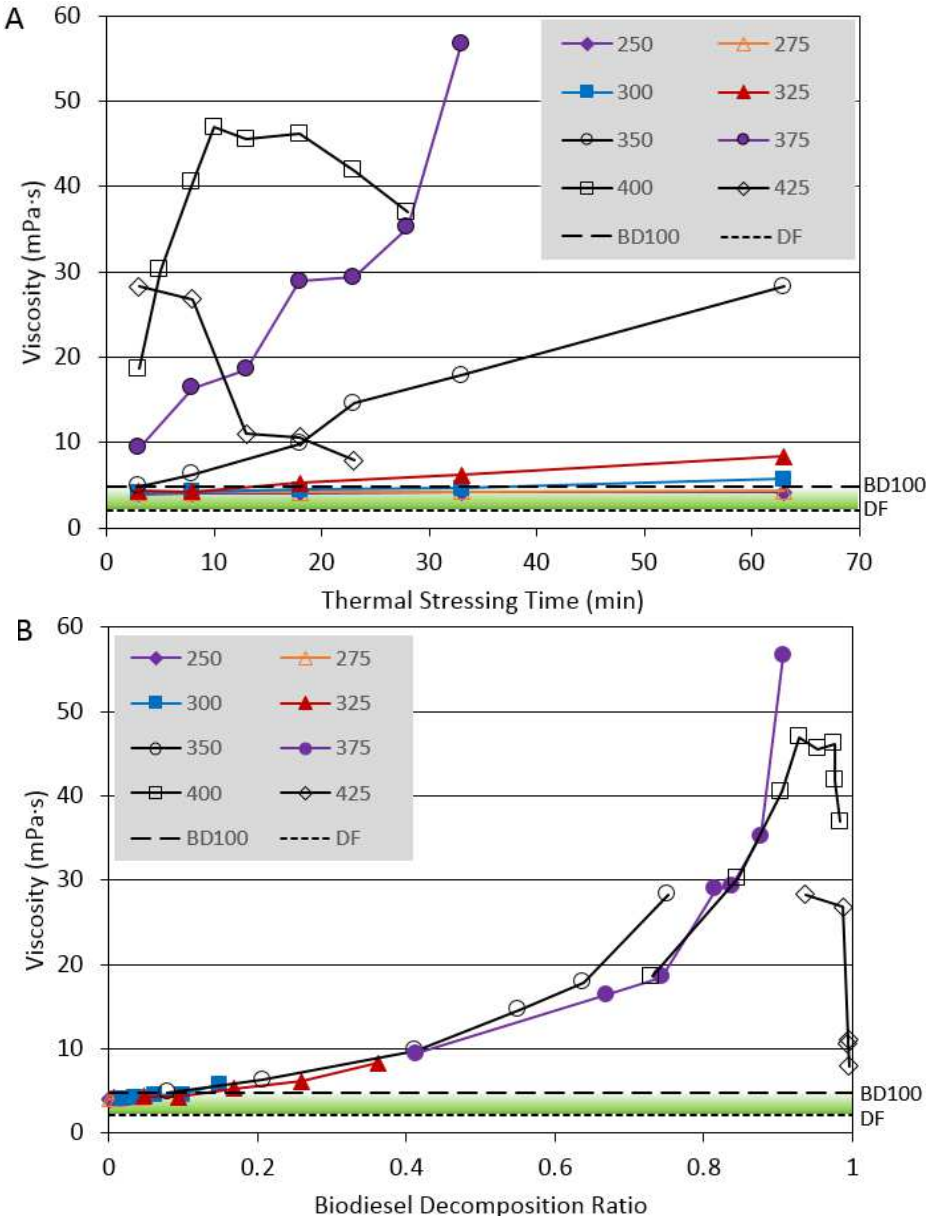

Figure 3-12. Viscosity at 40 ºC of stressed FAEEs biodiesel fuel (A) as a function of thermal stressing duration at varying thermal stressing temperatures, (B) as a function of decomposition at varying thermal stressing temperatures.

The slight increase of viscosity of FAEEs at low temperatures (250, 275, and 300 ^{o}C) is due to the isomerization reactions which generates trans-type isomers with higher viscosity [42] and the pyrolysis reactions which generated small amounts of carboxylic acids at 275 and 300 ^{o}C. When the temperatures were further increased to 325-350 ^{o}C, pyrolysis became more significant, and it generated C16-18 carboxylic acids which increase the viscosity to higher values. However, the viscosity of FAEEs heated at 375 ^{o}C and 33min (56.7 mPa·s), and 400 ^{o}C and 13 min (45.6 mPa·s) are much higher than viscosities of the C16-18 carboxylic acids (less than 25 mPa·s) [43]. This indicates the formation of more viscous compounds. As shown in the GC MSD chromatograms of **Figure 3-13**, for samples stressed at 375 ^{o}C, new peaks at GC retention time of 70 min, as circled by the blue dash rectangles, emerged after the C16-18 carboxylic acids, which means those compounds were less volatile and probably had higher molecular weight than the acids. The area of these peaks increase with thermal stressing time, and it indicates that the corresponding compounds were accumulating with the heating process at those temperatures.

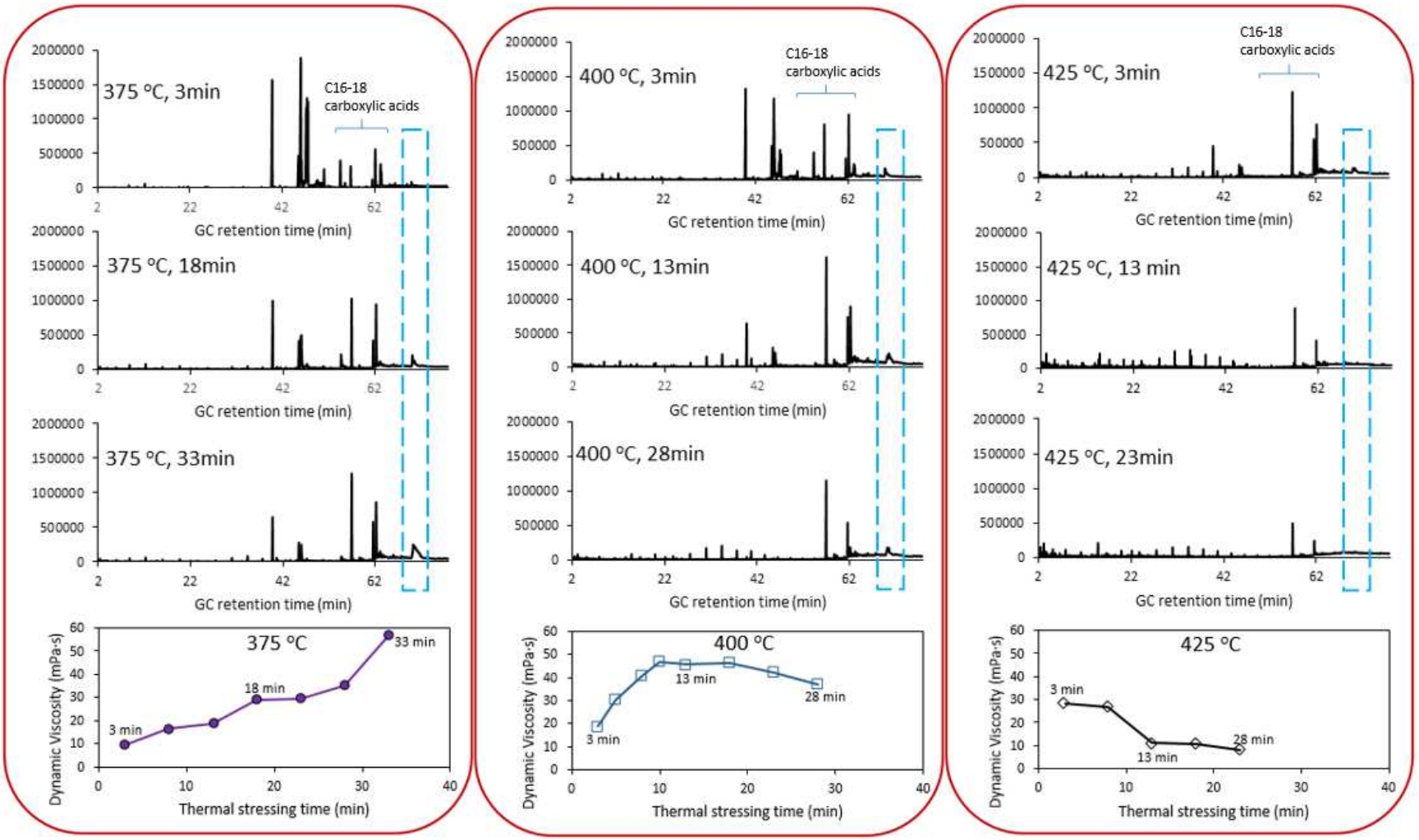

Figure 3-13. Corresponding change of dynamic viscosity at 40 °C of FAEEs biodiesel fuel stressed at 375, 400, and 425 °C to the change of peak at GC retention time of 70 min (circled by dash rectangles).

At 400 ºC, the area of the peaks circled by the blue dash rectangles increased with extending the heating time from 3 min to 13 min, and then decreased when heating for 28 min, however the peaks area for 28 min was still larger than 3 min. This means the compounds represented by the peaks were not stable at 400 ºC, and the sample heated for 28 min contains more of those compounds than the 3 min sample and less than the 13 min sample. At 425 ºC, the peaks circled by the blue rectangle decreased with heating time, and they can be barely observed at 13 min. For all the three temperatures, the viscosity changed correspondingly with these peaks areas, which accordingly implies that the high viscosities were due to the presence of the compounds represented by these peaks such as dimers and polymers formed via polymerization reactions, even though the detailed molecular structure for these peaks cannot be determined by the GC MSD analysis due to limited data source.

As a conclusion, the isomerization reactions that form trans-type isomers resulted in a slight increase in viscosity. Significant changes in viscosity were observed due to the effects of both pyrolysis reactions and polymerization reactions.

3.4.6 Effect of thermal degradation on FAEEs cold flow property

As shown in **Figure 3-14**, the crystallization onset temperature of fresh FAEEs biodiesel, diesel fuel, and FAEEs-diesel blends were measured and compared with the commercial FAMEs biodiesel and FAMEs-diesel blends [25]. The onset temperature of diesel fuel purchased for the current study is -14.42 ºC, and is slightly higher than the diesel fuel used in the previous study [25]. The onset temperature of pure FAEEs is -2.99 ºC which is lower than the value of FAMEs of -0.86 ºC, and this implies that the cold flow properties of the FAEEs are superior to those of the FAMEs. For the biodiesel-diesel blends, FAEEs-diesel has a lower crystallization onset

temperature than FAMEs-diesel for same blending ratio. As expected, the onset temperature of FAEEs-diesel blends increases with addition of FAEEs.

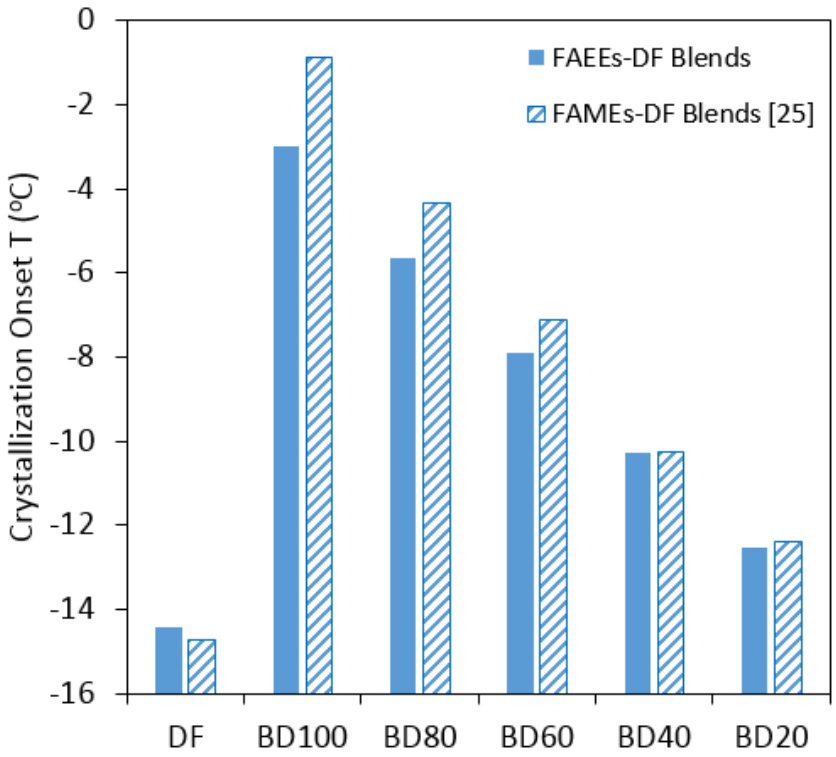

Figure 3-14. Crystallization onset temperature of fresh FAEEs/ FAMEs biodiesel fuel (BD), diesel fuel (DF) and FAEEs/ FAMEs-diesel blends. Data for FAMEs and its related fuels are from our previous study [25], and are reused here with Elsevier's permission.

Figure 3-15A shows the crystallization onset temperatures of thermally stressed FAEEs changing with heating durations at the experimental temperatures. At the temperature ranging from 250 to 300 °C, the onset temperature fluctuated between -4.45 and -3.28 °C at heating duration from 3 to 63 min. At 325 °C, no obvious change of the onset temperature was found until heating duration beyond 33 min. At 350 and 375 °C, the onset temperatures significantly increased with heating time, and the values were far beyond the value of B100 except for conditions of 350 °C and 3 and 8 min. The increase on the onset temperatures were due to the

accumulation of C16-18 carboxylic acids from pyrolysis reactions and dimers/polymers from polymerization reactions. At 400 ^{o}C, the onset temperatures increased up to 11.42 ^{o}C and then slowly decreased with heating duration. At 425 ^{o}C, the onset temperature increased to 9.34 ^{o}C at 3 min, then dramatically decreased to -5.87 ^{o}C at 23 min which is close to the value of B80. Similar with the viscosity change, the decrease on the onset temperatures were due to breaking down of acids and dimers/polymers into smaller molecular compounds which have improved cold flow properties.

Figure 3-15B shows a relationship between the crystallization onset temperature and FAEEs decomposition degree at the experimental conditions. Within 20% thermal decomposition, the onset temperatures of FAEEs change negligibly. This is due to the fact that the decomposition which occurred at lower temperatures (250, 275, and 300 ^{o}C) was mainly isomerization reactions, and it implies that the isomer products merely influence the cold flow properties of FAEEs. The onset temperature increased significantly up to 12.86 ^{o}C beyond decomposition ratio of 20%. Again, this increase was brought by carboxylic acids from the pyrolysis reactions and dimers/polymers formed from polymerization reactions. At 400 and 425 ^{o}C, a sharp decrease of the onset temperature was observed at the decomposition ratio beyond 90%. This was due to the corresponding further decomposition of acids and dimers/polymers into smaller chain compounds which have better cold flow properties.

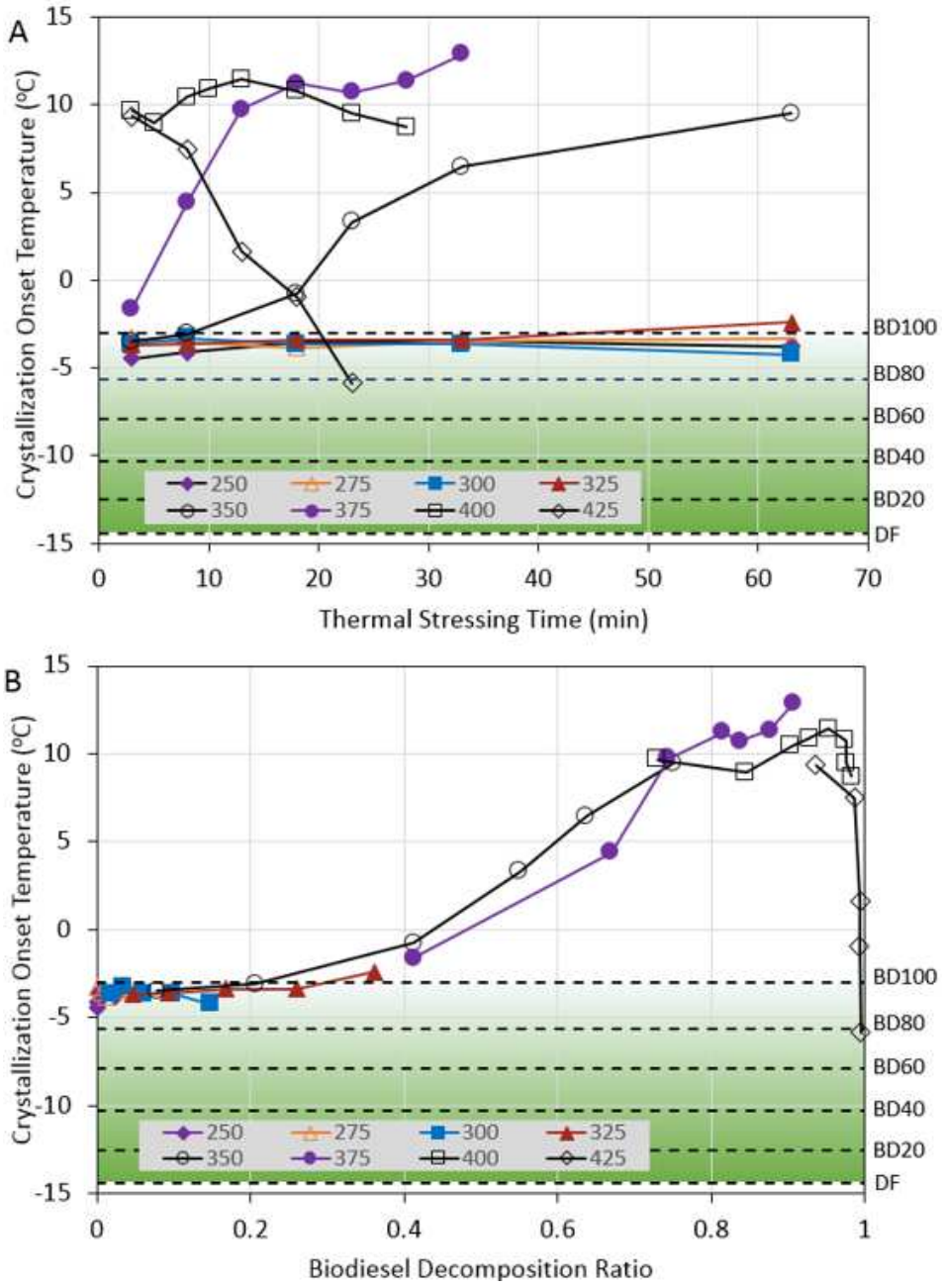

Figure 3-15. Crystallization onset temperature of stressed FAEEs biodiesel fuel (A) as a function of heating durations at different temperatures, (B) as a function of decomposition at different temperatures.

3.5 Conclusion

FAEEs biodiesel were prepared via the KOH-catalyzed method to be used for the thermal stressing experiments and to test fresh FAEEs properties. Viscosity of the prepared FAEEs was

within the ASTM standards limit, and the FAEEs had improved cold flow properties over the FAMEs biodiesel. The viscosities of FAEEs-diesel blends at FAEEs percentage of 20-60% satisfy the ASTM standard limit for diesel fuel. The FAEEs were then thermally treated at 250-425 ^{o}C for 3-63 min. Decomposition of the unsaturated and saturated FAEEs started from 250 and 300 ^{o}C, respectively. The decomposition reactions were mainly isomerization reactions ($T \geq$ 250 ^{o}C), polymerization reactions ($T \geq$ 350 ^{o}C), and pyrolysis reactions ($T \geq$ 275 ^{o}C). Compared with thermal decomposition of FAMEs, the prepared FAEEs were more unstable at high temperatures, and the pyrolysis products included significant amounts of carboxylic acids which were not present in similar FAMEs decomposition reactions. The proposed three-lump model well predicted experimental data for decomposition for temperatures from 250 to 325 ^{o}C. Two one-step reaction models were applied to predict the degree of FAEEs decomposition, and it was found that the reversible model performs better than the irreversible model except for the data at 425 ^{o}C. The presence of ethanol reduced the pyrolysis decomposition via esterification reactions. The isomerization reactions had negligible effect on the viscosities and crystallization onset temperatures, whereas, these properties were significantly influenced by the polymerization and pyrolysis reactions. Both viscosities and crystallization onset temperatures increased with the accumulation of polymerization and pyrolysis products and then decreased with subsequent decomposition of those compounds into smaller molecular components. These results suggest that during the non-catalytic FAEEs production, it is important to keep the reaction temperature below 350 ^{o}C to avoid the polymerization and pyrolysis reactions. Accordingly, the highest experimental temperature is set as 325 ^{o}C in the future as shown in Chapter 4 and 5.

Acknowledgements

We thank Professor Katie Cadwell in the Department of Biomedical and Chemical Engineering for allowing us to access the m-VROC viscometer and training on the instrument. We acknowledge Professor Patrick T. Mather for providing the differential scanning calorimetry (DSC), and Dr. Eric Finkelstein for the training on the DSC. We thank Professor Jesse Q. Bond for allowing us to use his GC-MSD, and Mr. Anargyros Chatzidimitriou for his help on using the instrument. We are also grateful to Syracuse University, College of Engineering and Computer Science for financial support.

3.6 References

[1] Gui MM, Lee KT, Bhatia S. Supercritical ethanol technology for the production of biodiesel: process optimization studies. The Journal of Supercritical Fluids 2009;49:286-92.

[2] Encinar J, González J, Rodríguez-Reinares A. Ethanolysis of used frying oil. Biodiesel preparation and characterization. Fuel Process Technol 2007;88:513-22.

[3] Marjanović AV, Stamenković OS, Todorović ZB, Lazić ML, Veljković VB. Kinetics of the base-catalyzed sunflower oil ethanolysis. Fuel 2010;89:665-71.

[4] Zhu L, Cheung C, Zhang W, Huang Z. Emissions characteristics of a diesel engine operating on biodiesel and biodiesel blended with ethanol and methanol. Sci Total Environ 2010;408:914-21.

[5] Mendow G, Veizaga N, Sánchez B, Querini C. Biodiesel production by two-stage transesterification with ethanol by washing with neutral water and water saturated with carbon dioxide. Bioresour Technol 2012;118:598-602.

[6] Yu D, Tian L, Wu H, Wang S, Wang Y, Ma D et al. Ultrasonic irradiation with vibration for biodiesel production from soybean oil by Novozym 435. Process Biochemistry 2010;45:519-25.

[7] Zexue D, Zhong T, Haijing W, Jianli Z, Yanfeng C, Enze M. Research and development of a sub-critical methanol alcoholysis process for producing biodiesel using waste oils and fats. Chinese Journal of Catalysis 2013;34:101-15.

[8] DU Z, WANG H, JIANG Y, CHEN Y, MIN E. Industrial Application and Life Cycle Analysis for Biodiesel Produced by SRCA Process From Waste Oils and Fats [J]. Acta Petrolei Sinica (Petroleum Processing Section) 2012;3:002.

[9] http://www.northstarbiofuels.com/. Last accessed on 09/16/2015.

[10] Kusdiana D, Saka S. Kinetics of transesterification in rapeseed oil to biodiesel fuel as treated in supercritical methanol. Fuel 2001;80:693-8.

[11] Farobie O, Matsumura Y. A comparative study of biodiesel production using methanol, ethanol, and tert-butyl methyl ether (MTBE) under supercritical conditions. Bioresour Technol 2015;191:306-11.

[12] Liu J, Lin R, Nan Y, Tavlarides LL. Production of biodiesel from microalgae oil (Chlorella protothecoides) by non-catalytic transesterification: Evaluation of reaction kinetic models and phase behavior. The Journal of Supercritical Fluids 2015;99:38-50.

[13] Ong L, Kurniawan A, Suwandi A, Lin C, Zhao X, Ismadji S. Transesterification of leather tanning waste to biodiesel at supercritical condition: Kinetics and thermodynamics studies. The Journal of Supercritical Fluids 2013;75:11-20.

[14] Nan Y, Liu J, Lin R, Tavlarides LL. Production of biodiesel from microalgae oil (Chlorella protothecoides) by non-catalytic transesterification in supercritical methanol and ethanol: Process optimization. The Journal of Supercritical Fluids 2015;97:174-82.

[15] Marulanda VF, Anitescu G, Tavlarides LL. Biodiesel fuels through a continuous flow process of chicken fat supercritical transesterification. Energy Fuels 2009;24:253-60.

[16] Marulanda VF, Anitescu G, Tavlarides LL. Investigations on supercritical transesterification of chicken fat for biodiesel production from low-cost lipid feedstocks. The Journal of Supercritical Fluids 2010;54:53-60.

[17] Imahara H, Minami E, Hari S, Saka S. Thermal stability of biodiesel in supercritical methanol. Fuel 2008;87:1-6.

[18] Shin H, Lim S, Bae S, Oh SC. Thermal decomposition and stability of fatty acid methyl esters in supercritical methanol. J Anal Appl Pyrolysis 2011;92:332-8.

[19] Quesada-Medina J, Olivares-Carrillo P. Evidence of thermal decomposition of fatty acid methyl esters during the synthesis of biodiesel with supercritical methanol. The Journal of Supercritical Fluids 2011;56:56-63.

[20] Jain S, Sharma M. Thermal stability of biodiesel and its blends: a review. Renewable and Sustainable Energy Reviews 2011;15:438-48.

[21] He H, Wang T, Zhu S. Continuous production of biodiesel fuel from vegetable oil using supercritical methanol process. Fuel 2007;86:442-7.

[22] Dunn RO. Effect of oxidation under accelerated conditions on fuel properties of methyl soyate (biodiesel). J Am Oil Chem Soc 2002;79:915-20.

[23] Windom BC, Bruno TJ. Pressure-controlled advanced distillation curve analysis of biodiesel fuels: assessment of thermal decomposition. Energy Fuels 2012;26:2407-15.

[24] Lin R, Zhu Y, Tavlarides LL. Mechanism and kinetics of thermal decomposition of biodiesel fuel. Fuel 2013;106:593-604.

[25] Lin R, Zhu Y, Tavlarides LL. Effect of thermal decomposition on biodiesel viscosity and cold flow property. Fuel 2014;117:981-8.

[26] Olivares-Carrillo P, Quesada-Medina J. Thermal decomposition of fatty acid chains during the supercritical methanol transesterification of soybean oil to biodiesel. The Journal of Supercritical Fluids 2012;72:52-8.

[27] Bertoldi C, da Silva C, Bernardon JP, Corazza ML, Filho LC, Oliveira JV et al. Continuous production of biodiesel from soybean oil in supercritical ethanol and carbon dioxide as cosolvent. Energy Fuels 2009;23:5165-72.

[28] Claudy P, Létoffé J, Neff B, Damin B. Diesel fuels: determination of onset crystallization temperature, pour point and filter plugging point by differential scanning calorimetry. Correlation with standard test methods. Fuel 1986;65:861-4.

[29] Garcia-Perez M, Adams TT, Goodrum JW, Das K, Geller DP. DSC studies to evaluate the impact of bio-oil on cold flow properties and oxidation stability of bio-diesel. Bioresour Technol 2010;101:6219-24.

[30] Heino E. Determination of cloud point for petroleum middle distillates by differential scanning calorimetry. Thermochimica Acta 1987;114:125-30.

[31] Blades AT. The kinetics of the pyrolysis of ethyl and isopropyl formates and acetates. Canadian Journal of Chemistry 1954;32:366-72.

[32] Chakrabarty M.M. Chemistry and Technology of Oils & Fats. New Delhi: Allied Publishers PVT. LTD.; 2003, p. 70.

[33] Ren W, Mitchell Spearrin R, Davidson DF, Hanson RK. Experimental and modeling study of the thermal decomposition of C3–C5 ethyl esters behind reflected shock waves. The Journal of Physical Chemistry A 2014;118:1785-98.

[34] Hurd CD, Blunck FH. The pyrolysis of esters. J Am Chem Soc 1938;60:2419-25.

[35] Bailey WJ, Turek WN. Synthesis and purification of fatty acids by the pyrolysis of esters. J Am Oil Chem Soc 1956;33:317-9.

[36] Zhang Y, Boehman AL. Experimental study of the autoignition of C 8 H 16 O 2 ethyl and methyl esters in a motored engine. Combust Flame 2010;157:546-55.

[37] Rennard DC, Dauenhauer PJ, Tupy SA, Schmidt LD. Autothermal catalytic partial oxidation of bio-oil functional groups: esters and acids. Energy Fuels 2008;22:1318-27.

[38] Mäki-Arvela P, Kubickova I, Snåre M, Eränen K, Murzin DY. Catalytic deoxygenation of fatty acids and their derivatives. Energy Fuels 2007;21:30-41.

[39] Snåre M, Kubičková I, Mäki-Arvela P, Eränen K, Wärnå J, Murzin DY. Production of diesel fuel from renewable feeds: kinetics of ethyl stearate decarboxylation. Chem Eng J 2007;134:29-34.

[40] American Society for Testing and Materials (ASTM). ASTM D6751-09, Standard Specification for Biodiesel Fuel Blend Stock (B100) for Middle Distillate Fuels. 2009.

[41] American Society for Testing and Materials (ASTM). ASTM D975-15b, Standard Specification for Diesel Fuel Oils. 2015.

[42] Knothe G, Steidley KR. Kinematic viscosity of biodiesel fuel components and related compounds. Influence of compound structure and comparison to petrodiesel fuel components. Fuel 2005;84:1059-65.

[43] Rabelo J, Batista E, Meirelles AJ. Viscosity prediction for fatty systems. J Am Oil Chem Soc 2000;77:1255-62.

Chapter 4: Continuous production of ethanol-based biodiesel under subcritical conditions employing trace amount of homogeneous catalysts

This chapter has been published as: Liu, Jiuxu, Yue Nan, and Lawrence L. Tavlarides. "Continuous production of ethanol-based biodiesel under subcritical conditions employing trace amount of homogeneous catalysts." Fuel 193 (2017): 187-196. It has been reused with permission from Elsevier.

4.1 Abstract

Syntheses of ethanol based biodiesel fuel (FAEEs) from corn oil were conducted at subcritical ethanol conditions (T: 175-225 ^{o}C, P: 80-200 bar) with the presence of trace amount of catalysts (0.1 wt% sulfuric acid, 0.05 and 0.1 wt% potassium ethoxide, based on oil mass). Experiments were conducted in a continuous tubular 316SS reactor. Potassium ethoxide showed a stronger catalytic ability than sulfuric acid at the same temperature of 225 ^{o}C, as the reaction yield reached 95% in five minutes with potassium ethoxide while only 25% yield was achieved for sulfuric acid. A three-step partially reversible model was determined to best fit the kinetic data for both catalytic reactions. To investigate the effect of water and free fatty acids (FFA) impurities on reaction yield under subcritical conditions, 10 vol% water (based on ethanol volume) and 30 wt% oleic acid (based on oil mass) were added to the reaction systems. For sulfuric acid, the reaction yield benefitted from the presence of these impurities. On the contrary, for reactions catalyzed by potassium ethoxide, the yield decreased from 96.8% to 15.3% and 2.6% when adding 10 vol% water and 30 wt% oleic acid, respectively. A pressure range of 80 to 200 bar at 225 ^{o}C was investigated to study the pressure effect on reaction yield. The reactions at

these pressures were observed to occur in the homogeneous phase, and the yields at all pressures were in the range of 94-96%, which implies that when the reactions are performed in the homogeneous state, pressure will have little effect on the yield.

4.2 Introduction

Acid/ base homogeneous catalysts are used in the conventional biodiesel fuel production industry. This technology has been criticized for two shortcomings that large amounts of waste water is generated when washing out catalysts from the product, and contaminants including water and free fatty acids (FFA) deactivate the catalysts [1]. These issues could be avoided by using non-catalytic sub/supercritical alcohol transesterification reactions (SCTE) [2]. The non-catalytic SCTE conditions are created by increasing the reaction temperature and pressure to have the reactions performed in a homogeneous reaction phase which minimizes mass transfer resistance and therefore significantly increases the reaction rate. The non-catalytic SCTE method is superior to the conventional technology in that it requires much less reaction time, the purification of biodiesel products is simplified because there are no catalysts to remove, and it is tolerant to poor-quality feedstocks containing FFA and water [2]. These benefits make it possible to use less expensive feedstocks such as waste cooking oil and animal tallows for biodiesel production via non-catalytic SCTE technology [3, 4]. Whereas conventional production methods require expensive high quality feedstocks such as refined oils and anhydrous alcohols which account for more than half of biodiesel production cost. Water content which exists in the low-quality oils and hydrous alcohols was shown to benefit biodiesel yield via the non-catalytic SCTE process [5-7]. This promising information makes the non-catalytic SCTE technology more competitive compared with conventional methods. Recent economic analyses of the non-

catalytic SCTE process have shown some encouraging results which support scaling up the technology to industrial levels [8-10].

However, when employing the non-catalytic SCTE technology, in order to reach a high reaction conversion, high temperatures have to be applied (supercritical conditions, T=250-400 ^{o}C) under which biodiesel fuel will be thermally decomposed [11-13], further degrading fuel qualities [14-16]. In order to complete the reactions at lower temperatures and shorter residence times to avoid decomposition reactions, some researchers have tried to solve this problem by adding heterogeneous [17, 18] or homogeneous catalysts [19-23]. Even though heterogeneous catalysts are believed to be superior to homogeneous catalysts in terms of generating less waste water and making the production process more environmental friendly, their industrial use is limited by the higher cost, undesirable stability, slower reaction rate, and leaching problems.

It is generally accepted that the most economical and practical choice is still homogeneous catalysts. However, it is critical to minimize their usage in order to decrease the amount of waste water generated in the product washing procedure. The dose of strong homogeneous catalysts can be reduced if the reaction conditions are extended from conventional conditions to sub/supercritical conditions. Recent work supports this conclusion. Zeng et al. [19] reached a FAMEs yield of 97.1% at temperature of 350 ^{o}C, pressure of 100 bar, residence time of 34 min, with the presence of 0.5 wt% sodium methoxide. Rodriguez-Guerrero et al. [20] conducted an optimization study in which the highest FAEEs yield was 98% at temperature of 300 ^{o}C, reaction time of 10 min, and 0.1 wt% sodium hydroxide. Liu et al. [21] reported a high yield of FAEEs of 95% under 175 ^{o}C and 240 min reaction time catalyzed by 0.1 wt% sulfuric acid. Besides strong acid/base catalysts, some researchers explored the possibility of applying weak acid/base catalysts in relatively large amount to catalyze the reactions. Caldas et al. [22]

used an ionic liquid with a concentration of 0.35 mL/1.5 g oil, and achieved a FAEEs yield of 97.6% at 255 ^{o}C, 100 bar, and 45 min reaction time. Six wt% of acetic acid was added by Go et al. [23] into subcritical methanol providing 95% yield at 250 ^{o}C, 72 bar, and 60 min.

Despite these studies the information regarding synthesizing FAEEs biodiesel fuel under subcritical conditions with trace amount of homogeneous catalysts is very limited. For example, it is not clear if impurities of water and free fatty acids would poison the catalysts under SCTE conditions, since these compounds deactivate acid/base catalysts under conventional conditions. Another limitation is that kinetics of ethanolysis with trace amounts of homogeneous catalysts under subcritical conditions are rarely reported in the literature, although kinetic studies for biodiesel production at conventional conditions with acid/base catalyst have received much attention over the past few decades [24-28].

This study aims (1) to explore the possibility of reaching a high biodiesel yield under subcritical conditions which are milder than the commonly used supercritical conditions (T:275-400 ^{o}C) at short residence times by adding acid and base catalysts, and (2) to study the kinetics for the catalytic reaction systems, neither of which is well addressed in the literature. In addition, mixing phenomena of ethanol-oil streams at elevated conditions were studied in order to determine the significance of mass transfer resistance on conversion. Also, trace amounts of homogeneous catalysts of sulfuric acid (0.1 wt%, based on oil mass) and potassium ethoxide (0.05 and 0.1 wt.%, based on oil mass) were employed at subcritical conditions (T:175-225 ^{o}C, P:200 bar). The small usage of catalysts will simplify the product purification process significantly. Other variables investigated were pressure and impurities of water and FFA on the reactions.

4.3 Experimental

4.3.1 Material

Anhydrous ethanol (200 proof, 100 vol%) and refined corn oil were purchased from Pharmco-Aaper and a local market, respectively. Potassium ethoxide, sulfuric acid, oleic acid, GC analytical standards for glycerides and FAEEs, *n*-Methyl-*n*-(trimethylsilyl) trifluoroacetamide (MSTFA) (GC derivatization synthesis grade) were purchased from Sigma Aldrich. n-*Heptane* (HPLC grade) was provided by Thermo Fisher Scientific. Gases (ultrahigh purity grade) used in gas chromatograph analysis were supplied by Airgas. Fatty acid profile of the corn oil includes 20 wt% C16:0, 6.5 wt% C18:0, 71 wt% unsaturated C18 and 2.5 wt% other species.

4.3.2 Transesterification reactions at subcritical conditions

Transesterification reactions of corn oil with ethanol were executed in a coiled tubular reactor (316SS, ID 1.753 mm*10m). Catalysts employed were 0.1 wt% sulfuric acid and 0.05 and 0.1 wt% potassium ethoxide (based on oil mass). They were dissolved in ethanol before mixing with the oil. Temperature (175-225 ^{o}C), pressure of 200 bar, and ethanol-to-oil molar ratio of 18:1 were employed to perform experiments for the kinetics study. For temperature at 225 ^{o}C, pressures ranging from 80 to 200 bar were applied to investigate the pressure effect. For reactions with sulfuric acid, the residence time ranged from 2 to 120 min, while it varied from 1 to 20 min for reactions with potassium ethoxide. As shown in **Figure 4-1A**, during experiments, corn oil and ethanol containing catalysts were pressurized and transported using high pressure syringe pumps (Teledyne ISCO 260 D), preheated by heating tapes, mixed by passing through a mixing tee, and flowed into the reactor which was heated by an electrical furnace (Briskheat). The entire experimental set-up for conducting the reactions was the same as employed in our

previous study including tubular reactor, high-pressure syringe pumps, furnace, temperature controllers, thermocouples, back-pressure regulator, and data acquisition system [29]. Each run was repeated twice, and the experimental errors were within 4%. Collected samples were washed with distilled water before GC analysis to remove the dissolved ethanol, glycerol, and catalysts.

Desired residence time was reached by precisely controlling pump flow rates, and it was defined as

$$\tau = \frac{V}{F_E(\rho_E/\rho'_E)+F_O(\rho_O/\rho'_O)} \qquad \text{Eq 4-1}$$

where V is volume of the reactor, F is volumetric flow rate provided by the pumps, ρ is density of the oil and ethanol (pump temperature, pump pressure), ρ' is density of the oil and ethanol at reaction conditions, whose values are determined from the literature [30]. E and O represent ethanol and oil, respectively.

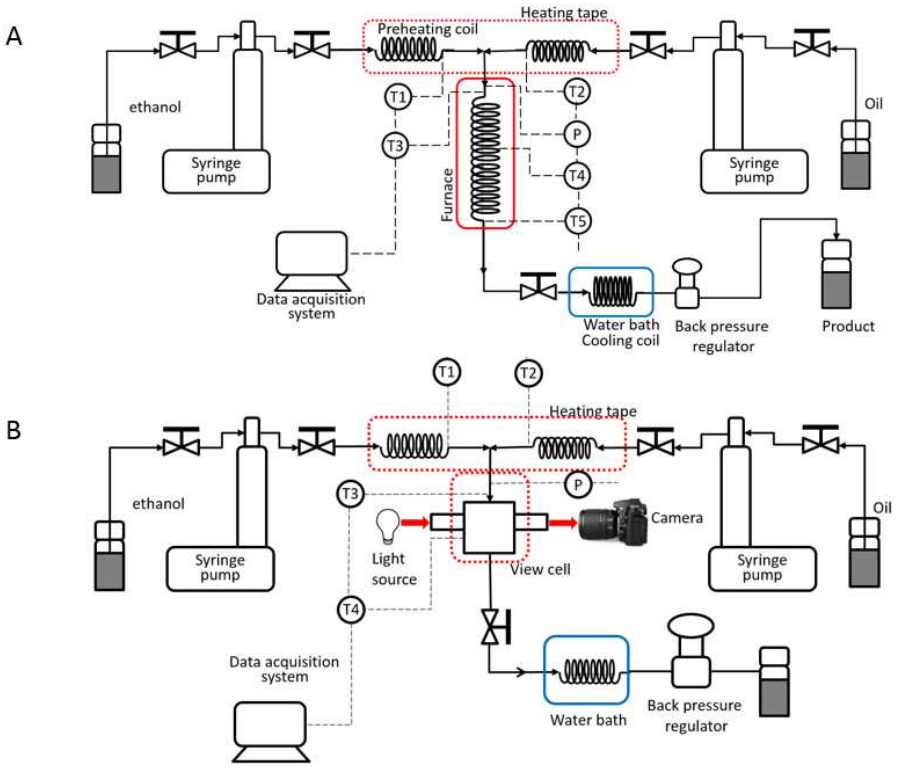

Figure 4-1. Schematic diagram of the experimental setup A) for non-catalytic transesterification of corn oil (P – pressure indicator, T1-T5 – thermocouples), B) for phase transition study (P – pressure indicator, T1-T4 – thermocouples). The diagrams from our previous work [29] are reused here with Elsevier's permission.

The mixing of ethanol-oil streams was physically observed through a view-cell system, as shown in **Figure 4-1B**, which consists of high pressure pumps (Teledyne ISCO 260 D), high pressure view-cell, a charge-coupled-device (CCD) camera with a micro-lens (Photron, model# FASTCAM-512PCI), light source, and data acquisition system. This experimental setup was also used in our previous study [29]. Corn oil and ethanol were pumped separately by two high pressure pumps (Teledyne ISCO 260D), preheated by two heating tapes, mixed in a mixing tee and then entered a high-pressure view cell which was heated by a heating tape.

4.3.3 Gas chromatogram analysis

For the analysis of the FAME profile, biodiesel samples were prepared by diluting 5 µl biodiesel into 1 ml hexane, making a total biodiesel concentration of 5000 ppm by volume. The samples were derivatized using MSTFA based on procedures provided in ASTM D6584 [31]. Quantitative analysis to measure the concentration of FAEEs and glycerides including unreacted triglycerides and the intermediates diglycerides and monoglycerides was conducted via a GC FID (HP 5890 Series II) equipped with an autosampler (HP 5890 Series II) and a Rtx-Biodiesel TG column (10 m × 0.32mmID × 0.10 µm, Restek) at splitless mode. Calibration curves for each compound were prepared by diluting the GC standards. Details of the temperature program was the same as in our previous work [29].

Concentrations of ethanol and glycerol were determined from mass balance calculations since the initial concentration of ethanol and triglycerides were known (MR of 18:1) and the

concentration of glycerides and FAEEs in the collected samples were measured from GC FID analyses.

4.4 Results and discussion

4.4.1 Mixing of ethanol-oil streams

Mixing phenomena of ethanol-oil streams was studied during the heating and pressurizing process via a view-cell experimental setup in order to determine the significance of mass transfer resistance on conversion. The flow rates of the mixture were the same to establish a one minute residence time in the 10-meter tubular reactor. Selected results are reported in **Figure 4-2**. It is known that at ambient conditions, ethanol is immiscible with oil. When increasing the temperature to 100 ^{o}C and pressure to 100 bar, a flow jet was observed, and the dark layer of the jet was believed to be corn oil, which indicates that under this flow condition the oil and ethanol were not fully miscible. After further elevating the reaction temperatures (175-225 ^{o}C) and pressure (100-200 bar), the ethanol-oil mixtures formed a homogeneous state, which indicates that at these specific conditions the reactions were performed in a homogeneous phase from the beginning and accordingly mass transfer resistance could not be significant.

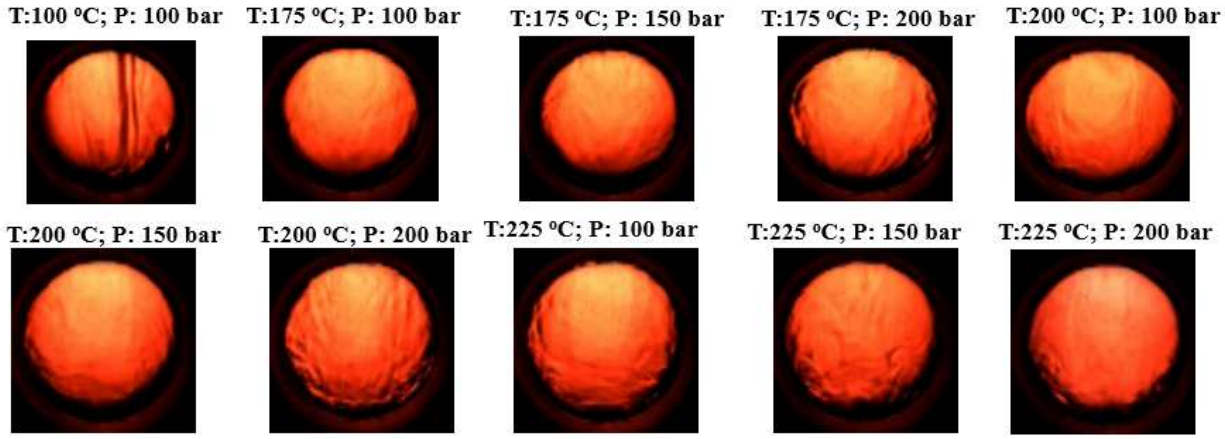

Figure 4-2. Ethanol-oil mixture (EtOH/oil molar ratio of 18) flowing through a view cell at 175-225 ^{o}C and 100-200 bar. The flow rates of the mixture were the same as ones which created one min residence time in the tubular reactor in the reaction experiments.

4.4.2 Kinetics of the transesterification reactions with trace amount of sulfuric acid and potassium ethoxide

Preliminary experiments using sulfuric acid at trace concentrations 0.1 and 0.2 wt% (based on oil mass) were executed and compared with non-catalytic reactions in order to determine if trace amounts of strong acid would perform well in this reaction system. As shown in **Figure 4-3**, at temperature of 200 ^{o}C, pressure of 200 bar, and residence time of 30 min, the yield for non-catalytic reactions was only 5% which means the reactions barely occurred without the presence of sulfuric acid. The yield was significantly increased to 81% and 92% when sulfuric acid was employed for concentrations of 0.1 wt% and 0.2 wt%, respectively. Similarly at temperature of 225 ^{o}C and residence time of 30 min, the yield was increased from 28% to 95% when increasing the sulfuric acid concentration from zero to 0.1 wt%. Further increasing the acid from 0.1 wt% to 0.2 wt% did not improve the yield any more, since the reactions had reached equilibrium. These phenomena demonstrate the strong catalytic ability of sulfuric acid even with a trace concentration on the transesterification reactions under subcritical conditions.

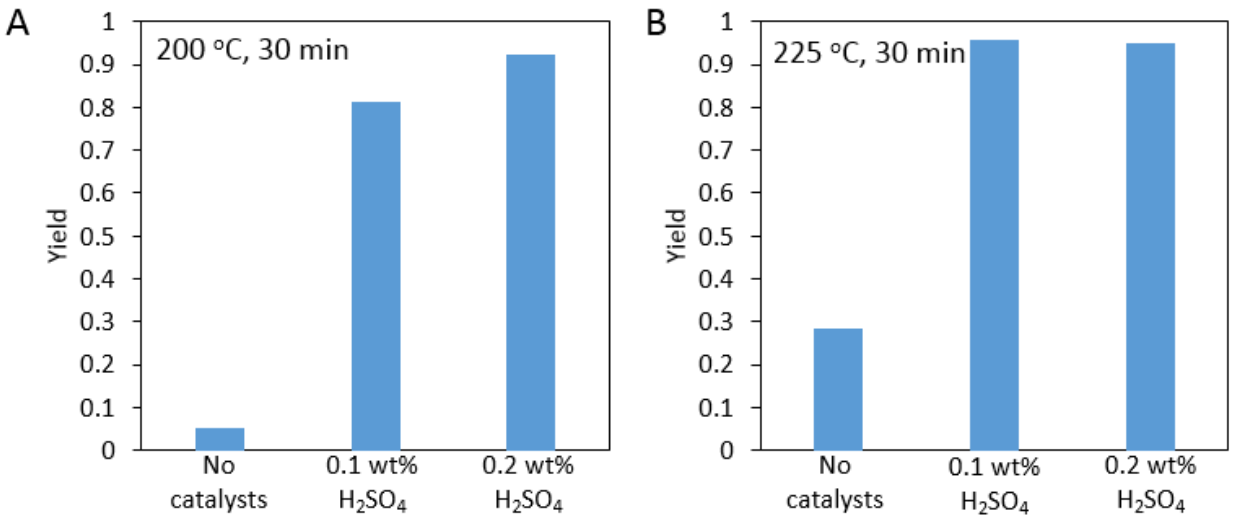

Figure 4-3. Comparison of FAEEs yield catalyzed by zero, 0.1, and 0.2 wt% sulfuric acid based on oil mass at (A) 200 ºC and 30 min, and (B) 225 ºC and 30 min. The reaction pressure was kept at 200 bar.

Since at subcritical conditions ethanol and oil are supposed to be in liquid state, the reaction mechanism in this study is assumed to be the same with one conducted at conventional conditions [32]. For sulfuric acid catalysis reactions, as shown in **Figure 4-4**, the carbonyl group in a triglyceride (TG) molecule is protonated by proton, which makes the adjoining carbon atom susceptible to nucleophilic attack. Then the oxygen atom in ethanol molecule attacks the protonated triglyceride to form a tetrahedral intermediate. This intermediate is broken down after proton migration to give a diglyceride (DG), FAEE, and proton. Then this sequence is repeated by diglyceride to form monoglycerides (MG) which further follows the same mechanism to produce glycerol (GL).

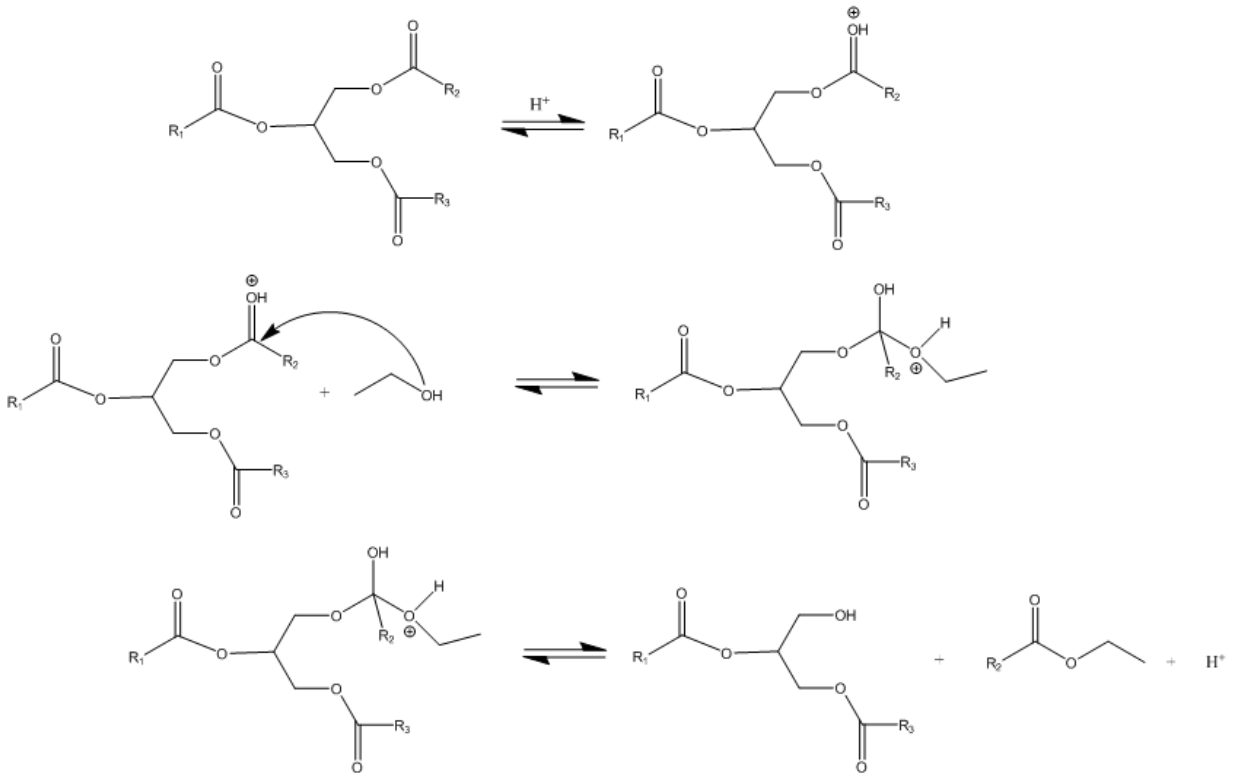

Figure 4-4. Mechanism of transesterification reactions of oil and ethanol catalyzed by homogeneous acid catalysts. R_1, R_2, R_3: carbon chain of fatty acids.

On the contrary, base catalysis follows a more direct and quicker reaction pathway, as shown in **Figure 4-5**. First the potassium ethoxide reacts with a subcritical ethanol molecule to produce the active ethoxide $CH_3CH_2O^-$ which then attacks a carbonyl group on the triglyceride (TG) molecule to form a tetrahedral intermediate. The intermediate then breaks down to generate FAEEs and the corresponding anion of triglyceride which is further reacted to produce diglyceride (DG) and regenerate the $CH_3CH_2O^-$ active compound. The diglyceride follows same mechanism to produce monoglycerides (MG) which further reacts to gives glycerol (GL). The above reaction mechanisms have been simplified into some commonly used kinetic models including one-step models [33-35] and three-step models [25, 36, 37].

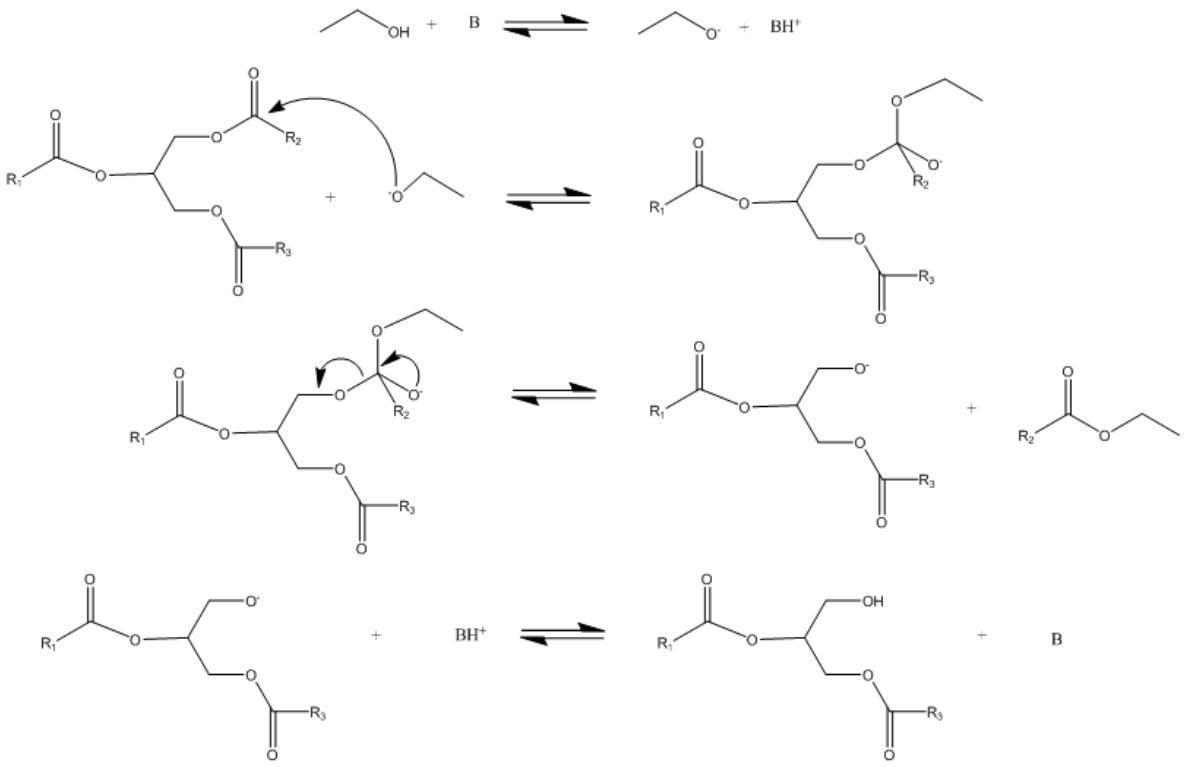

Figure 4-5. Mechanism of transesterification reactions of oil and ethanol catalyzed by homogeneous base catalysts. B: base catalysts. R_1, R_2, R_3: carbon chain of fatty acids.

Figure 4-6A-C illustrate the concentration profile of each compound including the original reactants, triglycerides (TG) and ethanol, intermediate products diglycerides (DG) and monoglycerides (MG), and final products FAEEs and glycerol (GL) produced at 175-225 ^{o}C with 0.1 wt% sulfuric acid. As expected, TG and ethanol were decreasing along with reaction time, whereas that of FAEEs and GL increased over time. The intermediate products DG and MG increased at the beginning stage of the reactions then decreased. At the last stage of reactions, the amount of TG and DG was reduced to a negligible level, however the MG were still present, which prohibited the reactions from being completed. This tendency was found regardless of the reaction temperatures. Specifically, at 175 ^{o}C and 60 min, 200 ^{o}C and 30 min,

and 225 ºC and 30 min, all TG and DG were almost reacted while intermediate product MG were always present and not fully converted to glycerol.

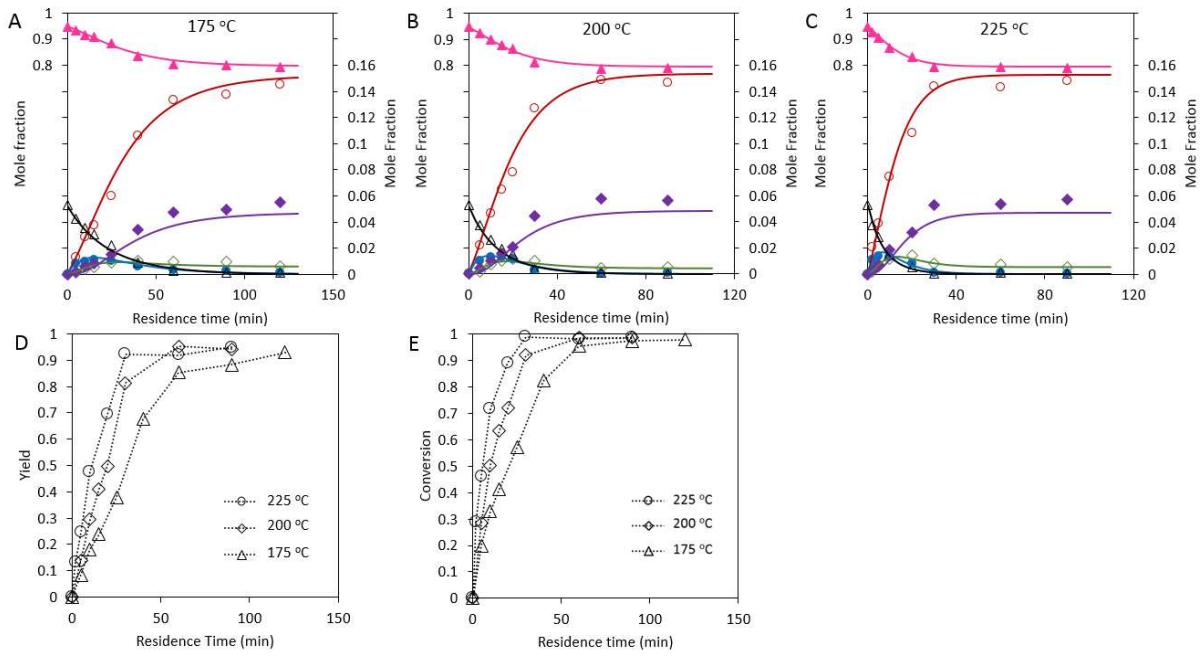

Figure 4-6. Curve fitting of kinetic data by the three-step partially reversible model under the subcritical conditions with 0.1 wt% sulfuric acid at (A) 175, (B) 200, and (C) 225 ºC. Key: (▲) ethanol, (○) FAEEs, (♦) GL, (Δ) TG, (●) DG, (◊) MG. Data of ethanol are plotted on the primary axis (left), and the rest are plotted on the secondary axis (right). (D) Yields of reactions, and (E) conversions of oil.

Also as shown in **Figure 4-6D**, the reaction rate started to decrease at these times in the reaction discussed above when TG and DG were gone and MG were still present. This demonstrates that with sulfuric acid as the catalyst, at the above times the transesterification reactions were approaching equilibrium so the reaction from MG to FAEEs are slower than that of TG and DG. As shown in **Figure 4-6D**, at 175 ºC with 0.1 wt% sulfuric acid, the yield increased to 85% in 60 min, and ramped up with a slower rate to 93% after 120 min. Higher temperatures allow the reactions to reach equilibrium in a shorter residence time. At 200 and 225 ºC, a yield of about 95% at equilibrium was reached after 50 min and 30 min, respectively.

Reaction conversions of triglycerides were included in **Figure 4-6E** which shows that the conversions exceeded 98% regardless of the temperatures indicating most of the triglycerides were reacted, which is consistent with **Figure 4-6A-C**.

For reactions catalyzed by 0.1 wt% potassium ethoxide, the concentration change of each compound was shown in **Figure 4-7A-C**. During the course of the reaction, the TG were almost completely reacted in one minute at all temperatures, while DG were accumulated in the beginning then quickly decreased. The intermediate product MG were found difficult to be fully consumed regardless of temperatures. The reactions rates were significantly enhanced by switching catalysts from 0.1 wt% sulfuric acid to 0.1 wt% potassium ethoxide. As shown in **Figure 4-7D,** the yield quickly increased to 85% in only one minute at the lowest reaction temperature 175 ^{o}C compared to 60 minutes at same temperature with 0.1 wt% sulfuric acid. The reactions reached equilibrium with yields higher than 94% in twenty, ten, and three minutes for temperatures of 175, 200, and 225 ^{o}C, respectively. The reaction rates significantly reduced after one minute when the major unreacted compound left was MG, as shown in **Figure 4-7A-C**, and this means that with potassium ethoxide as the catalyst, the reaction step from MG to FAEEs was still the slowest compared to the ones of TG and DG at the above times. Decreasing the potassium concentration to 0.05 wt% significantly reduced the reaction rate as shown in **Figure 4-7D**. Only 15% yield was achieved in one minute at 175 ^{o}C compared to 85% for potassium concentration of 0.1 wt%. At 0.05 wt% potassium ethoxide, the yield slowly ramped up to 82% at 225 ^{o}C after 20 min residence time, however it only took less than one minute when the catalyst concentration was 0.1 wt%. **Figure 4-7E** presents the reaction conversions of triglycerides at all temperatures with both concentrations of potassium ethoxide. For 0.1wt% potassium ethoxide, the conversion exceeded 97% in one minute at all temperatures, while it

took about 20 minutes at the highest temperature 225 ºC for 0.05 wt% potassium ethoxide to reach similar conversion.

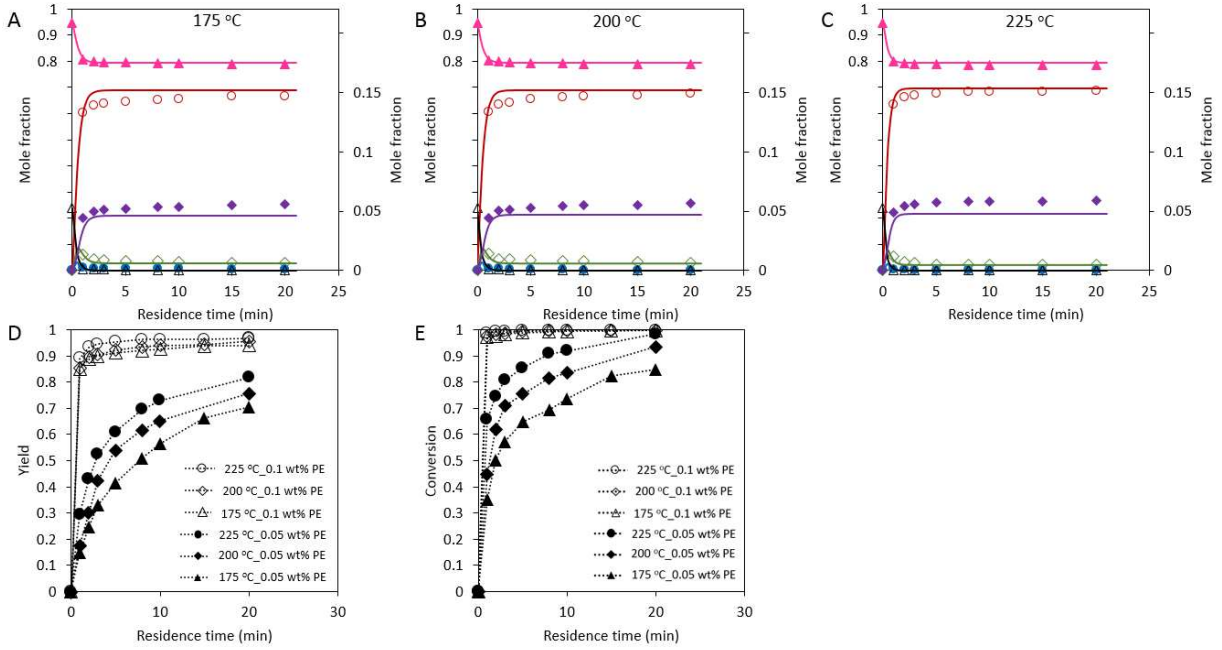

Figure 4-7. Curve fitting of kinetic data by the three-step partially reversible model under the subcritical conditions at (A) 175, (B) 200, and (C) 225 ºC with 0.1 wt% potassium ethoxide. Key: (▲) ethanol, (○) FAEEs, (♦) GL, (Δ) TG, (●) DG, (◊) MG. Data of ethanol are plotted on the primary axis (left), and the rest are plotted on the secondary axis (right). (D) Yields of reactions with 0.1 and 0.05 wt% potassium ethoxide, and (E) conversions of oil with 0.1 and 0.05 wt% potassium ethoxide.

In this study, a three-step partially reversible kinetic model, as shown in Eq 4-(2-4), was determined to best fit the data of reactions with sulfuric acid after comparing with other three-step and one-step models. For all the kinetic modelling in this study, the mass transfer resistance was neglected according to the results from the view-cell experiment which was conducted to observe the mixing of ethanol and oil at the desired reaction conditions.

$$TG + EtOH \xrightarrow{k_1} DG + EE \qquad \text{Eq 4-2}$$

$$DG + EtOH \xrightarrow{k_2} MG + EE \quad \text{Eq 4-3}$$

$$MG + EtOH \underset{k_{-3}}{\overset{k_3}{\rightleftharpoons}} GL + EE \quad \text{Eq 4-4}$$

In this model, the first two reaction steps are assumed to be irreversible while the last step is assumed to be reversible. The reaction order for each step was determined as second order. Micromath Scientist 3.0 software was used for data fitting to calculate the reaction rate constants at each step via the least-squares regression. For the reactions catalyzed by 0.1 wt% sulfuric acid, **Figure 4-6** also clearly shows this model well predicted the data change. The R^2 values for data fitting as shown in **Table 4-1** are greater than 0.99 for all temperatures which also indicates a good data fit. The calculated reaction rate constants are presented in **Table 4-1**. Using the Arrhenius equation, $k(T) = k_0\exp(-E_a/RT)$, the activation energies, E_a, for each reaction step were determined based on the k values as presented in **Table 4-2**, and they are compared with the values reported in the literature [21]. The different activation energies between this work and one from Liu et al. [21] can be due to the result of different triglycerides feedstocks and different reaction system in terms of different mixing and physical state transitions. Van't Hoff equation was employed to estimate the standard reaction enthalpy and entropy change for the third step reaction by using data in **Table 4-1**. For sulfuric acid system, the standard reaction enthalpy change and entropy change was calculated as 2.3 kJ/mol and 17.2 J/mol/K, respectively. For potassium ethoxide system, the standard reaction enthalpy change and entropy change was calculated as 1.8 kJ/mol and 13.3 J/mol/K, which is relatively consistent with the values derived from the sulfuric acid system. Both analyses shows the third reaction step to be slightly endothermic and entropically favorable. And by comparing the values of the third step reaction for the oil-methanol system, we can found that both the standard reaction enthalpy and entropy

change for the oil-ethanol system are significantly lower than the ones for the oil-methanol system (ΔH^0: 2.3 vs 79.3 kJ/mol; ΔS^0: 17.2 vs 137.2 J/mol/K).

Table 4-1. Reaction rate constants ($(mol/g)^{-1}$ min^{-1}) derived from the three-step model and R^2 values for the data fitting at each temperature.

Catalyst	T (°C)	k_1	k_2	k_3	k_{31}	R^2
0.1 wt% H_2SO_4	175	0.046 ± 0.003	0.102 ± 0.022	0.125 ± 0.043	0.079 ± 0.038	0.999
	200	0.082 ± 0.006	0.15 ± 0.032	0.183 ± 0.059	0.087 ± 0.053	0.999
	225	0.149 ± 0.012	0.2 ± 0.039	0.259 ± 0.123	0.116 ± 0.072	0.999
0.1 wt% PE	175	3.252 ± 0.558	9.388 ± 3.351	3.115 ± 2.404	2.155 ± 1.912	0.992
	200	3.337 ± 0.61	10.034 ± 3.062	3.392 ± 1.414	2.254 ± 1.016	0.993
	225	4.113 ± 0.829	11.78 ± 4.259	4.553 ± 2.482	2.374 ± 1.031	0.994

Table 4-2. Estimated activation energy (kJ/mol) for each reaction step.

	0.1 wt% H_2SO_4 This study	**0.1 wt% PE This study**	**0.06 wt% H_2SO_4 [21]**
TG→DG	43.1	8.6	47.4
DG→MG	25.0	8.4	55.8
MG→GL	17.6	13.9	46.0
GL→MG	13.9	3.6	58.1

Also as shown in **Figure 4-7** that with potassium ethoxide as the catalyst the amount of triglycerides and diglycerides decreased to a negligible level after one minute. These results imply that the reactions catalyzed by potassium ethoxide under the conditions from triglycerides to diglycerides and from diglycerides to monoglycerides would be irreversible. Accordingly the

partially reversible model was employed again for data fitting. Each step was determined to be second order reaction. The reaction rate constants for potassium ethoxide catalysis reactions can be found in **Table 4-1**, and it shows that each value was considerably increased compared to the reactions with sulfuric acid. R^2 values of the data set for each temperature for data fitting as shown in **Table 4-1** demonstrate the model can describe the reaction procedures accurately. The estimated activation energy for each reaction step is shown in **Table 4-2**. The value for each specific reaction step with potassium ethoxide is lower than that of sulfuric acid. This can be explained by the different reaction pathways due to the different catalysts, as discussed above, that transesterification reactions with base catalysts are easier to execute than those with acid catalysts.

4.4.3 Effect of impurities on the reactions

More than half cost of biodiesel fuel comes from refined oil and anhydrous alcohol costs which are required by the conventional biodiesel industry, since common impurities in the feedstocks of water and free fatty acids (FFA) deactivate the catalysts as FFA react with base catalysts via saponification reactions, and water poisons both base and acid catalysts under conventional biodiesel synthesis conditions. In a previous study [21], water content at 1 and 3 wt% were found to barely influence the reactions at a similar reaction condition (T=175 ^{o}C, with 0.06 wt% sulfuric acid). However usually water content in cheaper feedstocks as waste cooking oil and hydrous ethanol before pretreatment exceeds 3 wt%. Accordingly in this study, ethanol solution which contains 10 vol% water was used to study water effect on the reactions. As shown in **Figure 4-8**, when conducting reactions at 225 ^{o}C with 0.1 wt% sulfuric acid as catalyst, increasing water content in the ethanol from zero to 10 vol% enhanced the yield from 48% to 60%, and from 69% to 73% at 10 min and 20 min, respectively. Similar phenomena was reported

in the literature [5-7] that water favors the yield of FAEEs at supercritical conditions. The possible mechanism could be that either water performed as another catalyst which further promoted the reaction rate, or water turned triglycerides via hydrolysis into FFA which can further react with ethanol via esterification reactions and have a faster reaction rate compared to triglycerides.

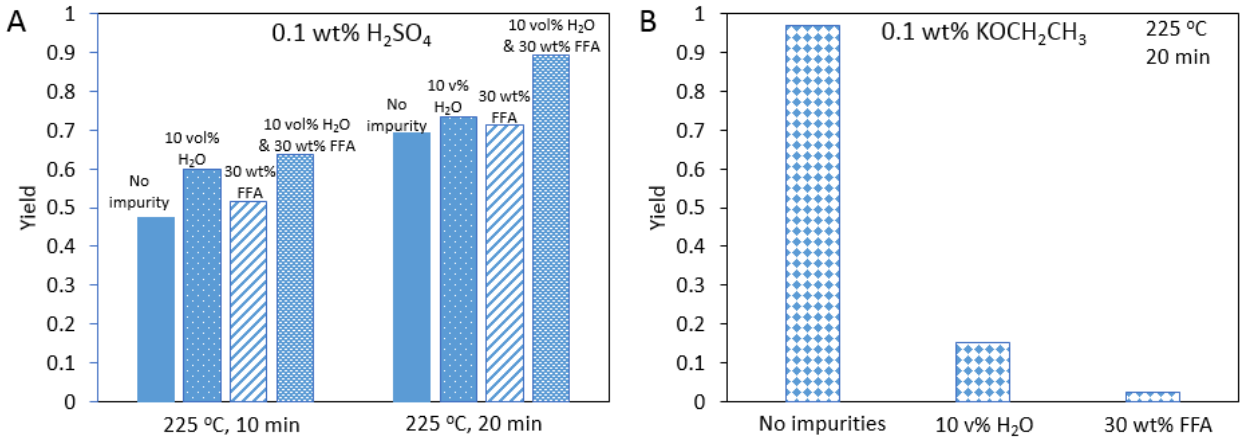

Figure 4-8. Effect of impurities on reactions catalyzed by (A) 0.1 wt% sulfuric acid at 225 °C and 10 and 20 min residence time, and (B) 0.1 wt% potassium ethoxide at 225 °C and 20 min residence time. The reaction pressure was 200 bar.

Besides water, waste cooking oil also contains large amount of FFA. In this study, tolerance to FFA was investigated by adding oleic acid to corn oil to simulate a waste cooking oil which has 30 wt% FFA. As shown in **Figure 4-8**, for the sulfuric acid catalytic system at 225 °C, the yield was found to slightly benefit from the addition of oleic acid. This benefit occurs because oleic acid can easily react with ethanol via esterification reactions catalyzed by sulfuric acid. By simultaneously adding both impurities, the yield was further increased to 64% and 89% at 10 and 20 min, respectively. These results demonstrate that cheap feedstocks as waste cooking oils which contain large amount of water and FFA can be used without pretreatment in the sulfuric acid catalytic system under subcritical conditions.

On the contrary, at 225 ºC and 20 min, when the same amount of water (10 vol%) and FFA (30 wt%) were added individually to the potassium ethoxide reaction system, the yield was dramatically decreased from 96% to 15% and 2%, respectively. This phenomena clearly proves potassium ethoxide is not tolerant at all to the impurities. The mechanism is believed to be that FFA can easily react with base catalysts via saponification reactions, and water can react with triglycerides via hydrolysis reactions to give FFA which further consumes base catalysts. Accordingly pretreatment of feedstocks to remove water and FFA is critical if potassium ethoxide is employed as the catalyst under subcritical conditions.

4.4.4 Effect of pressure on the reactions

High pressures of 150-300 bar are commonly used in studies related to sub/supercritical biodiesel synthesis in order to pressurize the reaction system into a homogeneous state. These required high pressure would bring potential safety issues and increase the cost of equipment. Adding co-solvent can improve solubilization of the alcohol-oil stream, but this also increases the product purification burden. In this study, pressure effect on reaction yield at subcritical conditions were investigated. As shown in **Figure 4-9**, at the stated conditions (T: 225 ºC, t: 20min, EtOH-Oil molar ratio: 18; 0.1 wt% potassium ethoxide), pressure range from 80 to 200 bar on yield was evaluated. At 200 bar, the yield was 96%. While dropping the pressure to 150, 100, and 80 bar, the yield slightly decreased to 95, 95, and 94%, respectively. The mixing of ethanol-oil stream was observed by the view-cell set-up, and it was found that in this pressure range the mixture formed a homogeneous state. This result demonstrates that the reaction yield will not be effected by pressure change as long as such change does not influence the reaction phase behavior. Experimental set-up such as a view-cell system and suitable equation of states can be employed to find minimum pressures experimentally and theoretically for specific

conditions including temperature, alcohol-to-oil molar ratio, and flow rate, which can create a homogeneous reaction state.

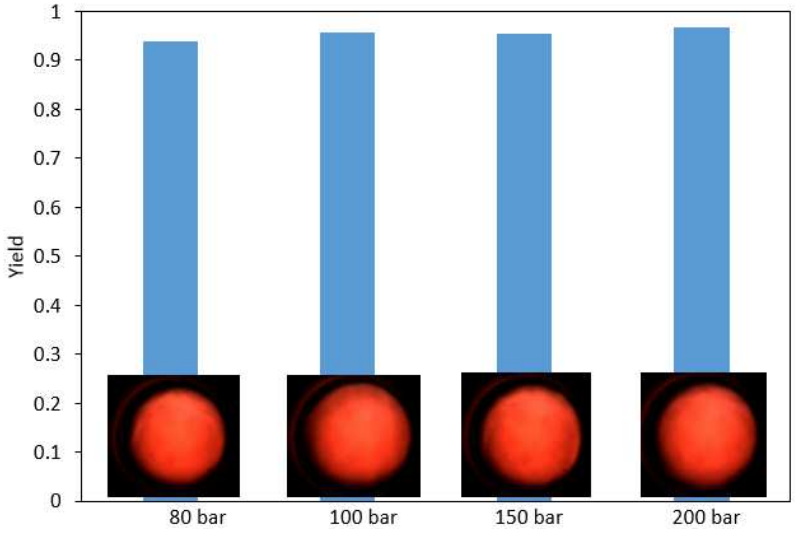

Figure 4-9. Effect of reaction pressure on yield. Reactions were catalyzed by 0.1 wt% potassium ethoxide at 225 ºC and 20 min residence time.

4.5 Conclusions

In this article, transesterification reactions of corn oil with subcritical ethanol were executed at T: 175-225 ºC, P: 80-200 bar, ethanol-to-oil molar ratio of 18, and residence time of 1-120 min. Two homogeneous catalysts with trace amounts, sulfuric acid and potassium ethoxide, were employed and discovered to have capacity of significantly increasing the reaction rate, especially for potassium ethoxide. By using these catalysts with only trace amounts, high yields over 95% were reached at the subcritical conditions which are milder than the commonly used supercritical conditions (T:275-400 ºC; P: 100-300 bar). The reaction mechanisms of the catalytic reactions under subcritical conditions were assumed to be the same as ones at conventional conditions, and were simplified to a three-step model. This model was used to fit the experimental data, and it was found that the first two steps are irreversible reactions, and the third step is reversible reaction. For each specific reaction step, the reaction rate constant for

potassium ethoxide is considerably greater than that for sulfuric acid, and the estimated activation energy of each step for potassium ethoxide is lower than that of sulfuric acid since potassium ethoxide provides a quicker reaction pathway compared to sulfuric acid. Effect of impurities of water and FFA on reaction yield were investigated. It is found that 10 vol% water based on ethanol volume and 30 wt% FFA based on oil mass increase the yield for sulfuric acid reactions, possibly due to the esterification reaction of FFA with ethanol. However, these impurities nearly terminated the reactions when potassium ethoxide served as the catalyst. Reaction mixtures of ethanol and oil formed a homogeneous state regardless of pressure change from 200 to 80 bar, and the reaction yields at all pressures were about 95%. This implies that the pressure effect is not important as long as the system is homogeneous, and that the lowest pressure to achieve homogeneity should be used to minimize operational costs in the future.

Acknowledgements

We are grateful to Syracuse University, College of Engineering and Computer Science for financial support.

4.6 References

[1] Meher L, Sagar DV, Naik S. Technical aspects of biodiesel production by transesterification—a review. Renewable and sustainable energy reviews 2006;10:248-68.

[2] Saka S, Kusdiana D. Biodiesel fuel from rapeseed oil as prepared in supercritical methanol. Fuel 2001; 80:225-31.

[3] Marulanda VF, Anitescu G, Tavlarides LL. Investigations on supercritical transesterification of chicken fat for biodiesel production from low-cost lipid feedstocks. The Journal of Supercritical Fluids 2010;54:53-60.

[4] Patil P, Deng S, Rhodes JI, Lammers PJ. Conversion of waste cooking oil to biodiesel using ferric sulfate and supercritical methanol processes. Fuel 2010;89:360-4.

[5] Gonzalez SL, Sychoski MM, Navarro-Díaz HJ, et al. Continuous catalyst-free production of biodiesel through transesterification of soybean fried oil in supercritical methanol and ethanol. Energy Fuels 2013;27:5253-9.

[6] Tan KT, Lee KT, Mohamed AR. Effects of free fatty acids, water content and co-solvent on biodiesel production by supercritical methanol reaction. The Journal of Supercritical Fluids 2010;53:88-91.

[7] Nan Y, Liu J, Lin R, Tavlarides LL. Production of biodiesel from microalgae oil (Chlorella protothecoides) by non-catalytic transesterification in supercritical methanol and ethanol: Process optimization. The Journal of Supercritical Fluids 2015;97:174-82.

[8] Deshpande A, Anitescu G, Rice P, Tavlarides LL. Supercritical biodiesel production and power cogeneration: technical and economic feasibilities. Bioresour Technol 2010;101:1834-43.

[9] Lee S, Posarac D, Ellis N. Process simulation and economic analysis of biodiesel production processes using fresh and waste vegetable oil and supercritical methanol. Chem Eng Res Design 2011;89:2626-42.

[10] Marulanda VF. Biodiesel production by supercritical methanol transesterification: process simulation and potential environmental impact assessment. J Clean Prod 2012;33:109-16.

[11] Imahara H, Minami E, Hari S, Saka S. Thermal stability of biodiesel in supercritical methanol. Fuel 2008;87:1-6.

[12] Shin H, Lim S, Bae S, Oh SC. Thermal decomposition and stability of fatty acid methyl esters in supercritical methanol. J Anal Appl Pyrolysis 2011;92:332-8.

[13] Quesada-Medina J, Olivares-Carrillo P. Evidence of thermal decomposition of fatty acid methyl esters during the synthesis of biodiesel with supercritical methanol. The Journal of Supercritical Fluids 2011;56:56-63.

[14] Liu J, Shen Y, Nan Y, Tavlarides LL. Thermal decomposition of ethanol-based biodiesel: Mechanism, kinetics, and effect on viscosity and cold flow property. Fuel 2016;178:23-36.

[15] Lin R, Zhu Y, Tavlarides LL. Effect of thermal decomposition on biodiesel viscosity and cold flow property. Fuel 2014;117:981-8.

[16] Dunn RO. Effect of oxidation under accelerated conditions on fuel properties of methyl soyate (biodiesel). J Am Oil Chem Soc 2002;79:915-20.

[17] Santana A, Maçaira J, Larrayoz MA. Continuous production of biodiesel from vegetable oil using supercritical ethanol/carbon dioxide mixtures. Fuel Process Technol 2012;96:214-9.

[18] Shin H, Ryu J, Bae S, Kim YC. Biodiesel production from highly unsaturated feedstock via simultaneous transesterification and partial hydrogenation in supercritical methanol. The Journal of Supercritical Fluids 2013;82:251-5.

[19] Zeng D, Li R, Feng M, Fang T. Continuous Esterification of Free Fatty Acids in Crude Biodiesel by an Integrated Process of Supercritical Methanol and Sodium Methoxide Catalyst. Appl Biochem Biotechnol 2014;174:1484-95.

[20] Rodriguez-Guerrero JK, Rosa PT. Production of biodiesel from castor oil using sub and supercritical ethanol: effect of sodium hydroxide on the ethyl ester production. The Journal of Supercritical Fluids 2013;83:124-32.

[21] Liu Y, Lu H, Ampong-Nyarko K, et al. Kinetic studies on biodiesel production using a trace acid catalyst. Catalysis Today 2016;264:55-62.

[22] Caldas BS, Nunes CS, Souza PR, et al. Supercritical ethanolysis for biodiesel production from edible oil waste using ionic liquid [HMim][HSO 4] as catalyst. Applied Catalysis B: Environmental 2016;181:289-97.

[23] Go AW, Sutanto S, NguyenThi BT, Cabatingan LK, Ismadji S, Ju Y. Transesterification of soybean oil with methanol and acetic acid at lower reaction severity under subcritical conditions. Energy Conversion and Management 2014;88:1159-66.

[24] Qing S, Jixian G, Yuhui L, Jinfu W. Reaction kinetics of biodiesel synthesis from waste oil using a carbon-based solid acid catalyst. Chin J Chem Eng 2011;19:163-8.

[25] Zheng S, Kates M, Dube M, McLean D. Acid-catalyzed production of biodiesel from waste frying oil. Biomass Bioenergy 2006;30:267-72.

[26] Berchmans HJ, Morishita K, Takarada T. Kinetic study of hydroxide-catalyzed methanolysis of Jatropha curcas–waste food oil mixture for biodiesel production. Fuel 2013;104:46-52.

[27] Noureddini H, Zhu D. Kinetics of transesterification of soybean oil. J Am Oil Chem Soc 1997;74:1457-63.

[28] Karmee S, Chandna D, Ravi R, Chadha A. Kinetics of base-catalyzed transesterification of triglycerides from Pongamia oil. J Am Oil Chem Soc 2006;83:873-7.

[29] Liu J, Lin R, Nan Y, Tavlarides LL. Production of biodiesel from microalgae oil (Chlorella protothecoides) by non-catalytic transesterification: Evaluation of reaction kinetic models and phase behavior. The Journal of Supercritical Fluids 2015;99:38-50.

[30] Bazaev A, Abdulagatov I, Bazaev E, Abdurashidova A, Ramazanova. A PVT measurements for pure methanol in the near-critical and supercritical regions. The Journal of supercritical fluids 2007;41:217-26.

[31] ASTM D6584-10a, Standard Test Method for Determination of Total Monoglycerides, Total Diglycerides, Total Triglycerides, and Free and Total Glycerin in B-100 Biodiesel Methyl Esters by Gas Chromatography, ASTM International, West Conshohocken, PA, 2012

[32] Lotero E, Liu Y, Lopez DE, Suwannakarn K, Bruce DA, Goodwin JG. Synthesis of biodiesel via acid catalysis. Ind Eng Chem Res 2005;44:5353-63.

[33] Choi C, Kim J, Jeong C, Kim H, Yoo K. Transesterification kinetics of palm olein oil using supercritical methanol. The Journal of Supercritical Fluids 2011;58:365-70.

[34] Kusdiana D, Saka S. Kinetics of transesterification in rapeseed oil to biodiesel fuel as treated in supercritical methanol. Fuel 2001;80:693-8.

[35] He H, Sun S, Wang T, Zhu S. Transesterification kinetics of soybean oil for production of biodiesel in supercritical methanol. J Am Oil Chem Soc 2007;84:399-404.

[36] Darnoko D, Cheryan M. Kinetics of palm oil transesterification in a batch reactor. J Am Oil Chem Soc 2000;77:1263-7.

[37] Diasakou M, Louloudi A, Papayannakos N. Kinetics of the non-catalytic transesterification of soybean oil. Fuel 1998;77:1297-302.

Chapter 5. Continuous esterification of oleic acid to ethyl oleate under sub/supercritical conditions over γ-Al_2O_3

5.1 Abstract

Esterification of oleic acid with ethanol was conducted under subcritical and supercritical conditions in a packed-bed reactor containing γ-Al_2O_3. The presence of γ-Al_2O_3 significantly improved the reaction rate such that the 42% yield achieved at 325 ºC, 200 bar, and 1-min residence time without the alumina was increased to 98% at the same conditions when alumina was present. The catalytic capacity was attributed to Lewis acid sites on the surface of alumina, and non Brønsted acid sites were detected. Experiments to study the kinetics were executed at a pressure of 200 bar, elevated temperatures (200, 225, 275, 300, and 325 ºC), and residence times of half to 8 minutes. Mass transfer limitations were estimated to be negligible via the Mears and Weisz-Prater criteria. Kinetic analysis based on the one-step model demonstrates that the overall reaction was endothermic, and an Eley-Rideal (ER) reaction mechanism was proposed to describe each elementary reaction step. The stability of γ-Al2O3 on product conversion was tested via a 25-hour operation under 325 ºC, 200 bar, and 1-min residence time, and decrease of the conversion was not observed. However, results of the catalyst analytical characterization shows a decrease of the acid site density and surface area, supporting the occurrence of catalyst degradation. The addition of water slightly decreased the yield, while the pressure change from 200 to 100 bar did not have an obvious effect on the conversion.

5.2 Introduction

Considerable amounts of wastewater is generated in biodiesel industry in order to remove the dissolved homogeneous catalysts from the product [1, 2]. Plus, the production cost of

biodiesel is expensive, since current industry uses refined soybean oil as the feed stock considering the homogeneous catalysts are sensitive to the presence of free fatty acids and water which are present in cheap low-quality oils [3]. These problems could be solved via subcritical and supercritical method (SC). The SC conditions are created by increasing the reaction temperature and pressure to values near or above the critical point of alcohol. Under such severe conditions, the properties of alcohol are changed such as density of hydrogen bonding in alcohols significantly decreases, and alcohols become nearly non-polar [4, 5, 6]. These changes contribute to the mixing of alcohols and oils to have the reactions performed in a homogeneous reaction phase which minimizes mass transfer resistance and therefore significantly increases the reaction rate. The high reaction temperatures also benefit the reaction rate. Due to the fast reaction rate under SC conditions, it is possible to perform the reactions non-catalytically, which eliminate the contamination problem as mentioned above. Besides, SC method could be more economically competitive compared to current industrial technology [7, 8], since it can directly use low-quality and low-cost oils and hydrous alcohols [9, 10, 11].

However, biodiesel fuel will be easily thermally decomposed when temperature exceed 350 ^{o}C [12, 13], which further degrades fuel qualities [14, 15, 16]. In order to complete the SC reactions at temperatures lower than 350 ^{o}C in short reaction times to avoid decomposition reactions, one can add catalysts into the SC reaction media. Some researchers showed that a near complete yield was reached at 225 ^{o}C, 200 bar and 5 minutes by adding trace amount of strong basic homogeneous catalysts [17]. Stable heterogeneous (solid) catalysts are also expected to provide a similar product yield under the SC conditions.

Solid catalysts can be acidic or basic. The popular basic catalysts include hydroxides, dolomites, hydrotalcites, mixed basic metal oxides, loaded and supported alkaline elements and

oxides, which are commonly used under conventional conditions in biodiesel synthesis. In specific, CaO-based compounds including pure CaO [18] and loaded CaO [19, 20], and potassium-based compounds including loaded KF [21], KI [22], and KOH [22] have drawn numerous attention due to their high activity and wide availability. Other alkaline metal oxides such as MgO [23], ZnO [24] and SrO [24] are also studied by different researchers. Even though high product yields were reached by applying these basic catalysts, serious leaching problems were found and the active compounds were detected in biodiesel product with high concentrations even at the mild conditions. The acidic catalysts to synthesize biodiesel include acidic metal oxides [25], sulfated/ tungstated metal oxides [26, 27, 28, 29, 30], sulfonic ion-exchange resin, heteropolyacids, zeolites, and etc. Since the catalytic capacity of the acidic solids is lower than solid bases, the reactions with the acids were executed under severer conditions. Similarly, most of the acidic solids were not stable under the reaction conditions due to leaching and other issues, despite high yields were achieved initially.

A literature review indicates that several synthesized compounds were found to be relatively stable even at temperatures higher than 190 ^{o}C including Zr-SBA-15 [31], $ZnAl_2O_4$ [32], and $ZnO–TiO_2–Nd_2O_3/ZrO_2$ [33]. Zr-SBA-15 (mixture of zirconia and mesoporous silica) was tested by Melero et al. in a packed-bed reactor at 210 ^{o}C, 70 bar, and residence time of 30 min that the reaction yield reached 96% with negligible catalyst leaching [31]. Biodiesel yield of 70% was obtained at 210 ^{o}C and 4-h reaction time in a batch reactor containing $ZnAl_2O_4$ reported by Pugnet et al. [32]. Zinc leaching was very low that no more than 4 ppm by weight were detected in the ester phase after 6 h of contact time. By conducting the reactions in a packed-bed reactor over ZnO-TiO2-Nd_2O_3/ZrO_2 at 200 ^{o}C and 69-min residence time, 95% biodiesel yield

was reported by Kim et al., and the leaching of ZnO was determined to be negligible by ICP analysis [33].

Some simple and largely available metal oxides such as titania, zirconia and alumina have been commonly used as catalyst supports due to their thermal and mechanical stability even at SC conditions. However, they did not show any catalytic ability under conventional conditions (T=70 ^{o}C, ambient pressure) due to their weak acidic properties. McNeff et al. reported that under SC conditions, reactions with alumina, zirconia, and titania, reached conversions over 90% at 360 ^{o}C and 200 bar [34]. However, the temperatures proposed were too severe, since biodiesel is rapidly decomposed at temperature higher than 350 ^{o}C [12, 13, 14, 15]. Due to the very limited information, the optimal SC conditions for biodiesel production over the simple metal oxides are still unknown.

Generally speaking, information regarding synthesizing FAEEs biodiesel fuel under SC conditions with heterogeneous catalysts is very limited. Besides, kinetics of the alcoholysis with heterogeneous catalysts under SC conditions are rarely reported in the literature, although kinetic studies for biodiesel production at conventional conditions with heterogeneous catalysts have received much attention over the past few decades [35, 36, 37, 38, 39, 40, 41, 42, 43, 44].

Accordingly, this study aims to (1) explore the possibility of converting free fatty acids, which largely exist in waste cooking oils and animal tallows, to biodiesel fuel under SC conditions at short residence times over alumina powder, and (2) to study the kinetics for the catalytic reaction systems, neither of which is well addressed in the literature. The reactions were performed in a packed-bed reactor containing γ-Al_2O_3 under SC conditions (temperature from 200 to 325 ^{o}C, and pressure from 100 to 200 bar).

5.3 Experimental

5.3.1 Material

Anhydrous ethanol (200 proof, 100 vol%) was purchased from Pharmco-Aaper. Oleic acid, GC analytical standards for oleic acid and ethyl linoleate, white quartz (50+70 mesh), n-methyl-n-(trimethylsilyl) trifluoroacetamide (MSTFA) (GC derivatization synthesis grade), and pyridine were purchased from Sigma Aldrich. n-Heptane (HPLC grade) was provided by Thermo Fisher Scientific. Deactivated glass wool used in reactor packing was purchased from Restek Corporation. Gases (ultrahigh purity grade) used in GC, FTIR, and TPD analysis were supplied by Airgas. γ-Al_2O_3 was provided by Acros in neutral form.

5.3.2 Catalyst characterization

Powder XRD investigation was performed using a Bruker D8 Advance ECO powder diffractometer with Cu Kα radiation (λ=0.154 nm) at 40 kV and 25 mA with a step size of 0.02 in the 2θ angle range of 15-70^o.

Scanning electron microscope (JEOL) was utilized to physically observe the morphology of the fresh and spent catalyst.

N_2 adsorption-desorption isotherms were conducted by Micromeritics ASAP 2020 (adsorption of N2 at 77 K). Prior to N_2 dosing, samples were degassed under vacuum (423 K, 8 h). Brunauer-Emmett-Teller (BET) and t-plot analyses were used to determine total and micropore surface areas. Barrett-Joyner-Halenda (BJH) analysis of the adsorption branch of N_2 isotherms was used to determine pore size distributions and average pore diameters. Pore volumes were calculated from cumulative nitrogen uptake at a relative pressure of 0.99.

Density of Lewis acid sites was determined from temperature programmed desorption (TPD) of ammonia [45]. Typically, approximately 70 mg of sample was inserted into a 1/2 inch

quartz tube between two quartz wool (Grace) end plugs and the whole tube was further placed in an Omega furnace. The temperature of the furnace was regulated by a process controller (Love, series 16A) and monitored by a type K thermocouple (Omega). All samples were calcined (4h, 723K, 3K/min) under air flow (50 sccm) before analysis. After cooling to 423K, samples were purged in dry He flow (100 sccm) for more than 90 minutes. Catalysts were further dosed with ammonia (1% ammonia and 1% argon, Airgas) flow. After saturation of ammonia on the surface, physically adsorbed ammonia was removed by applying a high He flowrate (400 sccm) for at least 1 hour. The furnace was then ramped to 973K (10 K/min) under He including 1% Ar serving as an internal standard. Chemisorbed ammonia was removed after ramping. During the whole process, a mass-selective residual gas detector (Stanford Instruments RGA 100) was used to track MS signals of ammonia (m/z=16) and Ar (m/z=40) in the effluent.

Brønsted acid sites to Lewis acid sites ratio was determined using pyridine FTIR (Nicolet 6700 DTGS detector). 15-25 mg of catalysts were pressed into a 13mm pellet through a hydraulic press. The pellet was loaded on an in-situ cell, designed and built in house. Samples were calcined as the procedure described before. Subsequently, the cell was cooled to 423K, and purged under a flow of 60 sccm of He. The He was purified by a liquid nitrogen trap followed by a moisture trap. The pellet was then dosed with 4 torr of pyridine (Sigma Aldrich, 99%). After the pellet was fully saturated, the cell was purged under a He flow of 200 sccm at 423K to remove physically adsorbed pyridine. Spectra were collected at 423 K. and Brønsted to Lewis ratios were determined by the ratio of the integrated IR bands at 1545 cm-1 (pyridimium ion) and 1455 cm-1 (pyridine) respectively, by applying the appropriate molar extinction coefficients [46]. However, the prime quantities of interest in this study are Lewis site densities since no

Brønsted acid sites was detected. The operation procedures for FTIR and TPD can be also found as described in prior publications, respectively [47, 48].

5.3.3 Esterification reactions under SC conditions

Esterification reactions of oleic acid with ethanol were executed in a downflow tubular reactor (316SS, ID 4.57 mm*25 cm). The γ-Al_2O_3 catalyst bed was held in place by two quartz wool plugs. The tube upstream and downstream of the catalyst bed was packed with white quartz to minimize dead volume.

Temperature (200-325 ^oC), pressure of 200 bar, and ethanol-to-oleic acid molar ratio of 18:1 were employed to perform experiments for the kinetics study. For temperature at 325 ^oC, pressures ranging from 100 to 200 bar were applied to investigate the pressure effect. The reaction residence time ranged from half to ten minutes. During experiments, oleic acid and ethanol were pressurized and transported using high pressure syringe pumps (Teledyne ISCO 260 D), preheated by heating tapes, mixed by passing through a mixing tee, and flowed into the reactor which was heated by an electrical furnace (Briskheat). The entire experimental set-up for conducting the reactions was similar as employed in our previous study, except for the reactor, including high-pressure syringe pumps, furnace, temperature controllers, thermocouples, back-pressure regulator, and data acquisition system [49]. The experimental errors were determined within 5%. Collected samples were washed with distilled water before GC analysis to remove the dissolved ethanol.

Desired residence time was reached by precisely controlling pump flow rates, and it was defined as

$$\tau = \frac{V_B \cdot \varepsilon}{F_E \cdot (\rho_E/\rho'_E) + F_O \cdot (\rho_O/\rho'_O)} \qquad \text{Eq 5-1}$$

where V_B is volume of the empty-bed reactor, ε is the fraction of void to bed volume and it was experimentally determined by immersing the catalytic bed in ethanol. F is volumetric flow rate provided by the pumps, ρ is density of the oleic acid and ethanol (pump temperature, pump pressure), ρ' is density of the oleic acid and ethanol at reaction conditions, whose values are determined from the literature [50]. E and O represent ethanol and oleic acid, respectively.

The mixing of ethanol-oleic acid streams before reaching the packed-bed was physically observed through a view-cell system which consists of high pressure pumps (Teledyne ISCO 260 D), high pressure view-cell, a charge-coupled-device (CCD) camera with a micro-lens (Photron, model# FASTCAM-512PCI), light source, and data acquisition system. This experimental setup was also used in our previous study [49].

5.3.4 Biodiesel sample analysis

For the analysis of the FAEE profile, biodiesel samples were prepared by diluting 4 µl biodiesel into 1 ml heptane, making a total biodiesel concentration of 4000 ppm by volume. The samples were derivatized using MSTFA based on procedures provided in ASTM D6584 [51]. Quantitative analysis to measure the concentration of FAEE and oleic acid was conducted via a GC FID (HP 5890 Series II) equipped with an autosampler (HP 5890 Series II) and a DB-WAX column (30 m × 0.32mmID × 0.50 µm, Restek) at splitless mode. Calibration curves for each compound were prepared by diluting the GC standards. The temperature program was as: held at 60 °C for 2 min, ramp at 6 °C/min from 60 °C to 240 °C, and held at 240 °C for 30 min. Concentrations of ethanol and water were determined from mass balance calculations since the initial concentration of ethanol and oleic acid were known (MR of 18:1) and the concentration of oleic acid and FAEE in the collected samples were measured from GC FID analyses.

5.4 Results and discussion

5.4.1 Mixing of ethanol-oleic acid streams

Mixing phenomena of ethanol-oil streams was studied during the heating and pressurizing process via a view-cell experimental setup in order to determine the significance of mass transfer resistance on conversion. Selected results are reported in **Figure 5-1**. It is known that at ambient conditions, ethanol is only partially miscible with oleic acid. Elevating the temperatures (175-325 ^{o}C) and pressure (80-200 bar), the ethanol-oleic acid mixtures formed a homogeneous state, which indicates that at the selected reaction conditions (T: 200-325 ^{o}C, P: 100-200 bar) the reaction streams were in a homogeneous phase before contacting with the packed-bed, and accordingly mass transfer resistance between ethanol and oleic acid boundaries could not be significant.

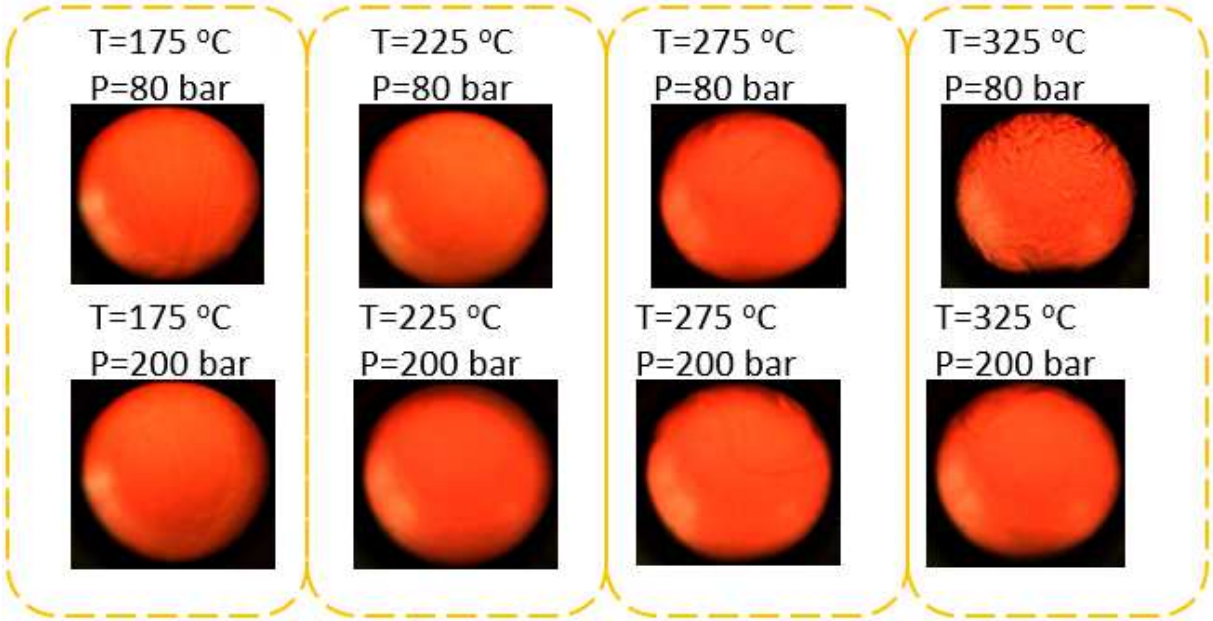

Figure 5-1. Mixtures of ethanol-oleic acid (EtOH/OA molar ratio of 18) flowing through a view cell (V ~ 1 ml) at various conditions (T = 175–325 ◦C, P = 80-200 bar)

5.4.2 Preliminary investigation on esterification of oleic acid over γ-Al_2O_3

Preliminary experiments using γ-Al_2O_3 were executed and compared with non-catalytic reactions in order to determine if the weak solid acid would perform well in this reaction system. As shown in **Figure 5-2**, at temperature of 200 °C, pressure of 200 bar, and residence time of 8 min, the yield for non-catalytic reactions was only 17%, while the yield was increased to 49% when γ-Al_2O_3 was employed. Similarly, at temperature of 225 °C and residence time of 5 min, the yield was increased from 24% to 62% when switching from non-catalytic to γ-Al_2O_3. Due to the weak acid property of alumina, the yield of the esterification reaction was not satisfying under the subcritical conditions in short residence times. The performance of the alumina was significantly enhanced under supercritical conditions. At 275 °C and 200 bar, the reaction with alumina reached a yield of 95% in three minutes compared to a non-catalytic yield of 40% at same condition. At 300 °C and 2 min, the yield of alumina-catalyzed reaction was 98% compared to a yield of 48% for the non-catalytic reaction. Similarly, at 325 °C and 1 min, near complete yield was obtained with alumina while only 42% was reached by non-catalytic reaction. The results above demonstrate a high catalytic capacity of γ-Al_2O_3 for the esterification reaction under supercritical conditions. No by-product was observed.

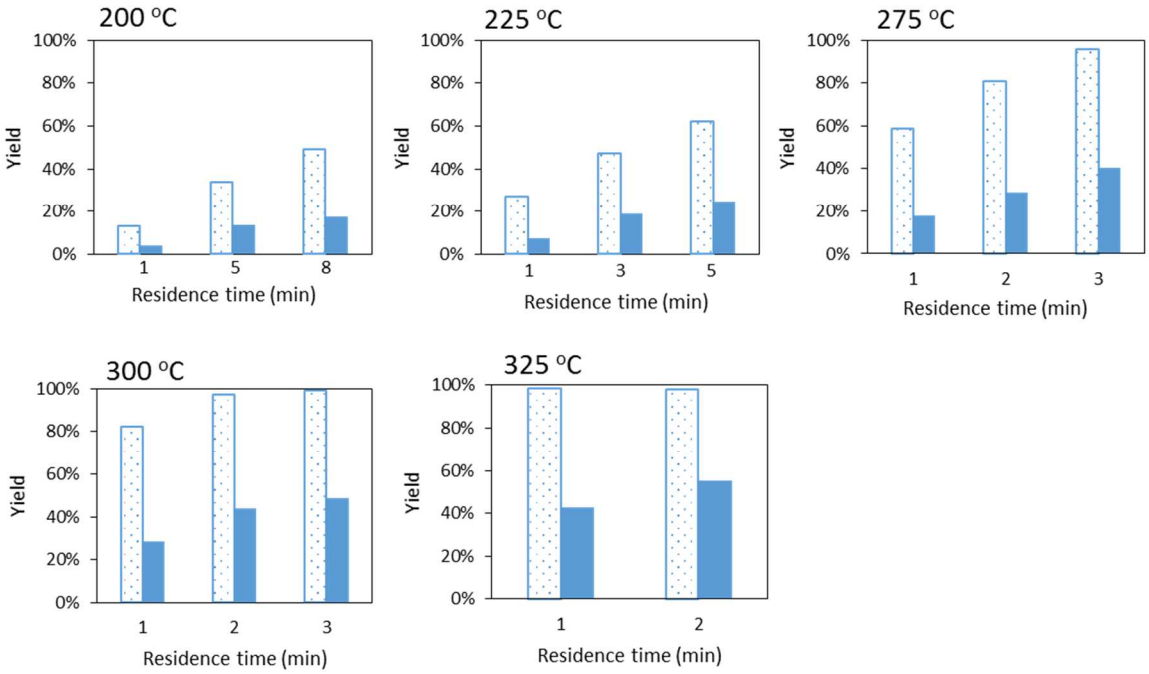

Figure 5-2. Comparison of biodiesel yield of the reaction catalyzed by alumina with the one without any catalysts. The reaction pressure was fixed at 200 bar.

5.4.3 Kinetics of esterification of oleic acid over γ-Al_2O_3

The reaction mechanism of esterification over heterogeneous Lewis acid was well described in the literature [52]. Similarly, in this study the mechanism, Eley-Rideal (ER), of the esterification reaction taking place between oleic acid and ethanol over γ-Al_2O_3 is proposed here as shown in **Figure 5-3**. The carbonyl group in oleic acid molecule is adsorbed on acidic site of the alumina surface which has positive formal charge. The interaction of the carbonyl oxygen of oleic acid with acidic site of the catalyst forms carbocation, which makes the adjoining carbon atom susceptible to nucleophilic attack. Then the oxygen atom in ethanol molecule attacks the carbocation to form a tetrahedral intermediate. Then the tetrahedral intermediate eliminates the water molecule via the esterification reaction to form one molecule of ethyl oleate. In the last step, the catalyst is regenerated by desorbing ethyl oleate from the Lewis acid site.

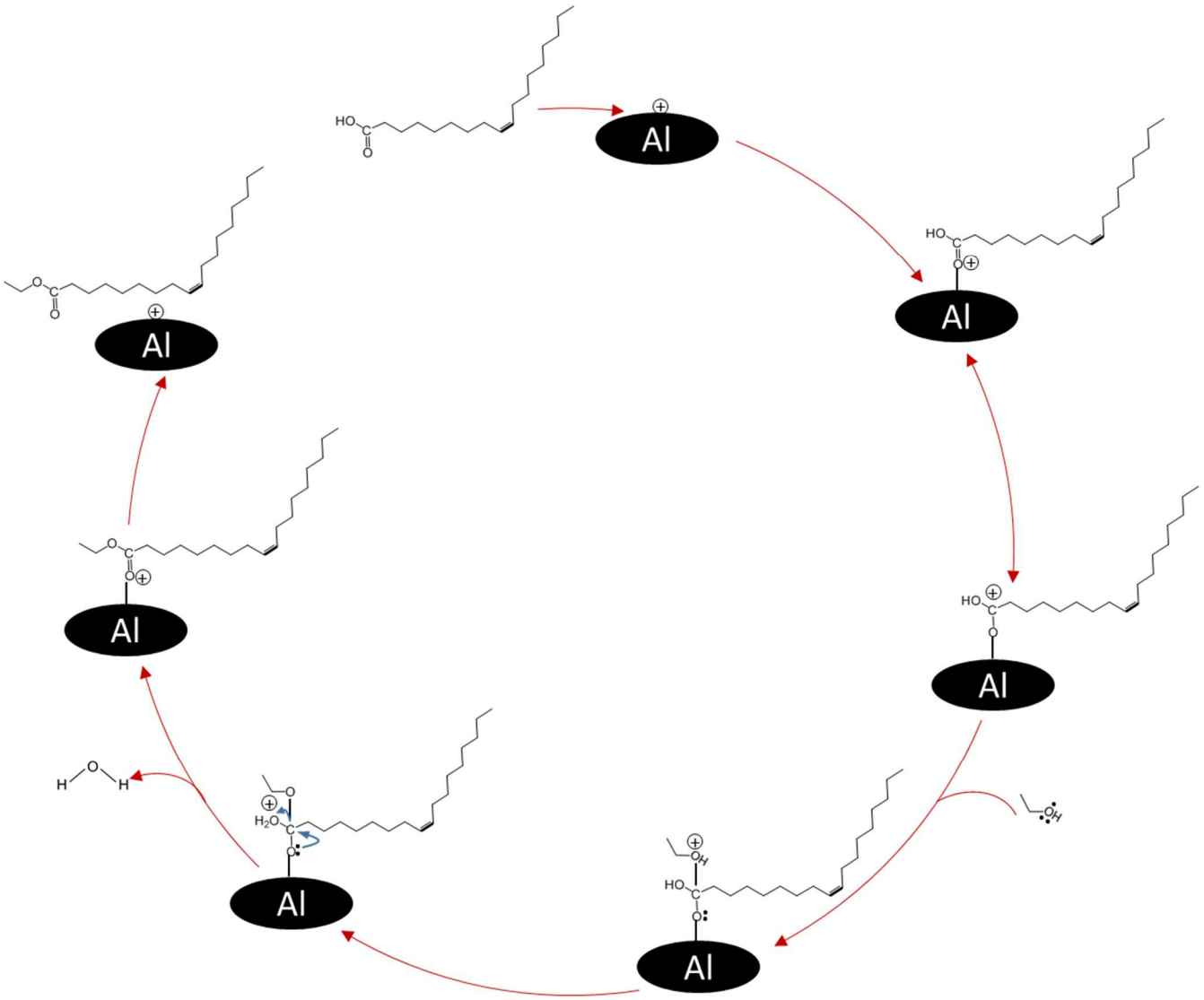

Figure 5-3. Mechanism of esterification of oleic acid with ethanol over alumina catalyst.

Data points in **Figure 5-4** illustrate the concentration profile of each compound including the original reactants, oleic acid (OA) and ethanol, and final products ethyl oleate (FAEE) and water produced at 275-325 ^{o}C with γ-Al_2O_3. As expected, concentration of OA and ethanol were decreasing along with reaction time, whereas that of FAEE and water increased over time. At the last stage of conducted reactions, the amount of OA was reduced to a negligible level under supercritical conditions, however significant amounts still remained under the subcritical

reactions. Specifically, at 275 ºC and 5 min, 300 ºC and 3 min, and 325 ºC and 1 min, most of OA was reacted providing yields over 98% as shown in **Figure 5-4**. However, trace amount of OA was still detected at these temperatures even if the residence time was extended, which implies the esterification reaction was reversible and had reached equilibrium. Also, the temperature changing from 275 to 325 ºC did not influence the final equilibrium significantly which indicates the reaction could be thermally neutral. Lower temperatures make the reactions perform with slower reaction rate. At 200 and 225 ºC with an 8-min residence time, a yield of only about 49% and 79% was reached, respectively, as calculated from data in **Figure 5-5**.

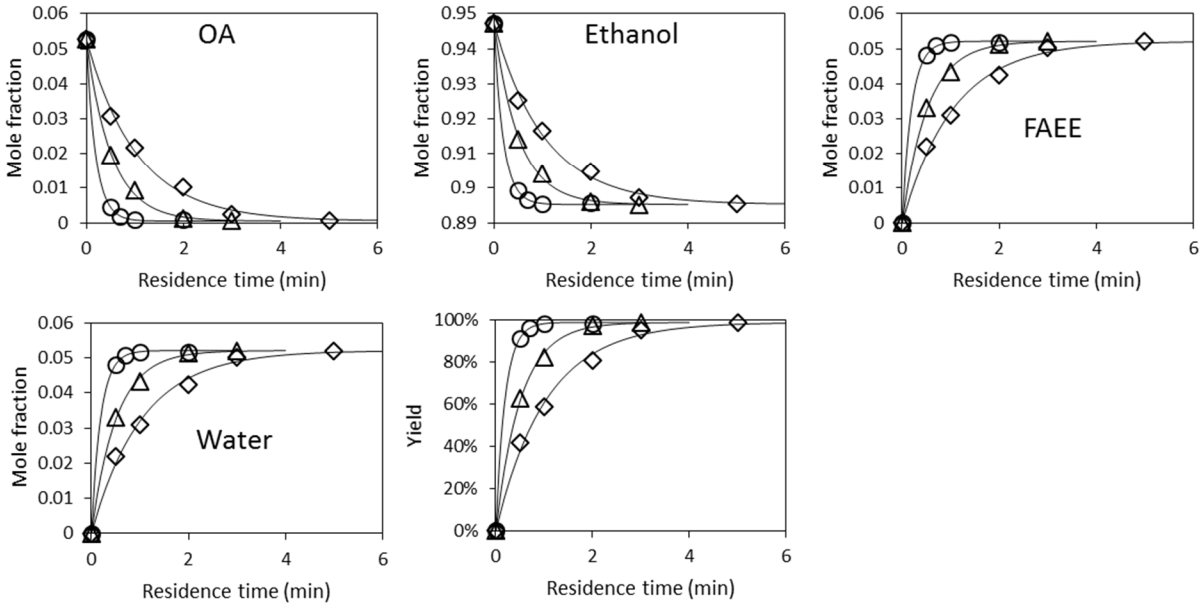

Figure 5-4. Data fitting by the one-step classic model under SC conditions (T: 275-325 ºC, P: 200 bar). Key: (◊) 275 ºC, (Δ) 300 ºC, (○) 325 ºC.

Theoretical analysis of transport limitations in the packed-bed reactor are discussed in supplementary material at the end of this chapter. Mears, as shown in Eq5-2, and Weisz–Prater,

as shown in Eq5-3, criteria were employed to estimate the interphase mass transfer limitations and intraparticle diffusion limitations, respectively, which were determined to be negligible.

$$\frac{-r_A \rho_b Rn}{k_c C_{Ab}} < 0.15 \qquad \text{Eq5-2}$$

where $(-r_A)$ is the rate of the reaction per bed volume (kmol/kg cat/s), ρ_b is the bulk density of catalyst bed (kg/m^3), R is the average radius of catalyst particles (m), n is the order of the reaction; C_{Ab} is the bulk concentration of the reactant oleic acid (kmol/m^3), and k_c is the mass transfer coefficient (m/s).

$$\frac{-r_A \rho_c R^2}{D_e C_{AS}} < 1 \qquad \text{Eq5-3}$$

where ρ_c is solid density of catalyst bed (kg/m^3), C_{AS} is the reactant concentration on alumina surface (kmol/m^3), D_e is the effective diffusivity of oleic acid in methanol.

By neglecting the external and internal mass transfer resistance and assuming a steady state and 2D scenario, the pack-bed reactor model was simplified from Eq5-4 to Eq5-5.

$$D_{AB}\left(\frac{\partial^2 C_A}{\partial x^2} + \frac{\partial^2 C_A}{\partial y^2} + \frac{\partial^2 C_A}{\partial z^2}\right) - U_x \frac{\partial C_A}{\partial x} - U_y \frac{\partial C_A}{\partial y} - U_z \frac{\partial C_A}{\partial z} + r_A = \frac{\partial C_A}{\partial t} \qquad \text{Eq5-4}$$

$$-U \frac{dC_{Ab}}{dz} + r_A = 0 \qquad \text{Eq5-5}$$

In order to perform the macroscopic kinetic analysis of the esterification reaction, a one-step reversible reaction model, as shown Eq5-6, with second order was used to predict the global kinetic parameters and simulate the experimental data. Accordingly, the reaction rate can be expressed as Eq5-7.

$$OA + C_2H_5OH \underset{k_{-1}}{\overset{k_1}{\longleftrightarrow}} FAEE + H_2O \qquad \text{Eq5-6}$$

$$r = k_1(C_{OA} \cdot C_{EtOH} - \frac{1}{K} C_{FAEE} \cdot C_{water}) \quad \text{Eq-7}$$

The simulation results for the supercritical reactions (T: 275-325 ºC, P; 200 bar) are plotted in **Figure 5-4** as solid curves which show a good data fitting. The estimated k values are reported in **Table 1** with the corresponding standard deviations. Then data of the subcritical reactions (T: 200 and 225 ºC, P; 200 bar) are compared with ones predicted by the model where the k values were estimated by using the Arrhenius Equation which was determined by data of the supercritical reactions. The result is shown in **Figure 5-5**, and it demonstrates a good predictability of the model.

Table 5-1. Estimated reaction rate constants for the one-step model

	k_1 ± S.D.[a]	**k_{-1} ± S.D. [a]**
200 ºC	0.089 [b]	0.046 [b]
225 ºC	0.230 [b]	0.093 [b]
275 ºC	1.015 ± 0.056	0.328 ± 0.237
300 ºC	2.078 ± 0.035	0.526 ± 0.212
325 ºC	5.554 ± 0.069	1.160 ± 0.109

a: standard deviation

b: The values for 200 and 225 ºC were estimated by using the Arrhenius Equation which was determined by the k values for 275-325 ºC.

The regressed values of K, the equilibrium constants, were plotted by the Van't Hoff equation, and the result shows a reasonable linearity with a R^2 of 0.98. Accordingly, the macroscopic reaction was experimentally found to be moderately endothermic ($\Delta H° = 15.9$ kJ mol−1) and entropically favorable ($\Delta S°=39.3$ J mol−1 K−1). Qualitatively, these values are consistent with-albeit higher than analogous thermochemistry estimated from a simulated equilibrium ($\Delta H° \approx 11$ kJ mol−1) [37]. The activation energy for the forward and reverse step is determined by applying the Arrhenius Equation as 74.9 and 58.9 kJ mol−1, respectively.

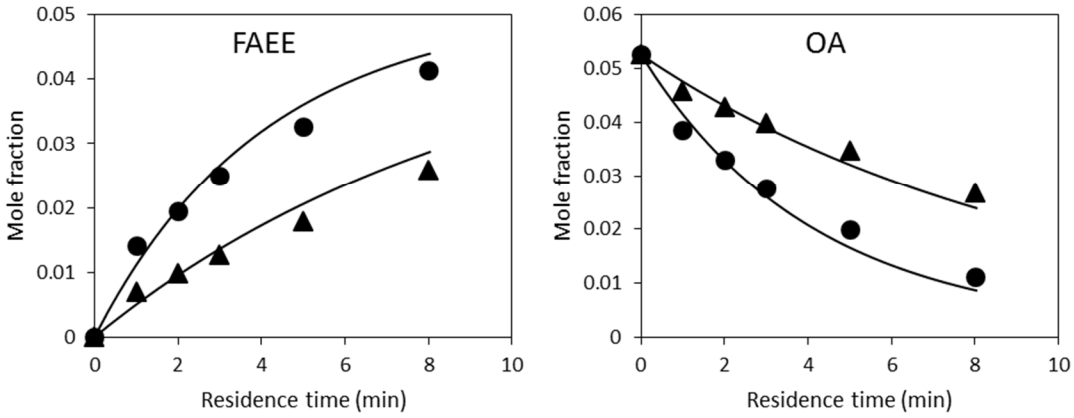

Figure 5-5. Data fitting by the one-step classic model under subcritical conditions (T: 200-225 ºC, P: 200 bar). Key: (▲) 200 ºC, (●) 225 ºC.

Based on the Eley-Rideal (ER) reaction mechanism discussed above in **Figure 5-3**, the elementary steps can be described as below. In this case, we consider that all adsorption and reaction steps involve a single type of active site, which is designated here as '∗'. In this sequence, a molecule of oleic acid (OA) adsorbs at a Lewis site (∗) on the surface as expressed in Eq5-8, then an ethanol molecule attacks the oleic acid to form one mole of ethyl oleate via esterification as written in Eq5-9. Finally, the catalyst is regenerated after desorbing ethyl oleate from the Lewis acid site as shown in Eq5-10. Accordingly, the equation of reaction rate can be expressed as in Eq5-11 if assuming the rate controlling step is the adsorption of oleic acid.

$$OA + * \xleftrightarrow{K1} OA* \qquad \text{Eq5-8}$$

$$OA* + C_2H_5OH \xleftrightarrow{K2} FAEE* + H_2O \qquad \text{Eq5-9}$$

$$FAEE* \xleftrightarrow{K3} FAEE + * \qquad \text{Eq5-10}$$

$$r = \frac{k_1(K_1K_2K_3C_{EtOH}C_{OA} - C_{FAEE}C_{WATER})}{K_1K_2K_3C_{EtOH} + K_1C_{FAEE}C_{WATER} + K_1K_2C_{FAEE}} \qquad \text{Eq5-11}$$

The data were fitted to calculate the reaction rate and equilibrium constants at each step via least-squares regression. The results indicate a good fit in terms of R^2 values over 0.995. Unfortunately, considering that the total number of data points were relatively limited, wide confidence intervals for the regressed kinetic parameters including K_1, K_2, and K_3 were found when employing this complicated model, so we currently are not able to regress all sets of the kinetic parameters from the experimental data to provide meaningful values. By conservative analysis using the Van't Hoff equation, the adsorption of oleic acid on the surface of alumina was estimated to be exothermic, the esterification and desorption of ethyl oleate from alumina were endothermic reactions. And the overall process in terms of a combination of the three elementary steps is endothermic based on the analysis from the one-step model.

5.4.4 Stability of the alumina catalyst under supercritical conditions

In order to determine the stability of the alumina catalyst under supercritical conditions, the pack-bed was utilized to carry out the esterification reaction at 325 ^{o}C, 200 bar, and 1-min reaction time continuously for 25 hours. Multiple biodiesel samples were collected and measured along with the process, and a decrease of the yield was not observed during this 25-hour test, as shown in **Figure 5-6A**. However, this does not prove the stability of the alumina catalyst, and it is very possible that there was more than enough catalyst in the reactor so the deactivation was not measurable even if it were occurring. Instead, the catalyst was taken out from the reactor, and analyzed by different characterization tools as below.

The XRD analysis, as shown in **Figure 5-6B**, tells that the fresh alumina was in gamma phase, and the spent alumina still remained in gamma phase, which demonstrates a stable crystal structure. In **Figure 5-6C** and **5-6D**, the morphology of the catalyst did not change obviously as observed by SEM analysis at different magnification.

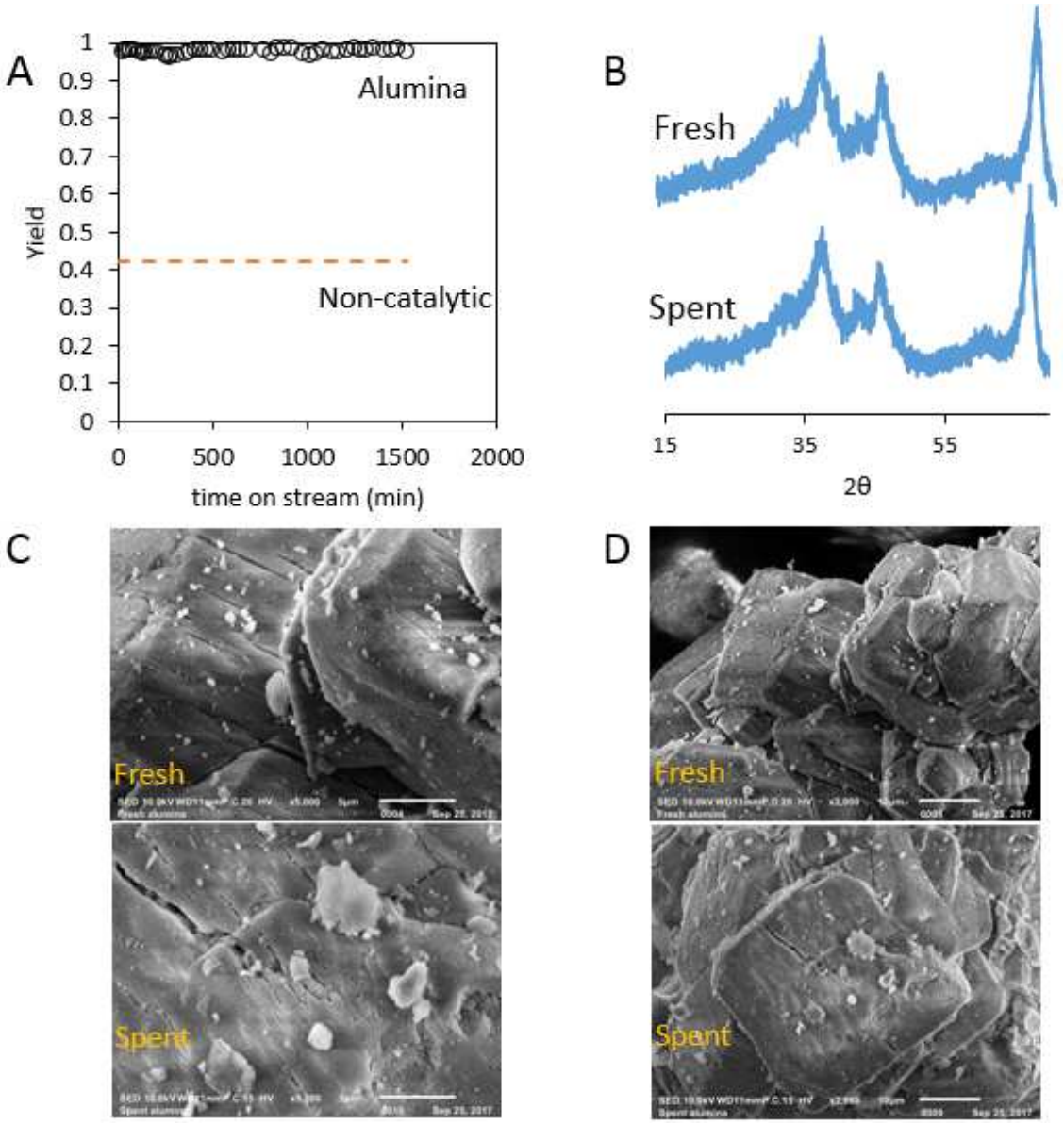

Figure 5-6. (A) Yield of biodiesel samples collected during the stability test at 325 °C, 200 bar, and 1-min residence time. (B) XRD analysis of the spent alumina catalyst before and after the stability test. Comparison of SEM analysis between fresh and spend alumina catalyst at magnification of (C) 5000 and (D) 2000.

However, data from BJH adsorption curve in **Figure 5-7A** clearly show a decrease of pore distribution between 3 and 7 nm pore-diameter after being treated under the supercritical reaction. The BET surface area decreased from 126.7 to 99.2 m^2/g, and BJH pore volume changed from 0.24 to 0.19 cm^3/g after the continuous reaction, as shown in **Table 5-2**. By

conducting the TPD analysis, we observed the Lewis acid site density dropped from 28.35 to 17.15 umol/g after the test, as also shown in **Figure 5-7B**. The cause could be due to carbon deposition, since we do observe the color of the alumina catalyst turned from white to gray. The mechanism and kinetics of the alumina degradataion will be included in future work by utilizing a differential reactor instead of a fully packed reactor.

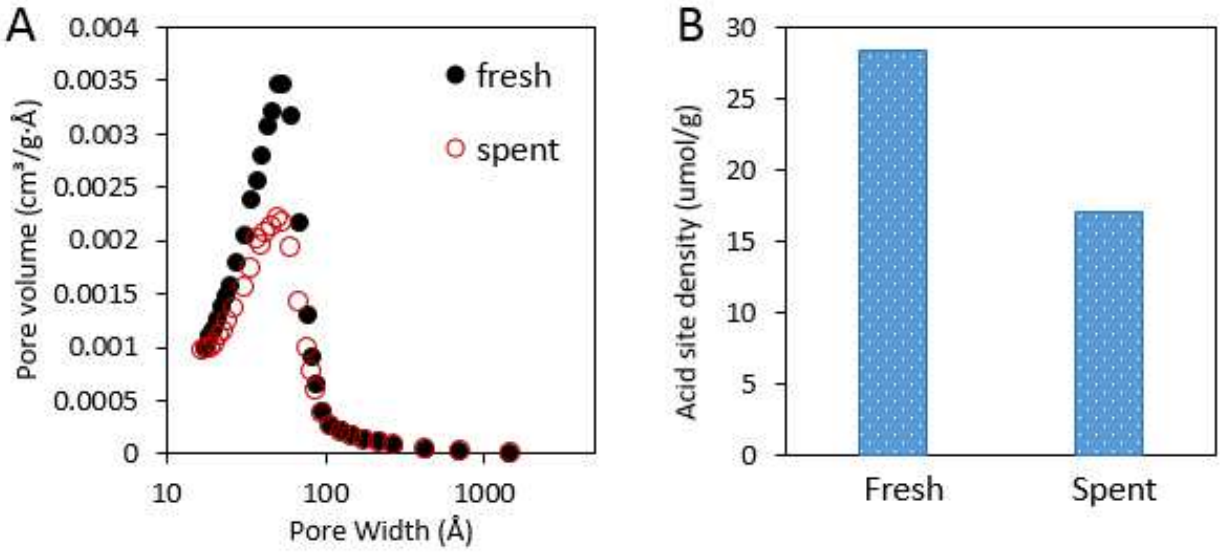

Figure 5-7. (A) BJH adsorption comparison and (B) Lewis acid sity density comparison between fresh and spent catalyst.

Table 5-2. Physical properties comparison of the alumina catalyst before and after the stability test.

	Lewis acid site density (umol/g)	**Bronsted acid site density (umol/g)**	**BET surface area (m^2/g)**	**BJH Pore volume (cm^3/g)**	**BJH Pore size (nm)**
Alumina before reaction	28.35	0	126.72	0.24	59.32
Alumina after reaction	17.15	0	99.16	0.19	59.16

5.4.5 Effect of water and pressure on the reactions

More than half cost of biodiesel fuel comes from refined oil and anhydrous alcohol costs which are required by the conventional biodiesel industry, since common impurities in the feedstocks of water and free fatty acids (FFA) deactivate the homogeneous catalysts as FFA react with base catalysts via saponification reactions, and water poisons both base and acid catalysts under conventional biodiesel synthesis conditions. Usually water content in cheaper feedstocks as waste cooking oil and hydrous ethanol before pretreatment exceeds 3 wt%. Accordingly, in this study, ethanol solution which contains 10 vol% water was used to study water effect on the reactions. As shown in **Figure 5-8A**, when conducting reactions at 325 and 300 °C, increasing water content in the ethanol from zero to 10 vol% making the yield decrease from 99% to 90%, and from 84% to 72% at 1 min, respectively. The yield decreasing could be due to that the large presence of water shifted the equilibrium to the left via hydrolyzing the FAEE to oleic acid since water is one of the product besides FAEE, or that it turned the reaction phase less homogeneity which increased the mass transfer resistance of the reaction system. Also as reported in the literature, the alumina will be turned into a hydrated boehmite (AlOOH) phase, and the acidity and surface area will be decreased under treatment of sub/supercritical water conditions [53]. Accordingly, water should be eliminated from the feedstock by pretreatment in order to prevent the yield from decreasing either from equilibrium shifting or alumina degradation by water.

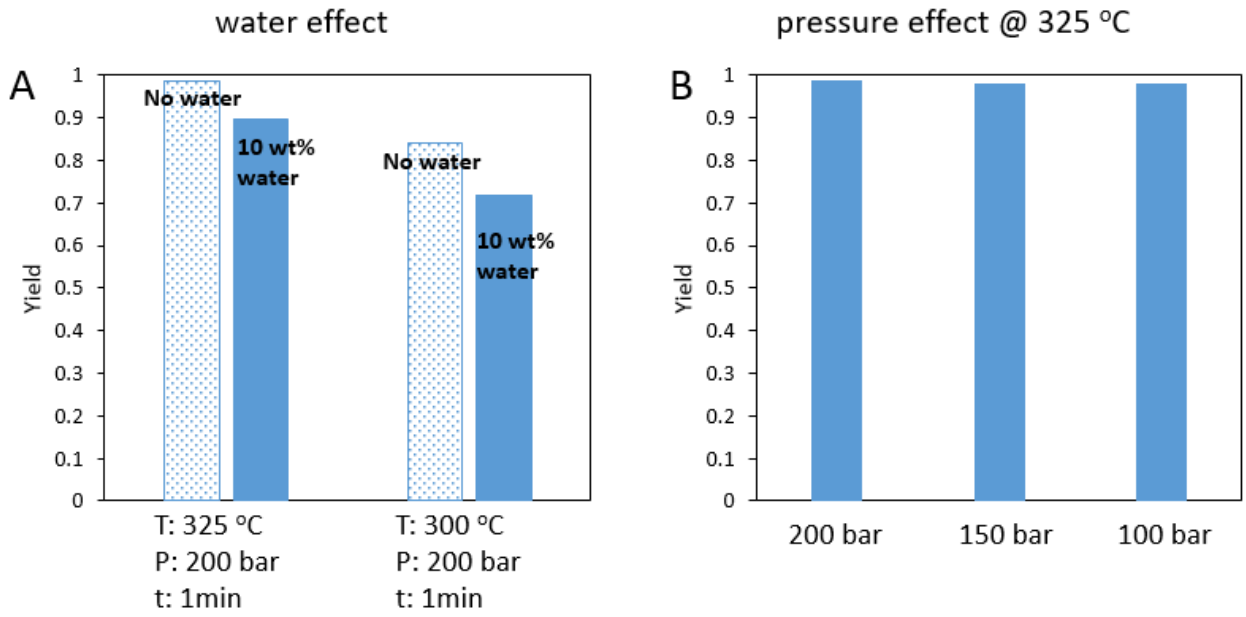

Figure 5-8. Effect of water and pressure on product yield.

High pressures of 150–300 bar are commonly used in studies related to sub/supercritical biodiesel synthesis in order to pressurize the reaction system into a homogeneous state. These required high pressure would bring potential safety issues and increase the cost of equipment. Adding co-solvent can improve solubilization of the alcohol-oil stream, but this also increases the product purification burden. In this study, pressure effect on reaction yield at supercritical conditions were investigated. As shown in **Figure 5-8B**, at the stated conditions (T: 325 °C, t: 1 min, EtOH-Oil molar ratio: 18), pressure range from 100 to 200 bar on yield was evaluated. The yield was monitored as nearly constant as 98%. The mixing of ethanol-oil stream was observed by the view-cell set-up, and it was found that in this pressure range the mixture formed a homogeneous state before contacting the packed-bed. This result demonstrates that the reaction yield will not be effected by pressure change as long as such change does not influence the reaction phase behavior. Experimental set-up such as a view-cell system and suitable equation of states can be employed to find minimum pressures experimentally and theoretically for specific

conditions including temperature, alcohol-to-oil molar ratio, and flow rate, which can create a homogeneous reaction state from the beginning.

5.5 Conclusions

The esterification of oleic acid with ethanol was carried out in a packed-bed reactor containing γ-Al_2O_3 catalyst under subcritical and supercritical conditions (T: 200-325 ^oC, P: 100-200 bar). The catalytic capacity of the alumina at supercritical conditions was considerably higher than at subcritical conditions, for example at pressure of 200 bar and one-minute residence time, about 99% yield was obtained at temperature of 325 oC and while only 27% yield was found at 225 ^oC. An one-step reaction model was used to well describe the data for the supercritical reactions, and it was capable of predicting the data for the subcritical reactions. The analysis demonstrates that the overall reaction including adsorption of oleic acid on the surface, the esterification reaction on the surface, and desorption of biodiesel from the surface is endothermic. Slowly deactivation of the catalyst was observed as a decreased acid site density and surface area, but the loss of product yield was not observed by the deactivation considering the large amount of catalysts employed. Large presence of water decreased the yield by around 10%, and dropping the pressure from 200 bar to 100 bar at 325 ^oC did not show obvious influence on the yield.

Supporting information (Theoretical Analysis of Transport Limitations)

1. Interphase mass transfer limitations

Mears criterion, as shown in Eq-S5-1, was employed to determine if the interphase mass transfer limitations are significant.

$$\frac{-r_A \rho_b Rn}{k_c C_{Ab}} < 0.15 \qquad \text{S5-1}$$

where $(-r_A)$ is the rate of the reaction per bed volume (kmol/kg cat/s), ρ_b is the bulk density of catalyst bed (kg/m^3), R is the average radius of catalyst particles (m), n is the order of the reaction assumed to be 2, C_{Ab} is the bulk concentration of the reactant oleic acid (kmol/m^3), and k_c is the mass transfer coefficient (m/s) for packed beds [54]. The equation for k_c is as below in Eq-S5-2.

$$k_c = 1.17U\left(\frac{U\rho d_p}{\mu}\right)^{-0.42}\left(\frac{D_{AB}\rho}{\mu}\right)^{2/3} \qquad \text{S5-2}$$

where U is superficial velocity (m/s) which would exist without packing, ρ is the density (kg/m^3) of the oleic acid-ethanol mixture, μ is the viscosity (Pa.S) of the mixture, and d_p is the diameter (m) of the catalyst particles. The individual density and viscosity of ethanol and oleic acid at different temperature and pressure was taken from NIST Standard Reference Database [55]. D_{AB} is the diffusion coefficient (m^2/s) as calculated by Eq-S5-3.

$$D_{AB} = \frac{7.4\cdot 10^{-12}(\phi_B \cdot M_B)^{1/2} T}{\mu V_A^{0.6}} \qquad \text{S5-3}$$

where A is solute (oleic acid), B is solvent (ethanol), ϕ_B is 1.5 for ethanol, M_B is the molecular mass of ethanol, V_A is the molar volume of oleic acid in cm^3/mol. The values of diffusion coefficients at pressure of 200 bar and temperature ranging from 200-325 ^{o}C were calculated and shown in **Figure S5-1**.

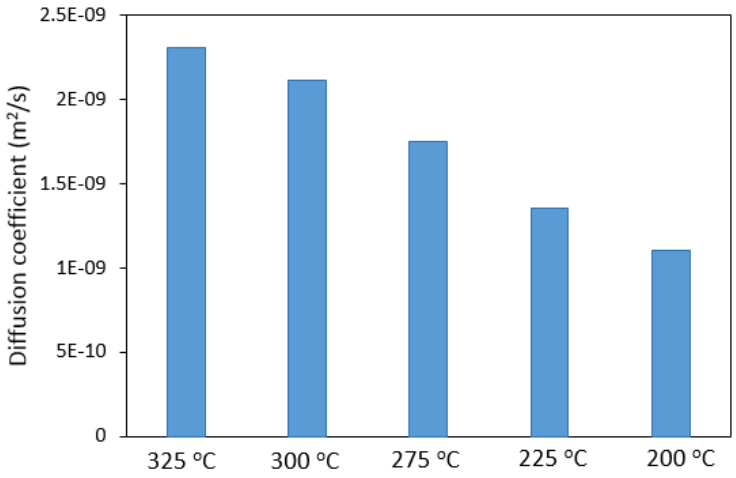

Figure S5-1. Diffusion coefficient at temperature of 200-325 °C, and pressure of 200 bar.

Considering the fact that the reactor employed in this study was not differential, the rate of reaction and reactant concentration were changing along the reactor. Instead, in Eq S5-1, we used the values of the initial rate of the reaction ($-r_{A0}$) and final reactant concentration (C_{A0}*(1-conversion)) to replace the real rate of reaction ($-r_A$) and reactant concentration (C_{Ab}) when applying Mears criterion, meaning the term we calculated was the possible maximum. The initial rate of the reaction was estimated from the experimental data in **Figure 5-4** of the manuscript by taking the derivative at the initial time (t=0). Also, the viscosity value was used as the one of oleic acid, since we did not find a correlation of oleic acid-ethanol mixture viscosity under the reaction conditions. The average radius of catalyst particle was taken as 0.000125 m which is the largest value of the catalysts, as described by the vendor.

The results satisfied the criterion, which implies that the interphase mass transfer resistance was not significant. Example for condition of 325 °C, 200 bar, and 1-min residence time was presented in **Table S5-1** showing that the value was 7.75×10^{-5}.

2. Intraparticle diffusion limitations

Weisz–Prater, as shown in Eq-S5-4, criterion was employed to determine if the intraparticle diffusion limitations are significant.

$$\frac{-r_A \rho_c R^2}{D_e C_{AS}} < 1 \qquad \text{S5-4}$$

where $(-r_A)$ is the rate of the reaction per bed volume (kmol/kg cat/s), ρ_c is solid density of catalyst bed (kg/m^3), C_{AS} is the reactant concentration on alumina surface (kmol/m^3), D_e is the effective diffusivity of oleic acid in methanol. The surface concentration is taken as equal to the bulk concentration of the reacting species, since the external diffusion is not kinetically controlling as estimated above. The equation for De is as below in Eq-S5-5.

$$D_e = \frac{D_{AB} \phi_p \sigma_c}{\tau} \qquad \text{S5-5}$$

where Φ_p is pellet porosity, σ_c is constriction factor, τ is tortuosity. The value of tortuosity, constriction factor were taken from heuristics provided in *Elements of Chemical Reaction Engineering* by Fogler [56].

Again similarly, we used the values of the initial rate of the reaction ($-r_{A0}$) and final reactant concentration (C_{A0}*(1-conversion)) to replace the real rate of reaction ($-r_A$) and surface concentration (C_{As}) when applying Weisz–Prater's criterion, meaning the term we calculated was the possible maximum. The results satisfied the criterion, which implies that the intraparticle mass transfer resistance was not significant. Example for condition of 325 ^{o}C, 200 bar, and 1 min residence time was presented in **Table S5-1** showing that the value was 2.72 x 10^{-3}.

Table S5-1. Parameters used in evaluating criteria for assessing the extent of transport control during reaction at temperature of 325 ^{o}C, pressure of 200 bar, and residence time of 1 min.

Item	symbol	unit	value

reactor diameter	d	m	4.57×10^{-3}
voild fraction of bed	Ɛ		0.7
bed length	L_b	m	0.14
catalyst mass	m_{cat}	kg	2.72×10^{-3}
Initial rate of reaction	$-r_{A0}$	kmol/(kg cat*s)	3.59×10^{-4}
catalyst bed density	ρ_c	kg/m^3	1.18×10^{-3}
porosity	φ_p		0.4
tortuosity	τ		3
constriction factor	σ_c		0.8
bulk density of catalst bed	ρ_b	kg/m^3	7.11×10^{-4}
catalyst particle diameter	d_P	m	2.5×10^{-4}
superficial velocity	U	m/s	4.167×10^{-3}
Superficial flow rate	Q	ml/min	4.10
Reynold number	R_e		1.0
diffusion coefficient	D_{AB}	m^2/s	2.31×10^{-9}
effective diffusivity	D_e	m^2/s	2.46×10^{-10}
molar volume	V_{nb}	cm^3/mol	420.9
Schmidt number	S_c		451.5
mass transfer coefficient	k_c	m/s	8.29×10^{-5}
bulk reactant concentration	C_{Ab}, assumed to be C_{A0}*(1-conversion)	$kmol/m^3$	9.94×10^{-3}
surface reactant concentration	C_{AS}	$kmol/m^3$	9.94×10^{-3}
initial bulk reactant concentration	C_{A0}	$kmol/m^3$	0.49
viscosity of oleic acid	μ_OA	Pa.S	4.24×10^{-4}
viscosity of ethanol	μ_ethanol	Pa.S	4.8×10^{-5}
density of oleic acid	ρ_OA	kg/m^3	670
density of ethanol	ρ_ethanol	kg/m^3	358
Mears			7.75×10^{-5}
Weisz–Prater			2.72×10^{-3}

Acknowledgements

We are grateful to Syracuse University, College of Engineering and Computer Science for financial support. We thank Mr. Richard Louis List for his help on using the SEM. This work also made use of the Cornell Center for Materials Research Shared Facilities which are supported through the NSF MRSEC program (DMR-1719875).

5.6 References

[1] Rattanapan, Cheerawit, et al. "Enhanced efficiency of dissolved air flotation for biodiesel wastewater treatment by acidification and coagulation processes." Desalination 280.1 (2011): 370-377.

[2] Phukingngam, D., S. Dararat, and O. Chavalparit. "Study of biogas production potential of biodiesel wastewater." Proceedings of the 7th National Environmental Conference, Environmental Engineering Association of Thailand, Bangkok, Thailand. CD-ROM. 2008.

[3] Meher, L. C., D. Vidya Sagar, and S. N. Naik. "Technical aspects of biodiesel production by transesterification—a review." Renewable and sustainable energy reviews 10.3 (2006): 248-268.

[4] Lu, Jie, et al. "Nearcritical and supercritical ethanol as a benign solvent: polarity and hydrogen-bonding." Fluid Phase Equilibria 198.1 (2002): 37-49.

[5] Lalanne, P., et al. "Hydrogen bonding in supercritical ethanol assessed by infrared and Raman spectroscopies." The Journal of Physical Chemistry A 108.18 (2004): 3902-3909.

[6] Hoffmann, Markus M., and Mark S. Conradi. "Are there hydrogen bonds in supercritical methanol and ethanol?." The Journal of Physical Chemistry B 102.1 (1998): 263-271.

[7] Deshpande, A., et al. "Supercritical biodiesel production and power cogeneration: technical and economic feasibilities." Bioresource technology 101.6 (2010): 1834-1843.

[8] Lee, Soojin, Dusko Posarac, and Naoko Ellis. "Process simulation and economic analysis of biodiesel production processes using fresh and waste vegetable oil and supercritical methanol." Chemical Engineering Research and Design 89.12 (2011): 2626-2642.

[9] Gonzalez, Samantha L., et al. "Continuous catalyst-free production of biodiesel through transesterification of soybean fried oil in supercritical methanol and ethanol." Energy & Fuels 27.9 (2013): 5253-5259.

[10] Tan, Kok Tat, Keat Teong Lee, and Abdul Rahman Mohamed. "Effects of free fatty acids, water content and co-solvent on biodiesel production by supercritical methanol reaction." The Journal of Supercritical Fluids 53.1 (2010): 88-91.

[11] Nan, Yue, et al. "Production of biodiesel from microalgae oil (Chlorella protothecoides) by non-catalytic transesterification in supercritical methanol and ethanol: Process optimization." The Journal of Supercritical Fluids 97 (2015): 174-182.

[12] Shin, Hee-Yong, et al. "Thermal decomposition and stability of fatty acid methyl esters in supercritical methanol." Journal of Analytical and Applied Pyrolysis 92.2 (2011): 332-338.

[13] Imahara, Hiroaki, et al. "Thermal stability of biodiesel in supercritical methanol." Fuel 87.1 (2008): 1-6.

[14] Lin, Ronghong, Yiying Zhu, and Lawrence L. Tavlarides. "Effect of thermal decomposition on biodiesel viscosity and cold flow property." Fuel 117 (2014): 981-988.

[15] Liu, Jiuxu, et al. "Thermal decomposition of ethanol-based biodiesel: Mechanism, kinetics, and effect on viscosity and cold flow property." Fuel 178 (2016): 23-36.

[16] Dunn, Robert O. "Effect of oxidation under accelerated conditions on fuel properties of methyl soyate (biodiesel)." Journal of the American Oil Chemists' Society 79.9 (2002): 915-920.

[17] Liu, Jiuxu, Yue Nan, and Lawrence L. Tavlarides. "Continuous production of ethanol-based biodiesel under subcritical conditions employing trace amount of homogeneous catalysts." Fuel 193 (2017): 187-196.

[18] Reyero, Inés, Gurutze Arzamendi, and Luis M. Gandía. "Heterogenization of the biodiesel synthesis catalysis: CaO and novel calcium compounds as transesterification catalysts." Chemical Engineering Research and Design 92.8 (2014): 1519-1530.

[19] Zabeti, Masoud, Wan Mohd Ashri Wan Daud, and Mohamed Kheireddine Aroua. "Biodiesel production using alumina-supported calcium oxide: an optimization study." Fuel Processing Technology 91.2 (2010): 243-248.

[20] Samart, Chanatip, Chaiyan Chaiya, and Prasert Reubroycharoen. "Biodiesel production by methanolysis of soybean oil using calcium supported on mesoporous silica catalyst." Energy Conversion and Management 51.7 (2010): 1428-1431.

[21] Kesić, Željka, et al. "Mechanochemical preparation and characterization of CaO· ZnO used as catalyst for biodiesel synthesis." Applied Catalysis A: General 427 (2012): 58-65.

[22] Islam, Aminul, et al. "Biodiesel synthesis over millimetric γ-Al 2 O 3/KI catalyst." Energy 89 (2015): 965-973.

[23] Di Serio, M., et al. "Transesterification of soybean oil to biodiesel by using heterogeneous basic catalysts." Industrial & Engineering Chemistry Research 45.9 (2006): 3009-3014.

[24] Yoo, Sung Jin, et al. "Synthesis of biodiesel from rapeseed oil using supercritical methanol with metal oxide catalysts." Bioresource technology 101.22 (2010): 8686-8689.

[25] Jitputti, Jaturong, et al. "Transesterification of crude palm kernel oil and crude coconut oil by different solid catalysts." Chemical Engineering Journal 116.1 (2006): 61-66.

[26] Garcia, Camila Martins, et al. "Transesterification of soybean oil catalyzed by sulfated zirconia." Bioresource Technology 99.14 (2008): 6608-6613.

[27] Furuta, Satoshi, Hiromi Matsuhashi, and Kazushi Arata. "Biodiesel fuel production with solid superacid catalysis in fixed bed reactor under atmospheric pressure." Catalysis communications 5.12 (2004): 721-723.

[28] Kansedo, Jibrail, Keat Teong Lee, and Subhash Bhatia. "Biodiesel production from palm oil via heterogeneous transesterification." Biomass and Bioenergy 33.2 (2009): 271-276.

[29] Park, Young-Moo, et al. "Esterification of used vegetable oils using the heterogeneous WO 3/ZrO 2 catalyst for production of biodiesel." Bioresource technology 101.1 (2010): S59-S61.

[30] Peng, Bao-Xiang, et al. "Biodiesel production from waste oil feedstocks by solid acid catalysis." Process Safety and Environmental Protection 86.6 (2008): 441-447.

[31] Melero, Juan A., et al. "Production of biodiesel from waste cooking oil in a continuous packed bed reactor with an agglomerated Zr-SBA-15/bentonite catalyst." Applied Catalysis B: Environmental 145 (2014): 197-204.

[32] Pugnet, Véronique, et al. "Stability, activity and selectivity study of a zinc aluminate heterogeneous catalyst for the transesterification of vegetable oil in batch reactor." Applied Catalysis A: General 374.1 (2010): 71-78.

[33] Kim, Manhoe, et al. "A new generation of zirconia supported metal oxide catalysts for converting low grade renewable feedstocks to biodiesel." Bioresource technology 118 (2012): 37-42.

[34] McNeff, Clayton V., et al. "A continuous catalytic system for biodiesel production." Applied Catalysis A: General 343.1 (2008): 39-48.

[35] Xiao, Yang, et al. "Experimental and modeling study of continuous catalytic transesterification to biodiesel in a bench-scale fixed-bed reactor." Industrial & Engineering Chemistry Research 51.37 (2012): 11860-11865.

[36] Ray, Nillohit Mitra, and Ajay K. Ray. "Determination of adsorption and kinetic parameters for methyl oleate (biodiesel) esterification reaction catalyzed by amberlyst 15 resin." The Canadian Journal of Chemical Engineering (2016).

[37] Tesser, R., et al. "Kinetics of oleic acid esterification with methanol in the presence of triglycerides." Industrial & engineering chemistry research 44.21 (2005): 7978-7982.

[38] Kapil, Ankur, et al. "Kinetic modeling studies of heterogeneously catalyzed biodiesel synthesis reactions." Industrial & Engineering Chemistry Research 50.9 (2011): 4818-4830.

[39] Allain, Florent, et al. "Estimation of kinetic parameters and diffusion coefficients for the transesterification of triolein with methanol on a solid ZnAl 2 O 4 catalyst." Chemical Engineering Journal 283 (2016): 833-845.

[40] Santacesaria, E., et al. "Kinetics and mass transfer of free fatty acids esterification with methanol in a tubular packed bed reactor: a key pretreatment in biodiesel production." Industrial & engineering chemistry research 46.15 (2007): 5113-5121.

[41] Dossin, Tanguy F., et al. "Simulation of heterogeneously MgO-catalyzed transesterification for fine-chemical and biodiesel industrial production." Applied Catalysis B: Environmental 67.1 (2006): 136-148.

[42] Veny, Harumi, Mohamed Kheireddine Aroua, and Nik Meriam Nik Sulaiman. "Kinetic study of lipase catalyzed transesterification of jatropha oil in circulated batch packed bed reactor." Chemical Engineering Journal 237 (2014): 123-130.

[43] Likozar, Blaž, Andrej Pohar, and Janez Levec. "Transesterification of oil to biodiesel in a continuous tubular reactor with static mixers: Modelling reaction kinetics, mass transfer, scale-up and optimization considering fatty acid composition." Fuel Processing Technology 142 (2016): 326-336.

[44] Xiao, Yang, et al. "Kinetics of the transesterification reaction catalyzed by solid base in a fixed-bed reactor." Energy & Fuels 24.11 (2010): 5829-5833.

[45] Emeis, C. A. Determination of Integrated Molar Extinction Coefficients for Infrared Absorption Bands of Pyridine Adsorbed on Solid Acid Catalysts. J. Catal. 1993, 141, 347.

[46] Farneth, W. E., & Gorte, R. J. (1995). Methods for Characterizing Zeolite Acidity. Chemical Reviews, 95(3), 615-635.

[47] Kellicutt, Aimee B., et al. "An examination of the intrinsic activity and stability of various solid acids during the catalytic decarboxylation of γ-valerolactone." Catalysis Science & Technology 4.8 (2014): 2267-2279.

[48] Bond, Jesse Q., Christian S. Jungong, and Anargyros Chatzidimitriou. "Microkinetic analysis of ring opening and decarboxylation of γ-valerolactone over silica alumina." Journal of Catalysis 344 (2016): 640-656.

[49] Liu, Jiuxu, et al. "Production of biodiesel from microalgae oil (Chlorella protothecoides) by non-catalytic transesterification: Evaluation of reaction kinetic models and phase behavior." The Journal of Supercritical Fluids 99 (2015): 38-50.

[50] Reference Fluid Thermodynamic and Transport Properties, NIST Standard Reference Database 23, Version 9.0., National Institute of Standards and Technology, Boulder, CO 80305.

[51] Standard Test Method for Determination of Total Monoglycerides, Total Diglycerides, Total Triglycerides, and Free and Total Glycerin in B-100 Biodiesel Methyl Esters by Gas Chromatography, ASTM International, West Conshohocken, PA (2012)

[52] Kulkarni, Mangesh G., et al. "Solid acid catalyzed biodiesel production by simultaneous esterification and transesterification." Green Chemistry 8.12 (2006): 1056-1062.

[53] Xiong, Haifeng, Hien N. Pham, and Abhaya K. Datye. "Hydrothermally stable heterogeneous catalysts for conversion of biorenewables." Green Chemistry 16.11 (2014): 4627-4643.

[54] E.L. Cussler, Diffusion mass transfer in Fluid Systems, Cambridge University Press, the Edinburgh Building, Cambridge CB2 8RU, UK (2009)

[55] Reference Fluid Thermodynamic and Transport Properties, NIST Standard Reference Database 23, Version 9.0., National Institute of Standards and Technology, Boulder, CO 80305.

[56] H.S. Fogler, Elements of Chemical Reaction Engineering, Pearson Education, Inc., Upper Saddle River, NJ, (2006).

Chapter 6. Future work

We have developed two methods for biodiesel production including homogeneous catalysis and heterogeneous catalysis under subcritical and supercritical conditions. In the developed homogeneous catalytic system, near complete biodiesel yields can be reached under the reaction conditions with only 0.1 wt% catalysts. The amount of catalysts were significantly reduced comparing to current industrial level. Ideally the heterogeneous system is superior to the homogeneous system in terms of reducing wastewater generation, if the heterogeneous catalysts can remain stable under the reaction conditions.

Speaking of the developed heterogeneous catalytic system in this study, gamma-alumina was demonstrated to be a good candidate to convert free fatty acids to biodiesel fuel under supercritical conditions. Even though the gamma-alumina was found to be much more stable than most of the reported heterogeneous catalysts in the literature, deactivation of the catalyst was observed after the packed-bed reactor was treated by supercritical reactions for 25 hours. To date, the mechanism and kinetics of the catalyst deactivation is still not clear.

The limitations of this study, which should be investigated in the future, include:

1. The gamma-alumina powder was determined as a good catalyst to esterify free fatty acids considering the fast reaction rate and relatively stable structure. However, its capacity of converting triglycerides to biodiesel fuel has not been studied yet. Considering that gamma-alumina is a weak Lewis acid solid, and triglycerides molecule size is bigger than free fatty acids which will bring diffusion problems, it is very possible that the alumina powder with its current form could not catalyze the transesterification reactions as well as the esterification reaction. Experiments should be designed and conducted to determine if gamma-alumina can catalyze the transesterification reactions of triglycerides, and the optimal reaction conditions.

2. As mentioned at the end of Chapter 5, the gamma-alumina was found to lose its active sites after being treated under 325 ^{o}C, 200 bar for 25 hours. The deactivation and mechanism should be studied, and the experiments should be carried out in a differential reactor. Also methods to regenerate the catalysts should be explored.

3. In Chapter 5, the gamma alumina was in powder form, and the mass transfer resistance was determined to be negligible based on estimation by Mears and Weisz-Prater criteria. If other types of alumina such as pellet form is used, both interparticle and intraparticle resistance should be reevaluated in order to determine the effect of mass transfer on the reaction kinetics.

4. In the introduction section of Chapter 5, we have summarized some stable solids which could be used under subcritical and supercritical conditions for biodiesel synthesis other than alumina. Among these solids, zirconium oxide could be another candidate to look at considering its simple and stable structure and Lewis acid property. Similar investigations on zirconium oxide can be conducted, and compared to the results of the alumina system.

VITA

NAME OF AUTHOR: Jiuxu Liu

PLACE OF BIRTH: Shexian, Hebei, China

DATE OF BIRTH: October 19, 1988

GRADUATE AND UNDERGRADUATE SCHOOLS ATTENDED:

Syracuse University, Syracuse, New York.

Hebei University of Technology, Tianjin, China.

DEGREES AWARDED:

M.Sc. in Chemical Engineering, 2013, Syracuse University, Syracuse, New York.

B. Eng. in Chemical Engineering, 2010, Hebei University of Technology, Tianjin, China.